NEUTRON AND GAMMA MEASUREMENTS

Dissertation

Väitös

Heikki Koskisen muistoa kunnioittaen

Servo Kasi

Neutron and gamma radiation transports are discussed. Radiation based meters (gauges) are described and own examples considered. When modelling a gauge, the transport equation and its adjoint can be solved both. Especially in Monte Carlo solution even in real geometry easily the combination of these give the counting rate of detector. Between gamma emission and detection (in a peak) is a ray, practically. Gauge sampling is discussed. A gauge should be calibrated in laboratory using materials with known elemental composition. Moisture measuring with neutron gauge used in soil moisture measurement in Finland is still not well done. Nondestructive determinations of ^{137}Cs profiles in soil have been performed.

CONTENTS	Page

Neutron and gamma measurements

1. Introduction.

The main sources for neutron measurements in industry and science, as in geophysics, have been the products of the reactions Am(α,n)Be and T(d,n)He, see Fig. 1 for their energy spectra. The last so-called neutron generator emits 14 MeV neutrons and can work in pulse. These and other sources and neutron physics have been described in the text books [1,2]. When neutrons interact

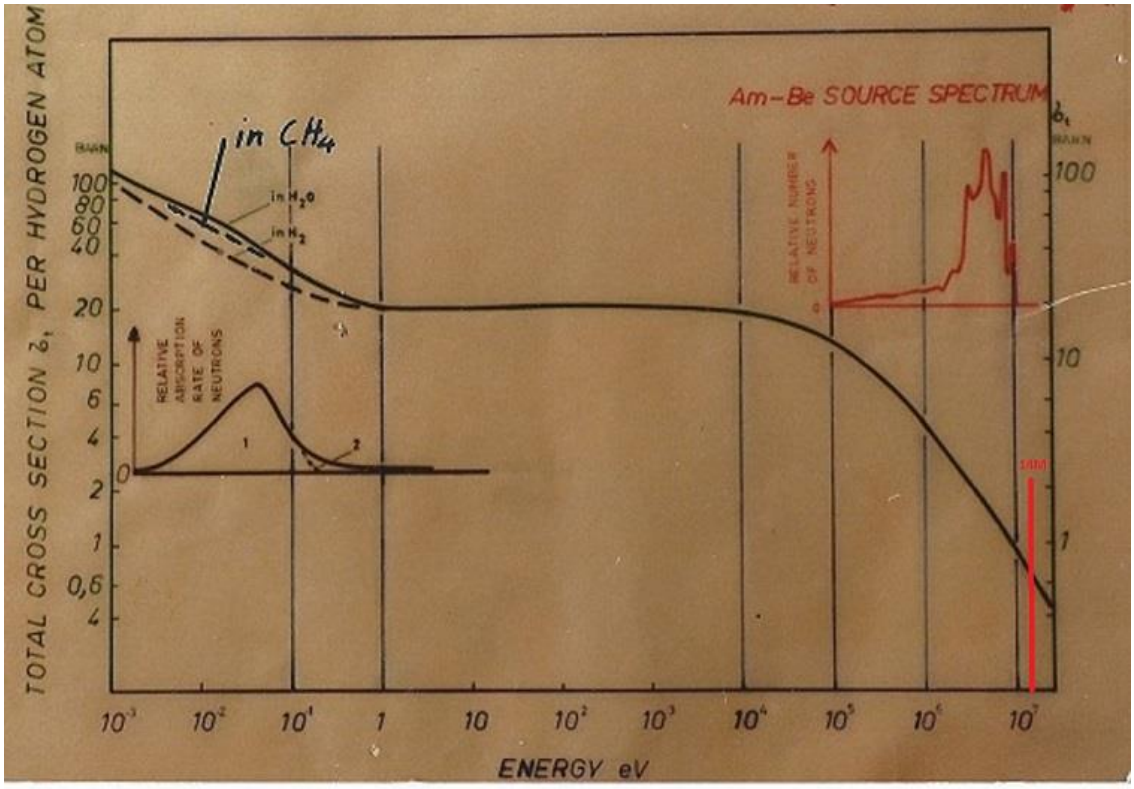

Fig. 1. Total hydrogen cross section ($\sigma_t = \sigma_s + \sigma_a$) over the neutron slowing-down energy range in H_2O and in two other molecules. σ_s is the scattering cross section. On the right AmBe-neutron source spectrum and 14 MeV neutron energy of DT-generator. On the left the energy distribution of absorption (σ_a) of 1 the thermal neutrons and 2 epithermal neutrons in homogeneous infinite mineral soil.

with matter often photons are emitted. These photons are in gamma energies, the physics of which have been described in [3]. The neutron induced gamma photons have been very useful in analytical works in geophysics and industry [4,5]. Also the capsulated point sources of gamma photons (^{137}Cs, ^{60}Co, ^{241}Am, etc.) have been used especially for density determination. The energies of the emitted neutrons and gamma are largely above thermal energies.

Poor neutron measurement (emission and detection) has been used for moisture determination (the neutron moisture gauge). When the source neutrons slow down in matter the hydrogen atoms influence strongly. Their scattering cross section is high. $\sigma_t = \sigma_s$ when energy is over about 1 eV, Fig. 1. In the hydrogen collision the neutron slow down on the average a half of its energy and

in the collision on other atoms considerably less, when neutron energy is below about 0.7 MeV. In larger energies the neutron inelastic scattering is significant, papers I and II.

I have mainly worked with moisture and density measurements. From [6] I found the adjoint flux for use in calculation. The poster [7] is a summary of this dissertation.

2. On neutron and gamma sources.

14 MeV neutron generator can be written DT. Also DD neutron generator (reaction D(d,n)^{3}He) is possible. It emits 2.5 MeV neutrons. Few cm size DT and DD neutron generators have been constructed (Neutristor) [8], but are they electrically safe? The fission neutrons have the energies of few MeV. ^{252}Cf-spontaneous fission source is used, though its half life is only 2.6 a. For the neutron moisture gauge the neutron source energies above 0.7 MeV are not good: there also influences the strong slowing down of inelastic scatterings of other atoms in matter (see Fig. 2 of Text I), and the effect of hydrogen scattering is about of the same order there. The AmLi neutron source should be good, because its energy is below or about 0.5 MeV [2]. I have found (I) that the iron reflector behind AmBe source clearly increase the sensitivity of moisture measurement.

The earth crust has the gamma-active ^{40}K (1461 keV), ^{208}Tl (2614 keV) and ^{214}Bi (1765 keV) nuclides. Their distribution in soil is almost a half infinite space. The attenuation of their radiation has been used for the survey of snow cover mass [9]. Today we have near the surface of soil the fall-out of ^{137}Cs from Chernobyl in Europe. It is almost a plane source of the ^{137}Cs gamma-radiation (662 keV), VII, [7]. Fig. 2.

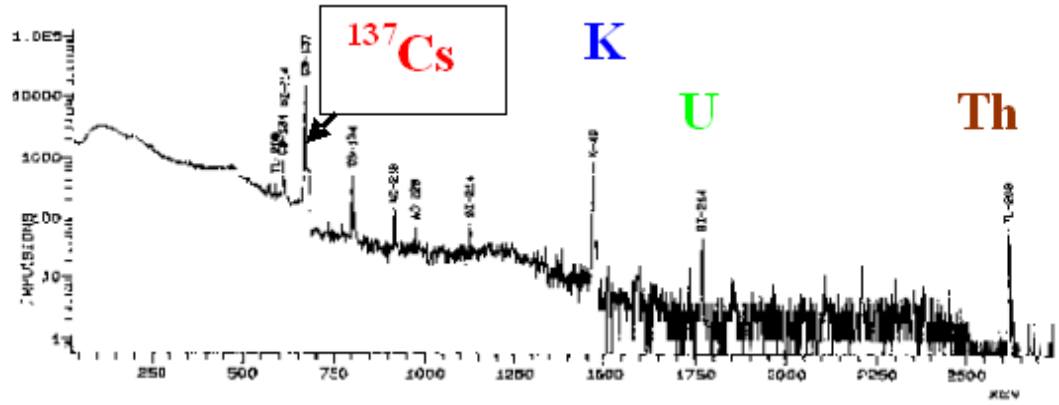

Fig. 2. Soil radiation with Ge-detector measured by the French group in the project RESUME in southern Finland 15.8.1995.

3. Neutron and gamma detectors.

The most methods of detection of neutrons and gamma photons have been presented by Knoll [10]. About epithermal detection, fig. 1, achieved by using Cd-foil around the neutron detector, Amaldi [2] has discussed thoroughly.

For measurements of relatively fast decaying numbers of particles (photons or others) I have made a paper [11] (with 8 references) declaring that instead of the Poisson distribution the binomial distribution works for any case of nuclear disintegration. In Appendix C [10] for the cases

of variable mean value during measurement the distribution C3 should agree with the corresponding binomial distribution

$$P(x) = \binom{N}{x}(1-e^{-\lambda T})^x (e^{-\lambda T})^{N-x}$$

I have in [11].

4. Radiation gauges

Near the radiation gauge one must consider the radiation level. It should not permanently exceed the dose level of environmental radiation. The dose on the worker is to be followed.

Radiation gauges are useful in industry, medicine and science. We consider the gauges where the response $R = R(x)$. x is the quantity to be determined. Mostly detection of a particle causes an electric pulse. The response R is the counting rate of pulses. It is determined the count number in a certain time interval, or the frequency R of pulses is determined electronically by a rate meter. The sensibility analysis discussed in IV is also applicable for other gauges than the moisture neutron gauge. For a radiation gauge with good calibration $R(x)$ the only significant error is caused by the statistics of radioactivity. I have presented a consideration for evaluation and design of radiation gauge[1] in this case and when the strength of radiation source does not change during the gauging. Then the statistical error $\Delta R = \sqrt{R/t}$, when the pulses in the time t are counted. When the rate meter is used then also $\Delta R \propto \sqrt{R}$ [10]. The error of x ,i.e.. $\Delta x = \Delta R / R'(x)$. In the former case $\Delta x = \sqrt{R(x)/t} / R'(x)$ and when we want the constant error expectation Δx in the interval (x_1,x_2), i.e. optimal calibration curve, and R_b is the background determined in time t_b, then those optimal calibration curves have the forms as presented in Fig. 3 for two Δx.

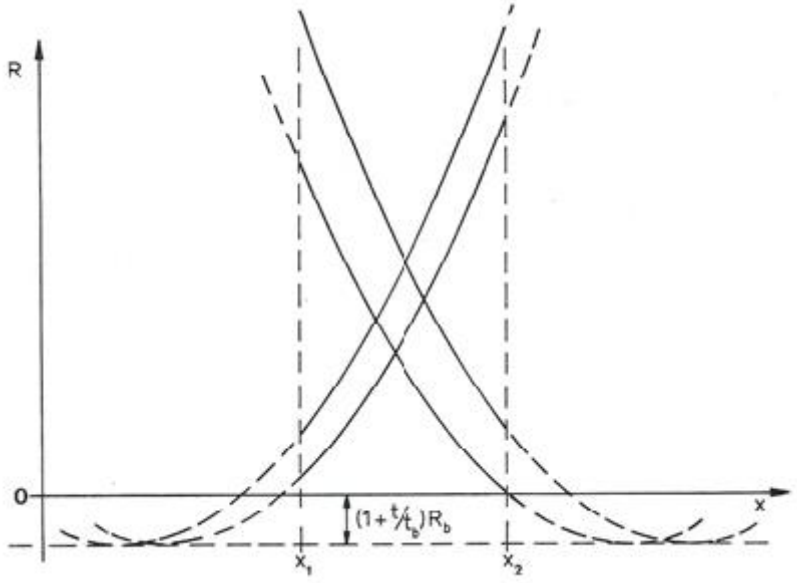

Fig. 3. Forms of optimal calibration curves for two constant values for error Δx, when background (the value R without radiation source measured in time t_b) also is concerned.

The neutron moisture measurement mentioned above is hydrogen content determination, III, IV, V and VI. Then the hydrogen content of bulk matter should be known, as well as its density, known or measured. The third parameter of the bulk matter when detecting thermal neutrons is their

[1] Report P5/1981 of Laboratory of Physics of Helsinki University of Technology is still unpublished. It is referred in text IV (ref. [6] there).

absorption cross section. In IV you see that the elements B, Gd, Sm, Eu and Cd effect strongly in the thermal measurement.[2] The thermal absorption cross section from a representative soil sample can be measured with at least three different methods (V). For the gauge some theoretical model can be developed good enough for practical measurements. The 3-group diffusion calculation used in IV maybe is not good enough for the model of gauge. In the calibration the parameters of the gauge model should be determined from measurements with known hydrogen content materials. Text V (Appendix) presents some proposals as to materials. Also $Al_2(SO_4)_3 \cdot 18\ H_2O$ may be included in the list.

The gamma gauge with a relatively long distance between the point source and detector has decreasing calibration curve (counting rate versus density). For peat measurements, 7.1, I have developed a gauge with increasing calibration curve. For it the calibration is good, though maybe the model function [12] of gauge (calibration function) with five parameters [7], I used, is not appropriate enough.

A plenty of neutron induced analysis of elements is possible [4,13,14]. The fast neutron inelastic scattering gamma-rays (FNIGR) can be used. Thermal neutron capture often causes the emission of prompt gamma-ray (TCPGR), which is characteristic for the absorbing element. The 2223 keV photon is characteristic for hydrogen. In the third type of elemental analysis there is activated mainly in a sample nuclides in captures of thermal neutrons or in reactions of fast (MeV) neutrons [4]. The neutron generator DT or DD can operate in pulse as in [15, 16], Fig. 4. I think the time T_1 is a little larger than the slowing-down time. In [15] $T_1 \cong 15$ µs and $T_2 \cong 85$ µs applicable in environmental measurements, which Tan shew in IRRMA 6 in Hamilton in Canada in 2005. During

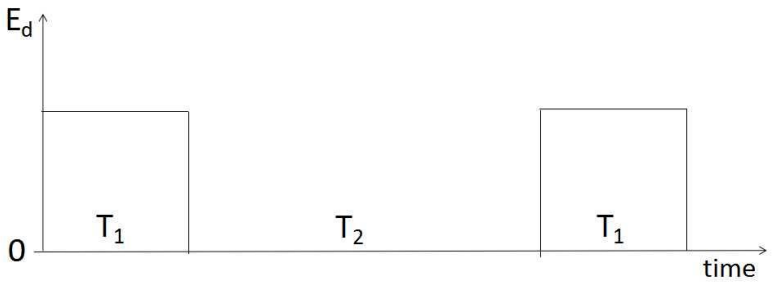

-

Fig. 4. Pulse train of neutron generator [15]. T_1 is the time when neutron generator is ON, then E_d in the DT generator is about 100 keV. T_2 is the time when the generator is OFF.

the time T_1 the FNIGR photons are measured and during T_2 the TCPGR photons [15].

For TCPGR measurement the hydrogen content of matter is significant parameter in quantitative analysis. Thermal neutron distribution influences.

[2] In IV two soil moisture measurement points are incorrectly too low. They are corrected in the poster [7] and in Fig. 14 a.

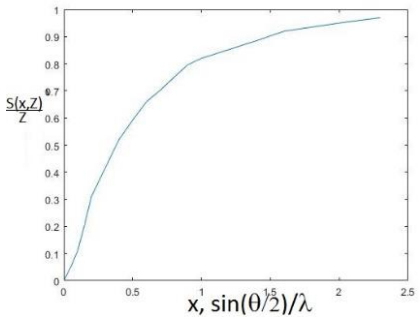

Fig. 5. Incoherent scattering function for aluminium [18]. θ is the scattering angle and λ is the wave length of photon.

It is amazing that the photopeaks of gamma photons are sharp, Fig. 2. For the small scattering angle θ the Klein-Nishina cross section σ_{KN}, [10], of Compton scattering is not valid. Then the real cross section of an element Z is $Z \cdot S(x,Z)/Z \cdot \sigma_{KN}$, when σ_{KN} is for a single electron. In tabulation [17] there is the incoherent scattering function S(x,Z)/Z for all elements, that for Al in Fig. 5. x in Fig. 5 is proportional to the momentum change in the scattering.

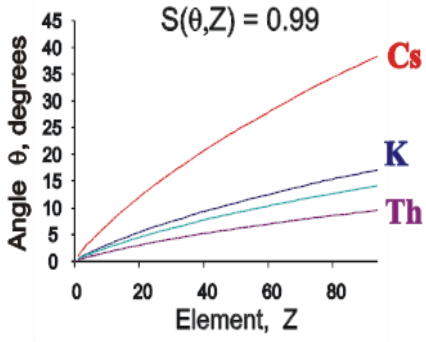

Fig. 6. When the scattering angle is between 0 and θ, then the Klein-Nishina cross section must be multiplied with the value S(θ,Z)/Z [17].

5. Calculation.

An introduction for this subject I have presented in Finnish [19]. Neutron or gamma is an electrically neutral particle. It moves in straight line until meets an atom. The interaction between the particle and atom is a rather accurately known event. It can be scattering or reaction. They have certain probabilities, the portions of the total cross section. The cross section σ is the area around the atom where the event occurs; its unit is barn = b = 10^{-24} cm^2. The density of atoms is $\rho A/M$, ρ is density of matter, M is atom number in weight unit/mole and A = 0.60221413 10^{24}/mole, the number of atoms in one mole. Then

$$\rho\Sigma = \frac{\rho}{M} A\sigma$$

is the probability of the event on the travel of the particle in a length unite.

$$\Sigma = \frac{A\sigma}{M}$$

is called mass attenuation coefficient or “macroscopic cross section”.

The exact calculation can be the Monte Carlo (MC) calculation or some accurate solution of the transport equation presenting the neutron or gamma process under the inspection.

5.1 Monte Carlo calculation

I made the first Monte Carlo (MC) calculation in the 60's, a forward calculation, I and II, for the neutron moisture gauge. There was assumed a point source (AmBe or relevant) of fast neutrons, Fig. 1. MC calculation selects the source energy E_0 of neutron to follow randomly with the random number R, which has the even distribution between 0 and 1. Neutron slows down in an elastic or inelastic scattering. For the event a random number R is selected. R selects the type of scattering. The point of the event, the decreased energy and the direction of scattered neutron is registered. The absorption too is possible. The weight number W, the value 1 in the start, is decreased with the multiplicator $1-\Sigma_a(E)/\Sigma(E)$ in each event. The interval from source and from a scattering point to the following one was selected randomly. Let us consider a beam of N neutrons. It is found that $N\exp(-\rho\Sigma s)$ is the number of neutrons after the distance s. Suppose $N = 1$, then we assume, when p is the *probability density function* of the event, that

$$\int_0^s p\,ds = 1-\exp(-\rho\Sigma s) = F(s) \qquad (1)$$

is the *cumulative distribution function* of the interval s. $F = R$ was selected and s was calculated from (1), the equation (7) in II.

{Instead of (1) the system (s,p,F) maybe can be another.[3] However, many simulation of measurements by using (1) have been excellent, e.g. [14].}

The neutron followed has four parameters with it: 1. position $\mathbf{r}$, 2. unite vector of direction $\boldsymbol{\Omega}$, 3. energy E or lethargy $u = \ln(E_0/E)$, 4. weight W. The neutrons have in I and II followed until the energy is below 0.75 MeV. My use of the inelastic scattering of fast neutrons have been presented in II. The neutron direction after the scattering is spherically symmetric. We suppose that elastic neutron scattering is cylindrically symmetric. In Fig. $\boldsymbol{\Omega}'$ is the direction of incoming neutron and θ is the scattering angle. In the elastic scattering from heavy elements (C and heavier) can the direction of outgoing neutron approximately be assumed spherically symmetric. However, the scattering from hydrogen is only symmetric in the center of mass system, but in environmental (laboratory) system we have the hydrogen scattering cross section $\Sigma_{sh} = \Sigma_s f(\mu)$, $\mu = \cos\theta$. and

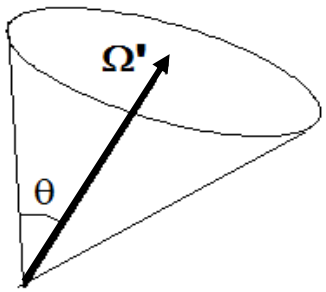

$$f(\mu) = 0 \text{ when } \mu \le 0 \text{ and } f = 2\mu \text{ when } \mu \ge 0. \qquad (2)$$

We can also make MC calculation in inverse direction starting from the detector with the detection probability for a neutron (or photon). First can the neutron thermalization to be treated roughly. We may then start with a certain detection energy, say 0.1 eV, and follow with the neutron upwards in energy. This idea I presented in my talk in 1982 in 50th Anniversary of the

[3] The disintegration of N radioactive nuclides has the similar value $N\exp(-\lambda t)$ after the time t (λ is the disintegration constant) and $1-\exp(-\lambda t)$ is c.d.f. for the disintegration of a nuclide [11].

Discovery of the Neutron in Cambridge [19]. In the neutron scatterings from heavy elements the approximation of spherical symmetry is not bad. In the hydrogen scattering, because it is spherically symmetric in c.m. system, only the directions of incoming neutrons are possible, and f is as in (2), but Θ is the angle of incoming neutron as to the direction of outcoming.

For the neutron moisture gauge we select an energy *E* between the source and detection energies [7]. Over the space we have the cloud of particles slowed down below *E* with their four parameters and the energy just below *E*. We also have calculated the cloud of detection probability "particles" with their similar parameters. We then sum up these two clouds over the space (9, p. 13). The result of computing is the counting rate of particles in the detector.

For TCPGR the neutron slowing down transport from source to thermal energies (Fig. 1) must be calculated. For TCPGR in [14] the writers see the MC library as a useful tool.

In the calculations of gamma photon fields (particle clouds in MC) the photon polarisation [3] is to be considered. The group of Fernandez in Italy have made that [20].

5.2 Ray theory.

We suppose simply that the particle (neutron or gamma) goes as a ray from the source. In a point it has an interaction with the matter and after that the same particle or some other particle goes as a ray to the detector. During the travel, say the interval *r*, the ray can interact according to (1). When the source strength of a point source is *S* particles per time unite then the intensity is:

$$I = S\frac{e^{-\rho\Sigma r}}{4\pi r^2} \qquad (3)$$

as the number of particles penetrating through a plane unite at the distance *r*.

The particle, that is emitted at the point ***r*** isotropically, is detected with the probability

$$D = \frac{e^{-\rho\Sigma a}}{4\pi a^2} A p_D \qquad (4)$$

in the detector at the distance *a*. Ap_D is the approximate constant for detection. More accurately we can calculate for a ray to penetrate the detector surface (in the direction $\boldsymbol{\Omega}$) at the distance a_1 and the second surface (possibly) at the distance a_2. Then

$$\frac{dD}{dA} = \int_0^{a_2-a_1} \frac{e^{-(\rho\Sigma a_1 + \rho_d\Sigma_d x)}}{4\pi(a_1+x)^2}\Sigma_D dx \qquad (5)$$

is detection probability which must be integrated over the area at the detector.[4]

In the FNIGR and TCPGR systems (as Fig. 4) we measure gamma rays characteristic for elements. The rays practically come in straight line from emitting element to the detector. For FNIGR the transport, before the inelastic scattering, may be treated ray-theoretically. The ray theory also may be applied for the gamma density measurements.

[4] Is the formula in [19] found from (5) correct?

5.3 Transport equation and its diffusion approximation.

The counting rate *C* of detector can be presented two ways [6]:

$$C = \int \Sigma_D \Phi(\mathbf{r}, \Omega, E)\, dE\, d\Omega\, dV_D = \int_V S(\mathbf{r},\Omega,E)\Phi^*(\mathbf{r},\Omega,E)\, d\Omega dV \qquad (6)$$

where $\Phi(\mathbf{r},\Omega,E)$ is flux and $\Phi^*(\mathbf{r},\Omega,E)$ is its adjoint flux (i.e. detection probability or so-called importance). The left integral is over the detector volume. In the right integral the energy *E* is some mean value in the energy interval of the slowing-down, and *V* is volume large enough. *S* is the slowing-down density over the energy *E*.

The transport equation [1,2,6] independent on time is

$$\Omega \bullet \nabla\Phi + \Sigma\Phi = \iint \Sigma_s(\mathbf{r},E',\Omega' \rightarrow E,\Omega)\Phi(\mathbf{r},E',\Omega')dE'd\Omega' + S(\mathbf{r},\Omega,E) \qquad (7)$$

and its adjoint [6]

$$-\Omega \bullet \nabla\Phi^* + \Sigma\Phi^* = \iint \Sigma_s(\mathbf{r},E,\Omega \rightarrow E',\Omega')\Phi(\mathbf{r},E,\Omega)dEd\Omega + \Sigma_D(\mathbf{r},E)$$

On the boundary against vacuum (or air) the incoming Φ and the outgoing Φ^* are zero. Basic simple geometries are spherical, cylindrical and plane ones. In my papers III-VI the diffusion approximation of (6) in spherical (and cylindrical) infinite geometry has been used. In I,II the point source in infinite space is assumed. The errors there in the calculated flux of dry density results have been eliminated by dividing in the energies 5 … 0.75 MeV the radius into intervals according to the slowing down length, Fig. 7.

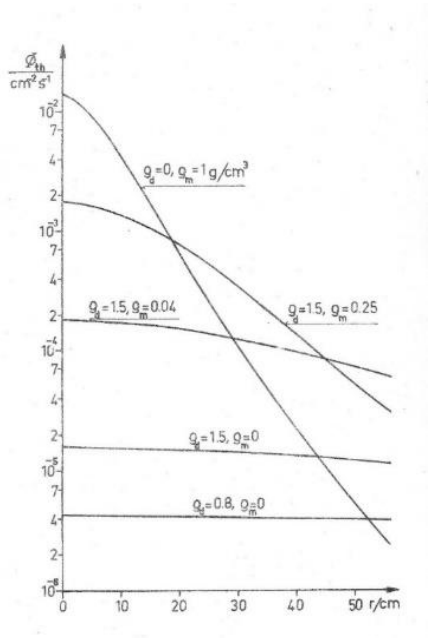

Fig. 7. Thermal flux around a point source 1 neutron/s in mineral source for some soil (ρ_d) and water (ρ_m) densities.

For the neutron gauge of moisture the cylindrical geometry should be better. Koskinen in I used this geometry with point source and slab. I started with a point source and point detector in homogenous infinite medium. In [21] Dunn and Gardner solve a point source on the surface of semi-infinite medium. They simulate detection with a line flux and an area flux. Later in IV we have

the neutron detector as a sphere away at the certain distance from the neutron source. In VII there is a plane geometry application.

In exact transport theory of neutron transport the good relevant models of measurements are not possible or difficult to find. In MC theory the good models of measurements are possible to find.

We suppose as in (2) that the elastic scattering in an atom is cylindrically symmetric around the direction $\mathbf{\Omega}'$ of the incoming particle to the angle θ. We have $\mu = \cos\theta$. Σ_s, ϕ and ϕ* can be developed in spherical harmonics. The diffusion approximation is found when in the developments only the terms P_0 and P_1 are included. For the scattering in hydrogen we have presented in (2) the function $f(\mu)$, where $f = 0$, when $\mu < 0$ and $f = 2\mu$, when $\mu \geq 0$.

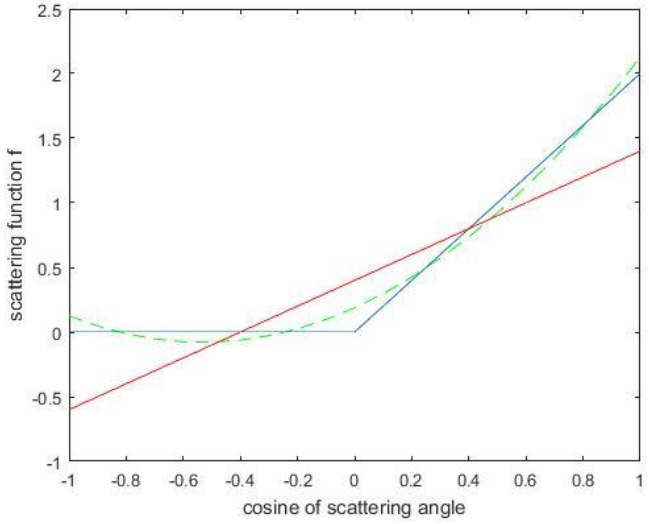

Fig. 8. Neutron scattering in hydrogen (blue line). Its P1-approximation is the red line, In the figure is also the P2(P3) approximation.

The diffusion (P1) approximation is bad for the medium what has hydrogen (Fig. 8). Therefor the diffusion results calculated for neutron moisture gauge should be controlled by using more accurate calculations. I have used the P1- (diffusion) calculation in I-VI. The diffusion calculation also as an approximation for the adjoint flux has been used [22].

Koskinen in I is trying toward the moisture distribution in slab. Calculated result of moisture distribution [23][5] can then be useful.

6. Sample size of gauge

We take Φ from (7) and integrate over the angles, and we have the particle flux $\phi(\mathbf{r}, E) = \int_{4\pi} \Phi(\mathbf{r}, E, \Omega) d\Omega$.

Then we define the characteristic of gauge $\Sigma\phi(\mathbf{r}, E)$, where Σ is:

1. element characteristic reaction or inelastic scattering cross section in neutron induced analysis FNIGR.
2. scattering cross section for the density gauge.

[5]Publication [23] is 3. part of Kasi's licentiate work.

3. hydrogen scattering cross section for moisture gauge.

1. Simple illustration for the gauge of elemental analysis with the neutron source and gamma detector system has been presented in Fig. 7, [24]. Here the attenuations of the source neutrons and emitted gamma photons, (3) and (4), I have assumed negligible. The curves are then the

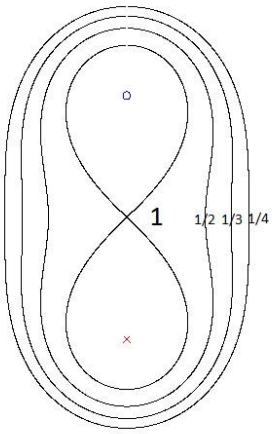

Fig. 9. Curves of equal count rate of detection. x is source and o is detector of gauge.

Cassini ovals. The numbers on the curves are relative weights. For FNIGR gauge the more accurate calculation of relative weights is simple. The quantity $dD/dA = \phi^*(\mathbf{r}, \Omega, E)$ at the point **r** in medium with the direction $\boldsymbol{\Omega}$ and at the energy *E* of emission is exact, for both FNIGR and TCPGR analysis.

For TCPGR gauge the neutron calculation is complicated.

2. For the density gauge the ray theory is not bad to be applied. The geometry can be realistic one.

More accurately and generally we can define the weight p_E from second equation (6), paper III,

$$p_E(\mathbf{r}) = \frac{dC/dV}{C} = \int_{4\pi} q(\mathbf{r}, \Omega, E)\, \Phi^*(\mathbf{r}, \Omega, E)\, d\Omega . \quad (8)$$

where as the source *S* is the slowing-down density *q*. The value of *E* is to be selected appropriately.

3. For the moisture gauge, Fig. 1, *E* of (8) is to be selected as a mean value of lethargy between the source and thermal energies [7]. The hydrogen scattering there is the most characteristic event. I think the most practical accurate calculational method to determine $p(\boldsymbol{r})$ is MC. We determine $q(\boldsymbol{r},\boldsymbol{\Omega},E)$ with forward MC and the importance $\phi^*(\mathbf{r}, \Omega, E)$ starting the backward MC from the detector. Then by integrating over the angles $p(\boldsymbol{r})$ is achieved.

In application we use in III only the P1-approximation of transport (diffusion), though its use is questionable, see Fig. 8. Then we calculate $p(r)$ for the point probe (the source and detector in a point, same for both) in infinite homogenous matter using 2- and 3-group diffusion (Fig. 10), as well as discussing the age-diffusion model application.

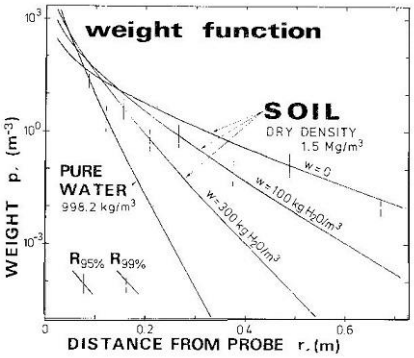

Fig. 10. Diffusion calculation of $p(r)$ for a point probe in infinite matter (soil) with 3 moistures and water. The radii of 95 and 99 % spheres are shown.

The sample radius R of the s % size from

$$\int_0^R p(r)4\pi r^2 dr = s\% \,.$$

has been calculated in III. I consider, the 3-group calculations are better than 2-group ones. Using the ratio between their values it is presented in IV the radius

$$R_{95\%} = \frac{4.3}{L_1^{-1} + L_2^{-1}},$$

where L_1 is the slowing-down length and L_2 is thermal diffusion length.

7. Some radiation gauges

In the measurements we have theoretical model of the gauge presenting the calibration function, as $R(x)$, 4. There we have two kind of parameters:

- parameters of the gauge
- parameters of matter

We consider at first density gamma gauges. The Compton (i.e. incoherent) scattering is proportional to the electron density (about ~Z, Z is the atomic number) in matter, except to H, then 2Z, and for heavy elements the Z effect reduces (because |M| > 2Z). Other photon interactions in matter are photoelectric absorption (cross section about $\sim Z^{4.5}$) below Compton scattering energies [10] and pair production ($\sim Z^2$) above them. The cross sections of these three interactions for different elements and many compounds are in the NIST tabulation, also graphically. ^{137}Cs is most used gamma source element. Its energy 662 keV is in the middle of the Compton dominance energies.

The calibration curve of cesium gamma gauge is decreasing, when the source-detector interval is long, but for relatively low densities (as the peat gauge 7.1.) the calibration curve is increasing when using smaller interval.

7.1 Peat density gauge

I have planned a gamma gauge of density, Fig. 11, where growing calibration curve, Fig. 12. Measurements

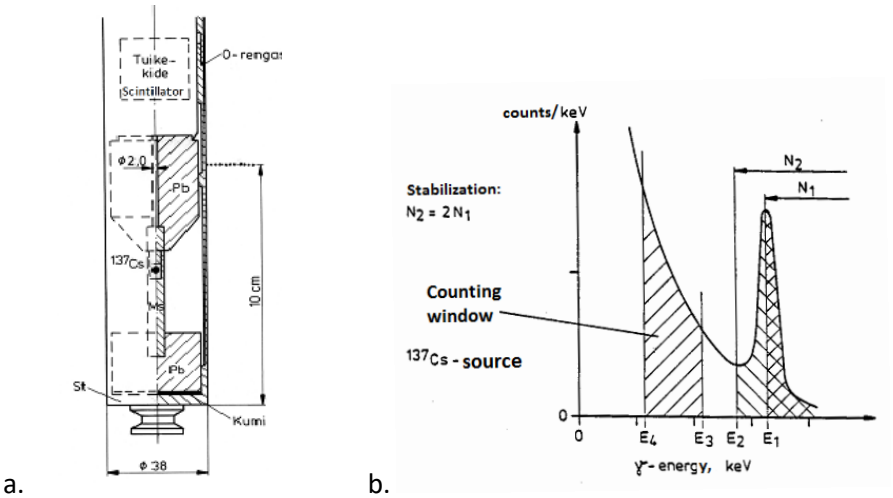

a. b.

Fig, 11. a. Peat density gauge. b. Its electronics, E_1 = 662 keV.

have been done with material with relatively well known chemical contents and densities (matter parameters). For the gauge the theoretical model has been taken from [12]. In the model 5 gauge-

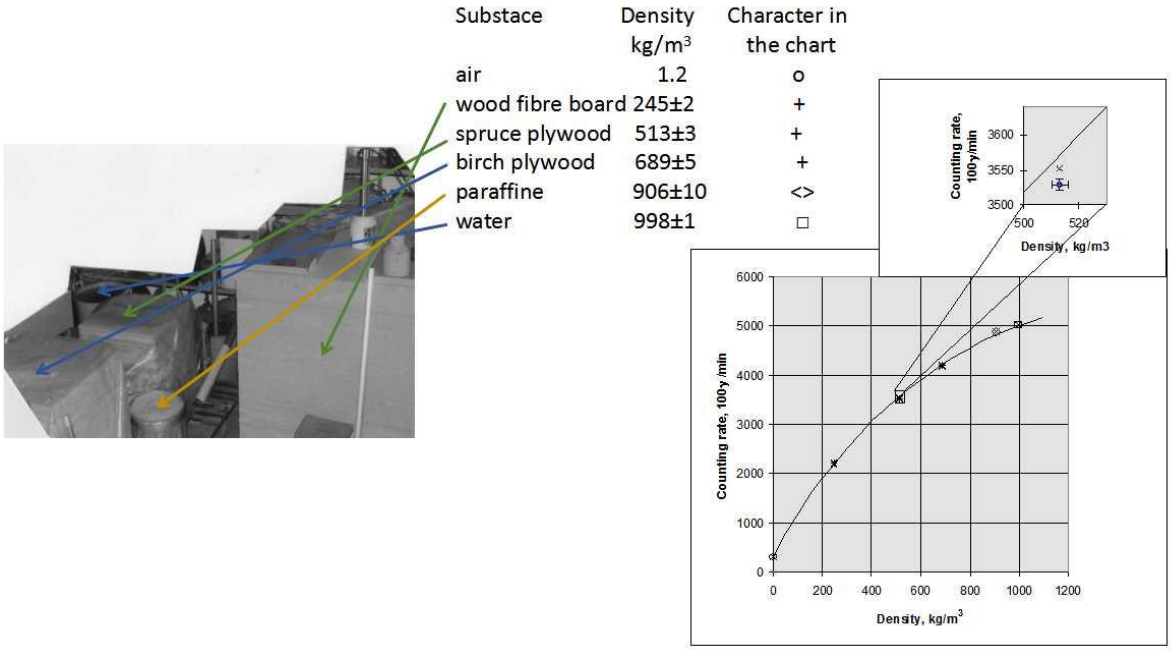

Fig. 12. Peat calibration of a gamma gauge. Characters x are results of calculation.

Table 1. Elements (%) in calibration substances.

Substance	water	C	H	O	N	Ar,Ca	Al,Fe,Si
air	1.12			23.2	75.6	1.2	
wood fibre	7.3	49.9	6.1	42.7	0,9	0.1	3·0.1
spruce	9.4	50.6	6.2	41.6	0.8	0.5	3·0.1
birch	9.3	49.7	6.1	42.7	0.9	0.3	3·0.1
paraffine	0	85.6	14.4				
water	100		11.1	88.9			

parameters were optimized. You see the accuracy, though maybe the theoretical model was too rough. See the small figure of calibration: the result of calculation for spruce plywood differs from the result of measurement more than its error limits.

7.2. Snow density gauge.

In the 5th Northern Research Basins Symposium in Finland 1984 I demonstrated a snow density gauge, Fig. 13.

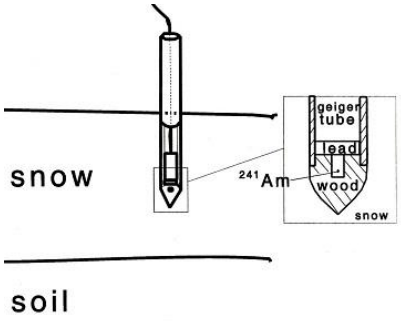

Fig. 13. Snow density gauge.

The energy of ^{241}Am gamma photon source is 60 keV. For H and O this energy is in the region of Compton scattering dominance. See the NIST tabulation.

7.3. Neutron gauge of moisture.

This meter has much been used for water content determination in mineral matters, as mineral soil. That this neutron gauge measures hydrogen content is due to hydrogen slowing-down power. The mean lethargy change is 1 for H, 0.158 for C, 0.120 for O, etc. decreasing with the atomic mass. For neutron moisture gauge also the calibration should be done in laboratory materials with known chemical contents. When using materials in [5, Appendix] at least as good calibration as in 7.1. is possible. However, the hydrated materials listed may be questionable. At least commercial aluminium sulfate is $Al_2(SO_4)_3 \cdot nH_2O$, where n = 14-18. In [21] polyethylene has been used successfully. As mentioned earlier (p. 3) from the matter parameters, when thermal neutrons are measured, they are:

1. hydrogen content,
2. density,
3. thermal absorption cross section of neutron.

In soil moisture measurement, when drilling a hole for the measuring, soil samples can be taken for the parameter determinations. Three methods to determine the absorption cross section have been referred in V. Let us add still the method of counting both with bare detector and with Cd-foil covered, [21].

For development of calibration of the moisture gauge the good neutron theory must be used. Papers I ja II are the start to this direction. Uses of realistic geometry and importance theory, I see, can be easily performed. The MC calculations are easy. In the forward MC starting from the source the “neutron cloud” we achieve at the mean lethargy (energy E in [7]) is the slowing-down density $q_E(\boldsymbol{r},\Omega)$. For thermal neutrons in realistic spatial conditions we take an energy distribution. Is that an Maxwellian in the temperature a little larger than that of environment? See [1], the ratio $\Sigma_a(non\ \ 1/v)/\Sigma_a(1/v) = 0.21$ for thermal neutrons using the element contents of table I in IV and the absorption cross sections of Table 1.4.1 of [1], v is neutron velocity. From the detector we transfer the detection probability during few interactions. After

that we from the thermalization energy, say 0.1 ev, and find the "detection probability cloud" at the energy *E* $\phi_E^*(\mathbf{r},\Omega)$. Then we have the counting rate

$$C = \iint_{V\,4\pi} \phi_E^*(\mathbf{r},\Omega) q_E(\mathbf{r},\Omega) d\Omega d\mathbf{r} \qquad (9)$$

where *V* is large enough.

However, now I can only present results of diffusion calculations [4], though they may include errors. In IV we found that the interference power of density is not effected by interference of the absorbing elements. That is because their contents are small. Gadolinium content can be more significant parameter than density [25]. In these calculations I had the point probe in infinite medium, as in III.

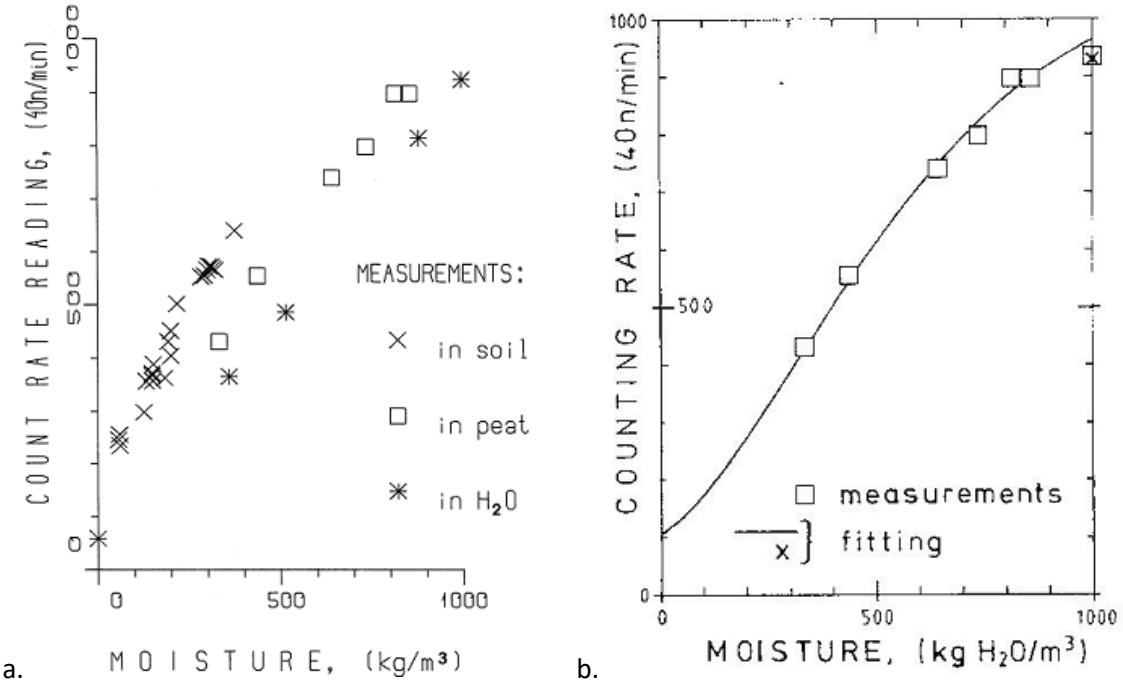

Fig. 14. a. Measurements of different soils, peats and snow-water. b. Fitting calculation to results of peat and water measurements.

In Fig. 14 there are measurements with a neutron gauge of Danish Nucletronics company. We developed 3-group diffusion calculation where it was homogeneous slowing down medium and detection sphere (radius *r*) at the distance *d* from the neutron source, and the sphere absorbs all thermal neutrons on it, and a part of epithermal neutrons. Using this calibration we made fitting application presented in Fig. 14b. We had five fitting gauge parameters: *r*, *d*, the portion of epithermal neutron detection, multiplier and constant term. It is sorry, that snow and soils were not included.

8. Cesium profiles nondestructively.

The most significant deposition nuclide from Chernobyl is ^{137}Cs. I have presented a method to determine cesium vertical profile nondestructively, VII-IX, Fig 15. In mineral soil ^{137}Cs may have stabilized close to its surface (VIII).

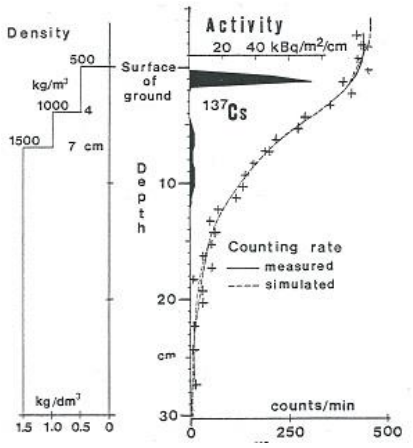

Fig, 15. Inversion determination of ^{137}Cs-profile in Lammi, Finland 1987/6. The detector in the soil tube was Ø1x1" NaI(Tl) scintillator crystal. On the left the assumed soil density profile.

In IX in Fig. 5 the ^{137}Cs local deposition values I measured for STUK.

9. Deposition of radioactive substances.

See the Fig. 16. The increase of the ^{239,240}Pu+^{241}Am-curve is due to the decay of ^{241}Pu, which

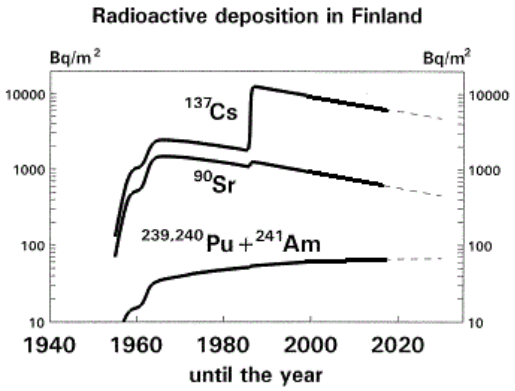

Fig. 16. Radioactive deposition in Finland.

half life is 14.4 a. The ^{137}Cs and Pu release in 2011 in Fukushima accident in Japan were similar than in Chernobyl accident in 1986 [26]. ^{137}Cs deposition in Finland in 2011 was below 1 Bq/m^2 [27].

ACKNOWLEDGEMENT

Prof. Erkki Laurila in 1963 proposed my diploma work on the neutron moisture measurement. Until 1986 I had to teach and study in Laboratory of Physics in Helsinki University of Technology, 1984-09 for the Academy of Finland in calibration of soil moisture neutron gauge. Computing facilities after 1986 I used in Hydrological Office and Helsinki University.

REFERENCES

[1] Beckurts, K. H., and K. Wirtz: Neutron physics. Springer 1964.

[2] Amaldi, Eduardo: The production and slowing down of neutrons. Pp. 1-659 of Handbuch der Physik XXXVIII/2, Springer 1959 .

[3] Fano, U., L. V. Spenger, M. J. Berger: Penetration and diffusion of X rays. Pp. 660-817 of Handbuch der Physik XXXVIII/2, Springer 1959.

[4] IAEA RADIATION TECHNOLOGY REPORTS No. 1, Neutron Generators for Analytical Purposes, INTERNATIONAL ATOMIC ENERGY AGENCY, VIENNA, 2012.

[5] Lim, C. S.: Recent developments in neutron-induced gamma activation for on-line multi-elemental analysis in industry. J. Radioanal. Nucl. Chem. 262(2) (2004) 525-532.

[6] Bell, G. I., and S. Glasstone: Nuclear reactor theory. Van Nostrand Reinhold 1970.

[7] Kasi, Servo: Modelling, calibration and errors of γ- and n-gauges. Poster presentation in ISRP-10, 2006.

[8] Elizondo-Decanini, J. M., D. Schmale, M. Cich, M. Martinez, K. Youngman, M. Senkow, S. Kiff, J. Steele, R. Goege, B. Wroblewski, J. Desko and A. J. Dragt: Novel surface-mounted neutron generator. IEEE Transactions on Plasma Science 40(9) 2145-2149, 2012.

[9] IAEA: Airborne Gamma Ray Spectrometer Surveying, INTERNATIONAL ATOMIC ENERGY AGENCY, Technical Reports Series No. 323, Vienna, 1991.

[10] Knoll, G. F.: Radiation detection and measurement. Wiley 2010.

[11] Kasi, S.: Error of number of radioactive disintegrations. Journal of Physical Science and Application 4 (3) (2014) 193-197.

[12] Rychlicki, S., and K. Umiastowski: Experimental verification of the universal calibration curve for gamma-gamma density logging. Nukleonika **15**(1970), 47

[13] Nargolwalla, S. S., and E. P. Przybylowicz: Activation analysis with neutron generators. John Wiley & Sons, 1973.

[14] Shyu, C. M., R. P. Gardner and K. Verghese: Developments of the Monte Carlo library least-squares method of analysis for neutron capture prompt gamma-ray analyzers. Nucl. Geophys. **7**(1993) 241-267.

[15] Tan, H., S. Mitra, A. Fallu-Labruyere, W. Hennig, Y. X. Chu, L. Wielopolsky and W. K. Warburton: A digital spectrometer approach to obtain multiple time-resolved gamma-ray spectra for pulsed spectroscopy. Nuclear Instruments and Methods in Physics Research **B 263**(2007) 63-66.

[16] Mitra, S. , L. Wielopolsky, H. Tan, A. Fallu-Labruyere, W. Hennig and W. K. Warburton: Concurrent measurement of individual gamma-ray spectra during and between fast neutron pulses. IEEE Transactions on Nuclear Science **54**(2007) 192-196.

[17] Hubbell, J. H., Wm. J. Veigele, E. A. Briggs, R. T. Brown, D. T. Cromer and R. J. Howerton: Atomic form factors, incoherent scattering functions, and photon scattering cross sections. Journal of Physical and Chemical Reference Data **4**(1975) 471-538.

[18] Ribberfors, R., and K-F. Berggren: Incoherent-x-ray-scattering functions and cross sections $(d\sigma/d\Omega')_{incoh}$ by means of a pocket calculator. Physical Review A **26**(1982) 3325-3333.

[19] Kasi, S. S. H.: (n,n)-, (n,γ)- ja (γ,n)-mittausten vasteen ja kohdekoon laskeminen (Calculation of the response and sample size in (n,n), (n,γ) or (γ,n) gauging). Arkhimedes **35**(1983) 142-148.

[20] Scot, V. and J. E. Fernandez: The Monte Carlo code MCSHAPE: Main features and recent developments. Spectrochimica Acta, part B: Atomic Spectroscopy **108** (2015) 53-60.

[21] Dunn, W. L., and R. P. Gardner: Development of mathematical models and the dual-gauge principle for surface-type neutron moisture content gauges. Nucl. Eng. Des. **32** (1975) 438-448.

[22] Gardner, R. P., and L. Liu: Monte Carlo simulation of neutron porosity oil well logging tools: combining the geometry-independent fine-mesh importance map and one-dimensional diffusion model approaches. Nucl. Sci. Eng. **133**(1999) 80-91.

[23] Kasi, S. S. H., and S. E. Pihlajavaara: An approximate solution of quasilinear diffusion problem; tables and nomograms for concentration in slabs in a special case. Valtion Teknillinen Tutkimuskeskus VTT, (1969) Publication 153.

[24] Fearon, R. E.: Neutron well logging. Nucleonics (1949, June) 30-42.

[25] Kasi,S.: Influence of rare earths on neutron moisture measuring. Nuclear Engineering and Design **8**, 317-320 (1968).

[26] Zheng, J., K. Tagami, Y. Watanabe, S. Uchida, T. Aono, N. Ishii, S. Yoshida, Y. Kubota, S. Fuma and S. Ihara: Isotopic evidence of plutonium release into the environment from the Fukushima DNPP accident. *Scientific Reports* **2**, Article number: 304 (2012), , https://www.nature.com/articles/srep00304#abstract

[27] Leppänen, A-P., A. Mattila, M. Kettunen and R. Kontro: Artificial radionuclides in surface air in Finland following the Fukushima Dai-ichi nuclear power plant accident. J. Environ. Radioact. **126**(2013), 273-283.

Servo Kasi's published texts:

I. Kasi, S., and H. Koskinen: Analysis, calculations and measurements concerning the moisture measuring by the neutron method. Nuclear Engineering and Design 3(1966), 74-82.
II. Kasi, Servo: Calculation of neutron flux in hydrogenous medium round a fast point source for application to moisture measurement by neutrons. The State Institute for Technical Research, Finland, Publication 99, Helsinki 1966.
III. Kasi, S. S. H.: An attempt to calculate correctly the region of influence in gauging moisture with neutrons. Int. J. Appl. Radiat. Isot. **33**(1982), 667-671.
IV. Kasi, S., J. Immonen and K. Saikku: Some considerations for soil moisture gauging with neutrons. Isotope and Radiation Techniques in Soil Physics and Irrigation Studies 1983, IAEA, 479-488.
V. Kasi, Servo: Spatial correlations of the soil quantities related with the neutron gage of soil moisture. Water in the Unsaturated Zone, NHP Report no. 15(1986), 113-118.
VI. Kasi, Servo S. H.: Soil water content more accurately by nuclear methods. XXI Nordic Hydrological Conference, 2000, NHP Report no. 46, 549-554.
VII. Kasi, S. S. H.: First radiocesium profile and snow cover mass measurements. Suomen Akatemian julkaisuja 5/1988, 101-105.
VIII. Kasi, S. S. H.: Cesium deposition in soil and its effects. Radiation Physics and Chemistry **61**(2001), 673–675.
IX. Kasi, Servo: Nondestructive determination of gamma-active nuclide profiles in soil. Nordic society for radiation protection, Proceedings of the NSFS XV conference in Ålesund Norway, May 2008, 104-107.

Text I

NUCLEAR ENGINEERING AND DESIGN 3 (1966) 74–82. NORTH-HOLLAND PUBLISHING COMP., AMSTERDAM

ANALYSIS, CALCULATIONS AND MEASUREMENTS CONCERNING THE MOISTURE MEASURING BY THE NEUTRON METHOD * **

S. KASI and H. KOSKINEN
Institute of Technical Physics, Institute of Technology, Otaniemi, Finland

Received 6 October 1965

This paper describes firstly a method of numerical analysis for the moisture measurement with neutrons, with special consideration of the effects of the dry density and the possible boron content of the material. Then a series of measurements performed by using an instrument including an additional iron reflector are rapported and the results analyzed. Finally some theoretical approaches of a more analytical nature are illustrated by applying simple physical models. Special attention is paid to the influence of a nonuniform distribution of moisture on the mathematical treatment.

Sections 2 and 3 are contributions of the first author, section 4 of the second author.

1. INTRODUCTION

The measurement of moisture with neutrons is based on the great neutron moderating power of hydrogen. The effect of the slowing-down upon the neutron densities in the vicinity of a point source of fast neutrons is twofold: the density of slow neutrons increases and the density of fast neutrons decreases. Therefore, by making observations on the spatial distributions of either slow or fast neutrons one can draw conclusions concerning the moisture in the medium. The measuring device consists of a point source of fast neutrons and a detector of slow or fast neutrons. A fast neutron detector is essentially a slow neutron detector surrounded by a block of paraffin or other hydrogenous material that converts the fast neutrons into thermal neutrons for the detection. So far, the neutron method has had its widest use in the measurement of the moisture of soil. Here two alternative arrangements have been employed. In the so-called depth measurement a probe including the source and a thermal detector is lowered into a hole in the soil, whereas in the surface measurement the instrument containing the source and the detector is placed in the vicinity of the surface of the medium to be investigated. The numerous publications rapporting on these measurements are collected in the reference lists of the articles [1] and [2]. In the moisture measurement of concrete slabs, walls, etc. the surface method is most easily applicable (see Pawlin and Spinks [3]), and two different alternatives can here be used. The surface measurement is called a reflection or a transmission experiment depending on whether the source and the detector are on the same side or on the opposite sides of the slab, respectively. The transmission method cannot always be used, but its advantage as compared with the reflection measurement lies generally in its insensitivity to nonuniformities in the spatial distribution of moisture. The reflected fast intensity is usually extremely small so that the fast reflection experiment can hardly be used. The fast transmission measurement, if it is in practice possible (and if the slab is not too thick), is instead very comfortable because it essentially constitutes a monoenergetic problem and thus quite elementary description of the neutron transport is sufficient to give a good agreement between theory and experiment. The measurements of the reflection and the transmission of the slow neutrons produced inside the hydrogenous slab are theoretically equivalent and their analysis is complicated because the whole slowing-down process must be described. On the other hand, the slow reflection principle is the easiest one for practical performance.

It is worth mentioning that as well the crystallized water as the loose water take part in the slowing-down of neutrons in concrete. Conse-

* Paper presented at RILEM/CIB Symposium, Moisture problems in buildings, at the State Institute for Technical Research, Otaniemi, Finland, September 1965.

** Accepted by A. Hönig.

quently, in comparison of the measurements on different walls one gets information concerning the total amount of water.

2. NUMERICAL ANALYSIS AND THE EFFECTS OF DRY DENSITY AND BORON

2.1. *The numerical method of computation*

The neutron sources most frequently used for these purposes are beryllium sources, and most of them the Ra-Be source despite its high gamma background. The Am-Be and Ac-Be sources are more advantageous in this respect, and their prices are of the same order as those of the Ra-Be source. In our calculations we have used the spectrum of the Ac-Be source [4] illustrated in fig. 2 including a peak at the energy of 0.1 MeV which contains 10% of all source neutrons, but the spectra of the other sources mentioned above are not very different.

The simple age-diffusion model proves to be unsatisfactory in the quantitative analysis of the neutron moisture measuring system when the moisture content exceeds 15% by volume, as is shown in the work by Westmeyer [5]. However, this method may be used, in the same way as the ray-theory described in section 4, for the qualitative investigation of some important effects, such as the influence of the composition and the density of the material. This has been done for instance by Semmler [2]. We have performed numerical calculations of the spatial neutron distributions for a model geometry consisting of a point source in an infinite medium. This situation is close to that of the depth measurement, but the tendencies shown by the results are probably common to all geometries. The code prepared for the computations [14] is based on a combination of the Monte Carlo technique with the method of Selengut and Goertzel. By using the Monte Carlo method [6] in this context it is possible to take into account the elastic and the very important inelastic scattering of neutrons by the atoms of heavy elements present in the material. The neutron events are followed by Monte Carlo until the neutron energy is below 0.75 MeV. The neutrons that have passed this energy value are divided further into two groups separated by the energy value 0.1 MeV. The lower group still contains the neutrons from the 0.1 MeV peak in the Ac-Be spectrum which have had three scattering events. Below the energy 0.75 MeV the diffusion of neutrons is described by a ninegroup diffusion approximation in the Selengut-Goertzel modification ([7], pp. 125–135). The width of the seven highest groups used is two lethargy units, the eighth group above 0.1 eV is a little shorter, and the thermal group consists of the neutrons below 0.1 eV. The two Monte Carlo groups serve as source terms for the two highest diffusion groups. The results of our computations are the spatial distributions of the epithermal flux ($E \approx 1.6$ eV) and the thermal flux. If we omit the errors near the origo introduced by certain oscillations in the calculations at very low moisture, a good agreement with experimental results is to be expected.

2.2. *The results of the computations*

The composition of our test material was: O 48%, MgAl 9%, Si 32%, KCa 5.4% and Fe 3.3% by weight. In the analysis the elements Mg and Al, and, respectively, K and Ca have been identified on the basis of the similarity of their neutron physical properties. The test values used for the density of this medium are 0.6 g/cm^3 and 2.0 g/cm^3, and those for the water content of 0%, 5%, 20% and 45% by volume.

As a result of the Monte Carlo calculation we present the function $4\pi r^2 S$, where S is the density of neutrons with an energy of 0.3 MeV, as a function of r, at different densities and water contents (fig. 1). The effect of the density upon

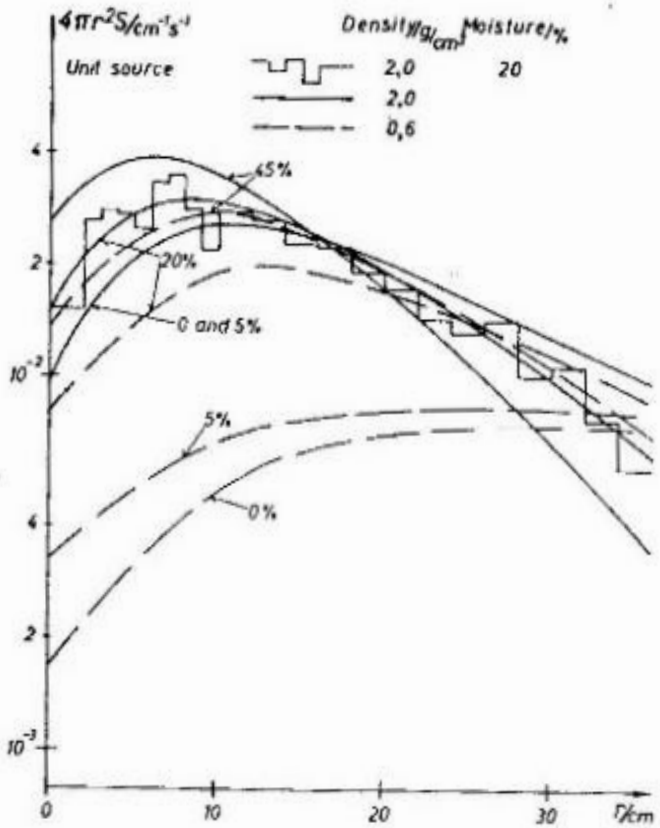

Fig. 1. Neutron distributions at energy 0.3 MeV.

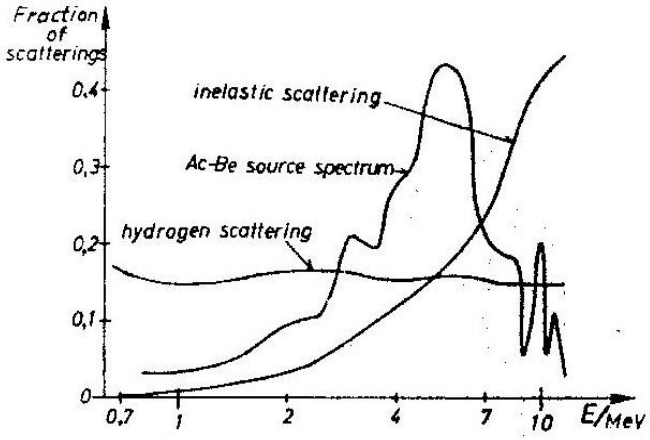

Fig. 2. Comparison of source spectrum at scatterings when density is 2.0 g/cm^3 and moisture 20%.

these results is remarkable. The difference between the density functions for dry material at 0.6 g/cm^3 and 2.0 g/cm^3 is a little greater than the difference between the curves at the water contents of 0% and 20% when the density is 0.6 g/cm^3. The reason for this effect is illustrated in fig. 2. Here the source spectrum and the relative probabilities for elastic scattering in hydrogen and inelastic scattering in the material are presented as functions of the energy. At the average source energy the probabilities for hydrogen and inelastic scattering are nearly equal, but even then the inelast.c scattering is dominating in the slowing-down of neutrons. This is due to the fact that the average energy loss per inelastic scattering is about 90% of the initial energy, as compared the corresponding number, 50% for the proton scattering. The hydrogen scattering dominates only below ca. 1 MeV. Hence we can conclude that the neutron energies of the usual sources are too high for an effective measurement. An ideal source is found not to exist, the most suitable spectrum is that of the Ra-γ-Be photoneutron source, which however has a very high gamma background. Other sources of possible use are the Po-Li source and the spontaneous fission sources.

It is apparent from the results of the multigroup calculations that, at a fixed moisture, the difference between the flux distributions corresponding to different dry densities is at the epithermal energy greater than at thermal energies. Therefore it is impossible to avoid the effect of the density by using epithermal detectors. The thermal flux Φ as a function of distance from the source is plotted in fig. 3. Fig. 4 shows the dependence of the thermal flux in the origo on the moisture at different dry densities of the material. In practice such curves that serve as calibration curves of the instrument

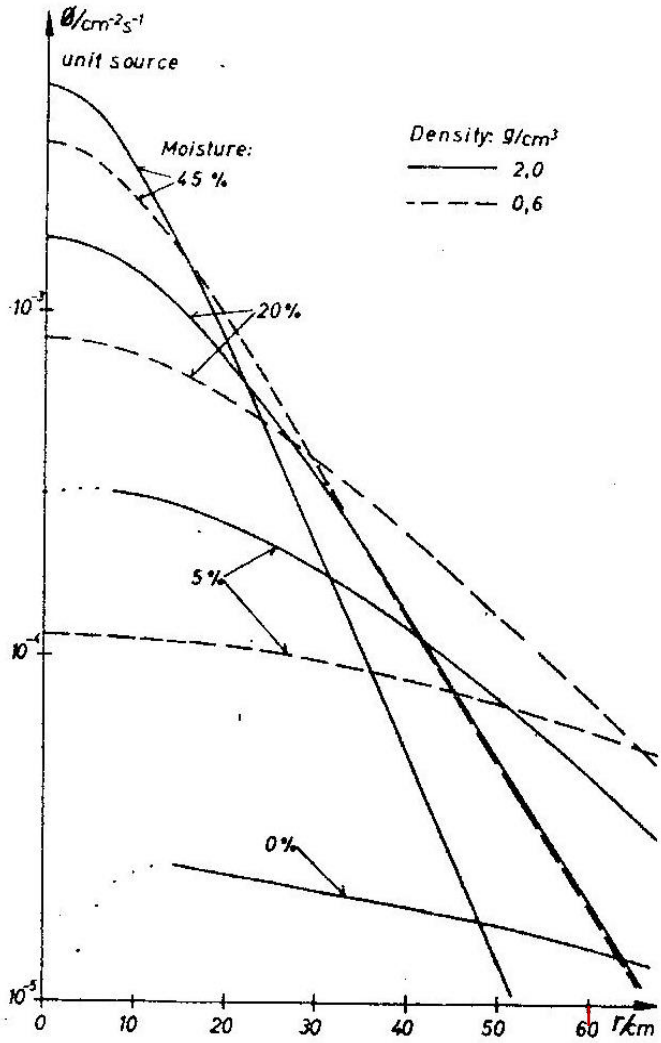

Fig. 3. Thermal flux.

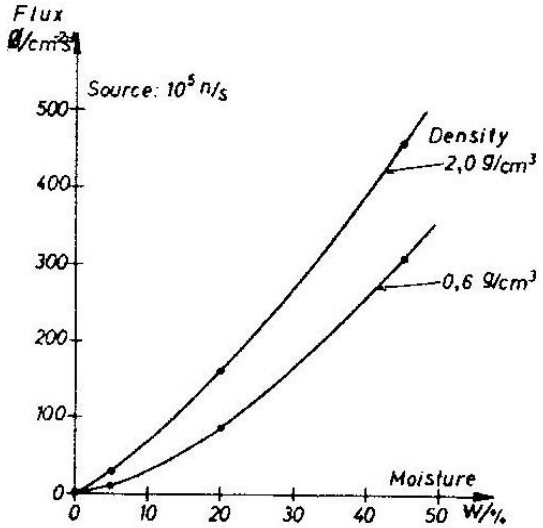

Fig. 4. Calibration curves at different densities.

are to be measured with samples of known composition and moisture. The strong dependence on dry density of the calibration curves has been observed experimentally by Unger and Claus [8].

The investigations concerning the influence of boron present in the material can be performed with the previous Monte Carlo results, because small amounts of this absorber change only the thermal cross sections remarkably. A multigroup calculation for the dry density of 2.0 g/cm^3 was carried out, and the influence of the additional absorber on the epithermal flux was found small as compared with the change in the thermal flux (fig. 5). For a moisture of 20% the relative changes per boron content in the thermal and epithermal fluxes in the origo were found to be 17.5%/0.005% and 0.5%/0.005%, respectively. Thus the effects of such additional absorbers as boron, cadmium etc. can be almost completely eliminated by the use of epithermal detectors like cadmium-covered BF_3-counters or cadmium-covered indium foils.

The numerical method of calculation rapported is applicable as well to other geometries, for instance to the reflection and transmission measurements on finite or semi-infinite slabs. It can also be modified so that computations for nonuniform distributions of moisture become possible.

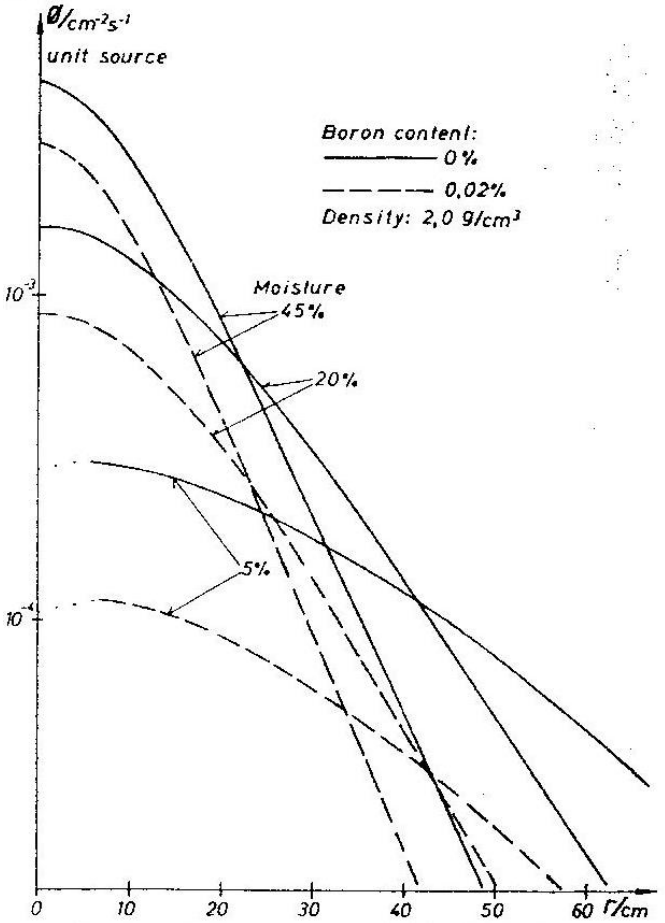

Fig. 5. Influence of boron on thermal fluxes.

3. MEASUREMENTS WITH AN IRON REFLECTOR AT THE BACK OF THE SOURCE

A series of measurements has been carried out to investigate the influence on the calibration curves of an additional iron reflector located behind the source. The arrangement is shown in fig. 6. The type of experiment was a surface measurement by Pawlin and Spinks [3] on a test material, which was fine sand of dry density 1.7 g/cm^3. The neutron source used was a Po-Be source of a strength of ~ 100 mC, and the detector was the BF_3-counter Philips ZP 1010 whose sensitivity is about 1 c/s per unit flux.

The resulting calibration curves obtained with and without the reflector are plotted in fig. 7. It is remarkable that the reflector does not raise the reading of the detector for dry material, but the sensitivity is considerably improved. This improvement is due to the reflection of inelas-

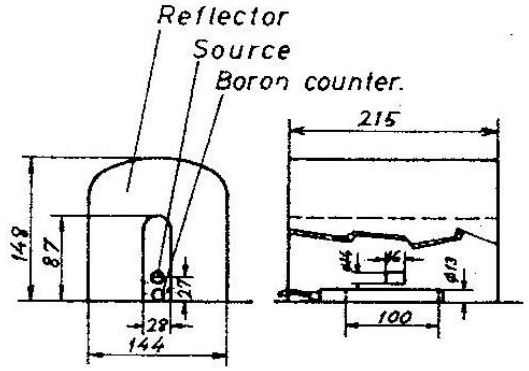

Fig. 6. Reflection measurement.

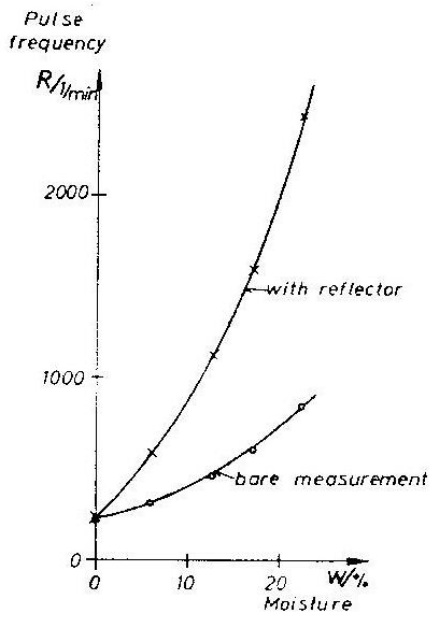

Fig. 7. Influence of reflector.

tically scattered neutrons from the iron, whereas the direction of motion of elastically scattered neutrons is mostly opposite. In the inelastic scattering the energy of the source neutrons decreases properly to the energies below 1 MeV so that they provide in the moisture measurement a better neutron source than the original source neutrons.

4. SOME MATHEMATICAL QUESTIONS OF THE ANALYSIS OF REFLECTION AND TRANSMISSION MEASUREMENTS ON SLABS

4.1. *The problem setting*

The aim of this section is to give a view on some basic ideas of the mathematical analysis of the reflection and transmission processes. The physical model subject to most of our considerations is diffusion theory for thermal neutrons and single-collision theory ("ray-theory") for fast neutrons. The ratio of the source term of thermal neutrons to the fast flux is assumed to be given by an effective cross section. This model is, of course, not totally justified in the analysis of the present problems, at least not when the moisture contert is low, but it is sufficient to give an insight into the main directions of a more complete analysis.

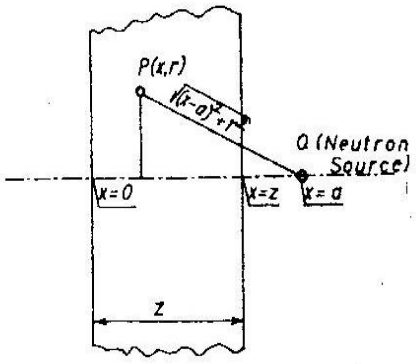

Fig. 8. The slab geometry.

We consider in a cylindrical system of coordinates a slab (fig. 8) extending from $x = 0$ to $x = z$, and to infinity in the radial direction. Suppose that a point source which emits isotropically Q_0 fast neutrons (energy E_0) per second is located in the point $x = a$, $r = 0$. We include all the possibilities $a > z$, $a = z$ or $a < z$. The slab is allowed to be stratified in the x direction in the sense that the content of hydrogen atoms per unit volume $N = N(x)$ is an arbitrary well-behaved function. Other atoms whose scattering and absorbing properties are accounted for are assumed to be space-independently distributed in the slab.

In general, the result of every measurement in the stationary case is a linear functional of the space, energy and direction dependent scalar flux $\varphi(r, E, \Omega)$, which is the solution of the energy dependent Boltzmann equation [9] under appropriate boundary and source conditions. Specifically, if the effects subject to our observations are the reflection from the face $x = z$ and the transmission through the face $x = 0$ of neutrons with different energies and directions of motion, the functional is of the form

$$I = \int_{E_{\text{th}}}^{E_0} \mathrm{d}E \int_{n\cdot\Omega>0} n\cdot\Omega \,\mathrm{d}\Omega \int_{x=0,\,x=z} f(s,E,\Omega)\,\varphi(s,E,\Omega)\,\mathrm{d}s\,, \qquad (1)$$

where the position vector r is denoted by s when lying on one of the surfaces and $\mathrm{d}s$ is the surface element. The vector n is the normal pointing outwards from the face under question. The function $f = f(s, E, \Omega)$ is an effectiveness function determined by the detector used. For instance, if we could select the neutrons from the infinitesimal energy interval $(E', E' + \mathrm{d}E)$ which are reflected from the surface element $\mathrm{d}s$ around s' into the infinitesimal solid angle $\mathrm{d}\Omega$ around the direction Ω', the effectiveness would be the delta function $f = \delta(s, s')\delta(E - E')\delta(\Omega, \Omega')$. For other types of functionals associated with this problem of measurement, see ref. [10].

Following observations may be directly made concerning the evaluation of the functional in eq. (1), independently of the physical model used. If the solution of the linear Boltzmann equation or its approximation for the whole volume of the slab, $\varphi(r, E, \Omega)$, is found, then (1) is easily obtained by substituting specifically $r = s$. There exists, however, an alternative basing on the fact that the whole solution $\varphi(r, E, \Omega)$ is actually not needed. The surface function is directly found in the method of invariant imbedding [9], in which the particular slab of thickness z is looked at as an element in the class of slabs of different thicknesses $z \geq 0$. In this technique, which is very useful in the description of stratified media, nonlinear initial value equations of Riccati type result for the reflection and transmission functions defined below in a special model. Furthermore, from the point of view of numerical computations the advantage of the reduction to initial value problems of boundary value prob-

lems wholly compensates the resulting non-linearity.

The boundary function $\varphi(s, E, \Omega)$ naturally depends on the coefficients of the Boltzmann equation or, in the other formulation, of the equations of invariant imbedding. Because we keep the other functions as well as the boundary and source conditions fixed but think of different hydrogen densities $N(x)$ this function must be added to the factors determining φ, or $\varphi = \varphi(s, E, \Omega; N(x))$. Let T denote the generally non-linear operator that carries $N(x)$ into the function $\varphi = \varphi(s, E, \Omega)$ defined in the proper phase space. If the functional of eq. (1) is written in the usual scalar product notation $I = [f, \varphi]$ and we wish to determine the change (variation) δI of I due to a little change $\delta N(x)$ of $N(x)$, we obtain for $\varphi = T(N(x))$:

$$\delta I = [f, \delta\varphi] = [f, \delta T(N(x))] = [f, T'(N(x))\delta N(x)], \quad (2)$$

where $T'(N(x))$ is the Fréchet derivative

$$T'(N(x)) = \lim_{|\delta N(x)| \to 0} \frac{T(N(x) + \delta N(x)) - T(N(x))}{\delta N(x)} . \quad (3)$$

Note that the two first forms in eq. (2) are exact because of the linearity of I as a functional of φ, whereas for the last expression the requirement $|\delta N(x)| \ll |N(x)|$ must be fulfilled. Eq. (2) has very important applications, arising from the fact that in general the derivative $T'(N(x))$ is more easily formed than T itself. A usual principle of perturbation theory consists of the following. Suppose that the neutron balance equations cannot be analytically solved for φ with a particular $N(x)$. It is, however, often possible to find a comparison function $N_0(x)$ that yields an analytical solution and from which $N(x)$ deviates only slightly. (The simplest case is that $N(x)$ deviates little from a constant.) Then, by using eq. (2) the functional $I = I_0 + \delta I$ pertinent to $N(x)$ can be evaluated. Another application is that N may depend on a real parameter, time, but let the variation be so slow that the stationary neutron equations can be used. This is the case for drying of a concrete slab. For $N = N(x; t)$, $dN = (\partial N(x; t)/\partial t)dt$ we obtain

$$\frac{dI}{dt} = \left[f, \frac{d\varphi}{dt}\right] = \left[f, T'(N(x; t)) \frac{\partial N(x; t)}{\partial t}\right] . \quad (4)$$

Thus, by making observations on dI/dt an experimental relation between $T'(N(x))$ and $\partial N/\partial t$ is established. This may be used in either directions depending on whether scattering of neutrons or drying of concrete is concerned. It is most interesting to note how the partial derivative in eq. (4) can be further transformed by using the diffusion equation for the moisture [11] itself.

4.2. *Use of linear equations in the diffusion approximation*

It is assumed that in the description of the neutron balance for the slab of fig. 8 the complete Boltzmann equation mentioned in our introductory chapter may be replaced by the diffusion equation

$$L\Phi \equiv -\nabla \cdot D(x)\nabla\Phi(x, r) + \Sigma_a(x)\Phi(x, r) = q(x, r), \quad (5)$$

where the thermal flux $\Phi = \Phi(x, r)$ is obtained from the scalar flux $\varphi(r, E, \Omega)$ by an integration over all directions of motion Ω and over the lowest, thermal part of the energy spectrum. Thus Φ depends only on the space coordinates x and r, if cylindrical symmetry is further assumed. The diffusion coefficient $D(x)$ is given by one third of the inverse transport cross section

$$D(x) = \frac{1}{3\Sigma_t(x)} ,$$

where

$$\Sigma_t(x) = \Sigma_{t0} + N(x)\sigma_t ,$$

and Σ_{t0}, σ_t are given constants. Likewise, $\Sigma_a(x) = \Sigma_{a0} + N(x)\sigma_a$, where Σ_{a0} and σ_a are given. The source term for thermal neutrons $q(x, r)$ is, as given by the ray theory of fast neutrons combined with the concept of removal cross section (see fig. 8):

$$q(x, r) = \frac{\Sigma_r(x) Q_0}{4\pi[(x - a)^2 + r^2]} \exp\left[-\frac{(x - a)^2 + r^2}{|x - a|} \int_{\min(z, a)}^{x} \Sigma_r(x')\, dx'\right] , \quad (6)$$

where the removal cross-section $\Sigma_r(x)$ is given by $\Sigma_r(x) = \Sigma_{r0} + N(x)\sigma_r$, and the constants Σ_{r0} and σ_r are supposed to be known. By $\min(z, a)$ we denote the smaller one of the quantities. The result (6) is formally one from the single-collision transport theory, but with respect to the production of thermal neutrons it is a highly artificial model that must be fitted to the experiments. It should be noted, however, as was mentioned in section 1, that in fast transmission measurements the transmitted fast intensity at distance r from the symmetry axis is in this approximation given by a geometrical factor times $\exp(-\int_z^0 N(x)\, dx)$ which yields the integrated moisture directly. If the source is moved along the axis of symmetry within the slab (lower limit

of the integral variable), there are possibilities for detailed determination of $N(x)$. In what follows only the thermal reflection experiment will be considered.

In the reflection experiment we assume that the functional of eq. (1) which gives the result of a single measurement depends only on the thermal flux (use of diffusion theory already implies independence on the direction of motion of neutrons) and is given by

$$I = \int_0^\infty f(r)\, J_{out}(z,r)\, 2\pi r\, dr$$

$$= \int_0^\infty f(r)\, [\tfrac{1}{4}\Phi(z,r) - \tfrac{1}{2}D(z)\Phi_x(z,r)]\, 2\pi r\, dr\,, \quad (7)$$

where $f(r)$ is the effectiveness "function" (also distributions allowed). The expression for the outgoing current J_{out} is one from the diffusion approximation. The functional of eq. (7) can be expressed by the use of the Parseval theorem for Hankel transforms also as follows:

$$I = 2\pi \int_0^\infty h\tilde{f}(h)\, \tilde{J}_{out}(z,h)\, dh\,, \quad (8)$$

where $\tilde{f}(h)$ and $\tilde{J}_{out}(z,h)$ denote the Hankel transforms

$$\tilde{f}(h) = \int_0^\infty J_0(hr)\, f(r)\, r\, dr\,,$$

$$\tilde{J}_{out}(z,h) = \int_0^\infty J_0(hr)\, J_{out}(z,r)\, r\, dr \quad (9)$$

($J_0(x)$ is the Bessel function of first kind and zero order). Eq. (8) gives a linear functional in the space of transformed functions. Two special cases resulting from the choice $f_1(r) = 1$ or $f_2(r) = \delta(r - r_0)/r_0$, respectively, yield $I_1 = 2\pi\tilde{J}_{out}(z,0)$ and $I_2 = 2\pi \int_0^\infty J_0(r_0 h)\tilde{J}_{out}(z,h)h\,dh$. To evaluate of eq. (8) we must solve eq. (5) under the boundary conditions of diffusion theory

$$J_{in}(0,r) = \tfrac{1}{4}\Phi(0,r) - \tfrac{1}{2}D(0)\Phi_x(0,r) = 0\,,$$
$$J_{in}(z,r) = \tfrac{1}{4}\Phi(z,r) + \tfrac{1}{2}D(z)\Phi_x(z,r) = 0\,, \quad (10)$$

which state zero ingoing thermal current from both faces. The next step consists of the reduction of eq. (5) with the boundary conditions (10) to a one-dimensional problem via the Hankel transform. The result is

$$-\frac{d}{dx}D(x)\frac{d\tilde{\Phi}(x,h)}{dx} + (\Sigma_a(x) + D(x)h^2)\tilde{\Phi}(x,h) = \tilde{q}(x,h) \quad (11)$$

with the associated transformed forms of eqs. (10). The Hankel transforms included in the previous equation have been defined analogously to eq. (9). We do not perform the transformation of q but assume that it is possible at least approximately. The solution of eq. (11) that satisfies the boundary conditions can be expressed in a standard manner

$$\tilde{\Phi}(x,h) = \int_0^z G_h(x,x')\, \tilde{q}(x',h)\, dx' \quad (12)$$

by using the Green's function $G_h(x,x')$ that satisfies

$$-\frac{d}{dx}D(x)\frac{dG_h(x,x')}{dx} + (\Sigma_a(x) + D(x)h^2)\, G_h(x,x') = \delta(x - x')\,, \quad (13a)$$

$$\tfrac{1}{4}G_h(0,x') - \tfrac{1}{2}D(0)\frac{dG_h}{dx}(0,x') = 0 \quad \text{for all } x'\,, \quad (13b)$$

$$\tfrac{1}{4}G_h(z,x') + \tfrac{1}{2}D(z)\frac{dG_h}{dx}(z,x') = 0 \quad \text{for all } x'\,. \quad (13c)$$

However, for our purposes we do not need $G_h(x,x')$ for all values of x. The reason for this is that the transformed outgoing (reflected) current $\tilde{J}_{out}(z,h)$ in the integral (8) is obtained as

$$\tilde{J}_{out}(z,h) = \tfrac{1}{4}\tilde{\Phi}(z,h) - \tfrac{1}{2}D(z)\tilde{\Phi}_x(z,h)$$
$$= \tfrac{1}{2}\int_0^z G_h(z,x')\, \tilde{q}(x',h)\, dx' \quad (14)$$

on the strength of eq. (12) and the transformed eqs. (10). Consequently the Green's function is actually needed only for $x = z$. Because the differential operator acting on $\tilde{\Phi}$ in eq. (11) is self-adjoint in the manifold defined by the transformed eqs. (10) the Green's function is symmetric in its arguments i.e. $G_h(z,x') = G_h(x',z)$. We must accordingly solve eq. (13) in the special case $x' = z$ and in the solution substitute x' for x. This problem proves to be identical with the solution of the following homogeneous equation with boundary conditions inhomogeneous at one end of the interval:

$$-\frac{d}{dx}D(x)\frac{dG_h(x,z)}{dx} + (\Sigma_a(x) + h^2)G_h(x,z) = 0\,,$$

$$\tfrac{1}{4}G_h(0,z) - \tfrac{1}{2}D(0)\frac{dG_h}{dx}(0,z) = 0\,, \quad (15)$$

$$\tfrac{1}{4}G_h(z,z) + \tfrac{1}{2}D(z)\frac{dG_h}{dx}(z-\epsilon,z) = 1\,.$$

Actually the second parameter z can be dropped out of the previous equations. For instance if the diffusion constant and the absorption cross section are space-independent the solution is easily

obtained. From the definitions of the cross sections introduced in eq. (5) we get:

$$\delta\Sigma_a(x) = \sigma_a \delta N(x) , \qquad \delta D(x) = -\frac{1}{3}\frac{\sigma_t}{\Sigma_t^2}\delta N(x) ,$$

$$\delta\Sigma_r(x) = \sigma_r \delta N(x)$$

as the small changes introduced in these functions by the little change $\delta N(x)$. If the operator in the first of eqs. (15) is denoted by L_{oh} and its change due to $\delta N(x)$ by δL_h

$$L_{oh} = -\frac{d}{dx} D_o(x) \frac{d}{dx} + \Sigma_{ao}(x) + D_o(x)h^2 ,$$
$$\delta L_h = -\frac{d}{dx} \delta D(x) \frac{d}{dx} + \delta\Sigma_a(x) + \delta D(x)h^2 , \tag{16}$$

but we restrict ourselves to variations $\delta D(0) = \delta D(z) = 0$ in order to remain in the same manifold of solutions, it follows from the condition $(L_{oh} + \delta L_h)(G_h + \delta G_h) = 0$ that $\delta G_h = -(G_h, \delta L_h G_h)$ when using the ordinary scalar product notation. If the variation $\delta\tilde{q}(x,h)$ is directly evaluated, we finally obtain the variation δI of eq. (8) as follows

$$\delta I \approx 2\pi \int_0^\infty h\tilde{f}(h) \tfrac{1}{2} \int_0^z [\delta G_h(x',z)\tilde{q}(x',h) + G_h(x',z)\delta\tilde{q}(x',h)]\, dx'\, dh , \tag{17}$$

where the expressions given above are to be substituted. This is a special case of eq. (2).

4.3. *Formulation of the problem via invariant imbedding*

In order to present new equations for the calculation of the transformed Green's function $G_h(x;z)$ of eq. (15) (the parameter z is here of special importance) we introduce the notations

$$u_h(x;z) = \tfrac{1}{4}G_h(x;z) - \tfrac{1}{2}D(x)\frac{dG_h(x;z)}{dx}$$

(right-going transformed current)

$$v_h(x;z) = \tfrac{1}{4}G_h(x;z) + \tfrac{1}{2}D(x)\frac{dG_h(x;z)}{dx}$$

(left-going transformed current)

so that the boundary conditions become $u_h(0;z) = 0$, $v_h(z;z) = 1$. The reduction of the first of eqs. (15) to a first-order system

$$\frac{du_h(x;z)}{dx} = -\left(\frac{1}{4D} + \tfrac{1}{2}\Sigma_a + \tfrac{1}{2}D(x)h^2\right) u_h(x;z) + \left(\frac{1}{4D} - \tfrac{1}{2}\Sigma_a - \tfrac{1}{2}D(x)h^2\right) v_h(x;z) , \tag{18a}$$

$$-\frac{dv_h(x;z)}{dx} = \left(\frac{1}{4D} - \tfrac{1}{2}\Sigma_a - \tfrac{1}{2}D(x)h^2\right) u_h(x;z) - \left(\frac{1}{4D} + \tfrac{1}{2}\Sigma_a + \tfrac{1}{2}D(x)h^2\right) v_h(x;z) \tag{18b}$$

subjected to the above conditions is quite classical and provides no difficulties. Of importance in the following are the coefficient functions which are here denoted by

$$a_h(x) = -\left(\frac{1}{4D(x)} + \tfrac{1}{2}\Sigma_a(x) + \tfrac{1}{2}D(x)h^2\right) ,$$
$$b_h(x) = \left(\frac{1}{4D(x)} - \tfrac{1}{2}\Sigma_a(x) - \tfrac{1}{2}D(x)h^2\right) . \tag{19}$$

They enter into the following Riccati equations for the reflection function $r_h(z) = u_h(z;z)/v_h(z;z) = u_h(z;z)$ and the transmission function $t_h(z) = v_h(0;z)/v_h(z;z) = v_h(0;z)$ as functions of the slab thickness z:

$$r_h'(z) = b_h(z) + 2a_h(z)r_h(z) + b_h(z)r_h^2(z) , \qquad r_h(0) = 0 ,$$
$$t_h'(z) = a_h(z)t_h(z) + b_h(z)r_h(z)t_h(z) , \qquad t_h(0) = 1 . \tag{20}$$

As concerns the derivation of these formulae we must refer to the literature [9]. Use is made of the so-called Hadamard variational formula which gives the dependence of Green's functions on variations of the boundary (here thickness z).

For the case of a moisture distribution symmetrical with respect to $x = \frac{1}{2}z$ (whence reflection functions are independent of direction) it can be shown [9] that our Green's function is expressed in terms of the solutions of eqs. (20) as

$$G_h(x,z) = \frac{t_h(x)[1 + r_h(z-x)]}{1 - r_h(x)r_h(z-x)} . \tag{21}$$

In the case of a semi-infinite slab all formulae are considerably simplified. With the aid of the eqs. (20) the following formulae may be obtained for the variations $\delta r_h(z)$ and $\delta t_h(z)$ of the reflection and transmission functions, caused by the variations $\delta a_h(z)$ and $\delta b_h(z)$ which again are due to the variation $\delta N(z)$:

$$\delta r_h'(z) = \delta b_h(z) + 2\delta a_h(z)r_h(z) + \delta b_h(z)r_h^2(z) + [2a_h(z) + 2b_h(z)r_h(z)]\,\delta r_h(z) .$$
$$\delta t_h'(z) = \delta a_h(z)t_h(z) + \delta b_h(z)r_h(z)t_h(z) + [a_h(z) + b_h(z)r_h(z)]\,\delta t_h(z) + b_h(z)t_h(z)\delta r_h(z) , \tag{22}$$

when small terms of the second order have been

dropped. These are linear equations for the variations sought and are more easily solvable than the complete eq. (20). Hence we can connect the variation of the hydrogen density $N(x)$ to the variations of the reflection and transmission functions, further to the variation of the Green's function (21), and finally to the variation δI of the functional (8). The generalization of the method of invariant imbedding to various formulations of the neutron transport theory is straight-forward.

4.4. *Remarks and conclusions*

One reason for the application of the physically unsatisfactory diffusion theory in this context was that the underlying methods, specifically that of invariant imbedding, prove certainly useful in the mathematical description of the diffusion of the moisture itself, in heat conduction etc. Many problems of space, time or concentration dependent diffusion coefficients etc. included in the reference [11] by Crank or [12, appendix 7] by Pihlajavaara may find their solutions by this method.

Very illustrative curves and tables which for various cases give the distribution of energy and direction of motion for neutrons reflected from a semi-infinite water medium, are found in our last reference [13].

REFERENCES

[1] R. Sweeney, Measurement of soil moisture and density by nuclear method, AERE-Bib 140 (1962).
[2] R. S. Semmler, Neutron-moderation moisture meters, analysis of applications to coal and soil, COO-712-73 (1963).
[3] J. Pawlin and J. W. T. Spinks, Neutron moisture meter for concrete, Can. J. Technol. 34 (1957) 503.
[4] W. R. Dixon, Alice Bielesch and K. W. Geiger, Neutron spectrum of an actinium–beryllium source, Can. J. Phys. 35 (1957) 699.
[5] H. Westmeyer, Uber Feuchtigkeitsmessung vermittels Neutronen, Kernenergie 6 (1963) 6.
[6] A practical manual on the Monte Carlo method for random walk problems, LA-2120, Los Alamos Scientific Laboratory (1957).
[7] W. C. Sangren, Digital computers and nuclear reactor calculations (Wiley and Sons, New York, 1960).
[8] K. Unger and St. Claus, Einfluss der Bodendichte auf radiometrische Feuchtigkeitsmessungen, Kernenergie 7 (1964) 567.
[9] G. M. Wing, An introduction to transport theory (Wiley and Sons, New York, 1962).
[10] G. I. Marchuk and V. V. Orlov, K teorii sopriazhennykh funktsii, in: Neitronnaia fizika, P. A. Krupchitsko, ed. (Moscow, 1961) p. 30.
[11] J. Crank, The mathematics of diffusion (Clarendon Press, Oxford, 1957).
[12] S. E. Pihlajavaara, Johdatus betonin kuivumisilmiöön, Valtion teknillinen tutkimuslaitos, Betoniteknillinen laboratorio, Helsinki (1964).
[13] M. J. Berger and J. W. Cooper, Reflection of fast neutrons from water, J. Res. Natl. Bur. Stand. 63A (1959) 101.
[14] S. Kasi, Calculation of neutron flux in hydrogenous medium round a fast point source for application to moisture measurement by neutrons. Will be published in these days in the series Acta Polytechnica Scandinavica.

Text II

UDC 539.125.5:543.712
620.171.33

VALTION TEKNILLINEN TUTKIMUSLAITOS
STATENS TEKNISKA FORSKNINGSANSTALT
THE STATE INSTITUTE FOR TECHNICAL RESEARCH, FINLAND

JULKAISU 99 PUBLICATION

CALCULATION OF NEUTRON FLUX IN HYDROGENOUS MEDIUM ROUND A FAST POINT SOURCE FOR APPLICATION TO MOISTURE MEASUREMENT BY NEUTRONS

SERVO KASI

HELSINKI 1966

VTT ROTAPRINTPAINO 1966
321/8

ABSTRACT

In this article, there is presented a semiapproximate method of calculating the thermal neutron flux around a point source of fast neutrons in an infinite hydrogenous medium. The calculations are based on the use of an Ac-Be source as the neutron emitter. At energies above 0.75 MeV, the Monte Carlo method is utilized, but below this limit the use of the nine-group Selengut-Goertzel modification of the age-diffusion approximation is satisfactory.

This method of computation has been developed for application in investigations of the neutron moisture device.

CONTENTS

1. GENERAL CONSIDERATIONS

The problem studied in this paper is that of finding the flux distribution of thermal neutrons when there is a point source of fast neutrons in an infinite hydrogenous medium.

Accurate treatment of slowing down in moderators which contain hydrogen is difficult, in view of the inapplicability of the age approximation of the transport equation. The latter is the basic equation in neutron transport; it is presented in the neutron physical literature, for instance in reference [10, p. 84]. In a hydrogen collision, the average change of lethargy is

$$\xi = \overline{\Delta u} = \overline{\ln \frac{E_1}{E_2}} = 1, \tag{1}$$

which is large in comparison with the corresponding value for scattering from a heavy element, where approximately

$$\xi \approx \frac{2}{A + \frac{2}{3}}. \tag{2}$$

E_1 and E_2 are the neutron energies before and after scattering, and A is the atomic mass number. As the lethargy changes are small, with a moderator of heavy elements use can be made of a continuous slowing down model, the basis of the age approximation. Nevertheless, in the treatment proper of hydrogen moderation application is necessary of more elaborate approximations of the transport equation, such as the method of moments, P_N- or B_N-approximations, or other methods, or the Monte Carlo techniques can be used.

Since the total macroscopic cross section of hydrogen is small at large energies, fast neutrons travel, on the average, long distances before being slowed down, but are then thermalized in relatively short distances. This is why a more exact treatment of very fast neutrons is needed. In this work, the Monte Carlo method was applied, and consideration was given to all possible neutron events, viz. absorption, elastic and inelastic scattering. In addition, account has been taken of the anisotropy of elastic scattering from heavy elements. Errors involved in the neutron physical data are the sole reason for inaccuracy of the Monte Carlo method if sufficient neutron histories have been calculated. After application of the Monte Carlo method, a multigroup Selengut-Goertzel modification of the age-diffusion

approximation is used, in which the Monte Carlo results act as source terms in the higher energy groups. The Selengut-Goertzel modification in this method eliminates some weaknesses of the age approximation arising from the presence of hydrogen.

Most neutron sources are made of some α-emitting material and beryllium. Their neutron spectra lie between 0.5 and 12 MeV, and the mean energy is about 4.5 MeV. Some, such as Ra-Be and Ac-Be (used in this work), probably have a peak at 100 keV [1] also.

2. MONTE CARLO CALCULATION

In the calculations, a random number generator gave evenly distributed numbers between 0 and 1 when required. Let us suppose that we have a distribution with the density function

$$p = p(x), \qquad a \leq x \leq b, \tag{3}$$

and the problem is that of choosing x at random according to this distribution. A random number R is selected, and then value x is found as the solution of the equation

$$R = F(x) = \int_a^x p(x)\,dx. \tag{4}$$

Three methods of solution have been employed in this work:

A. Direct integration of equation (4).

B. Discrete numbers p_i have been determined along $p(x)$ at points x_i at intervals Δx_i, and a numerical integration has been performed to find x_i corresponding to R. The original density function can also be piecewise constant.

C. If the analytical form of $p(x)$ is known, the method of von Neumann [2, p. 23] can be applied. Function y has been formed such that

$$y = p(x)/\max p(x), \tag{5}$$

$$a \leq x \leq b, \qquad 0 \leq y \leq 1.$$

Two random numbers R' and R" are selected, and the computation made:

$$\zeta = (b-a)R' + a, \tag{6}$$

and $y = y(\zeta)$. Now, if $R'' < y$, $x = \zeta$; otherwise the process is repeated for new values of R' and R".

In the programme, a neutron is followed from the source until its energy is less than 0.75 MeV, or for three collisions if it started with an energy of 100 keV. During processing, the following quantities are computed:

E	neutron energy
g	energy group
r	distance from the source
$\omega = \cos\vartheta$	cosine of the directional angle of the neutron with respect to the radius vector

ν number of collisions

W probability of no absorption in collisions occurring previously

Five energy groups were chosen between 11.75 and 0.75 MeV, and one below 100 keV. At the source, W = 1, which diminishes after every collision if absorption is possible.

Macroscopic cross sections for various elements in the different energy groups have previously been computed [3, 4, 5 and 6]. The cross sections for both elastic and inelastic scattering, and absorption are required.

The initial energy of a neutron was determined from formula (4) by method B. For neutron collision distance, there can be obtained direct from (4), by method A, [2, pp. 49 ··· 51]

$$\lambda = \frac{1}{\mu_t} \ln R, \tag{7}$$

where μ_t is the total macroscopic cross section. The values of r' and ω' for the new collision point are easily calculable from λ and the values of r and ω at the previous collision point. After collision,

$$W' = (1 - \mu_a/\mu_t)\, W, \tag{8}$$

where μ_a is the macroscopic absorption cross section.

The random number routine selects, by method B, an element which scatters either elastically or inelastically. In the elastic scattering with heavy elements the cosine of the scattering angle, $\delta = \cos\theta$, has been divided into 6 intervals. The probabilities for each interval were determined from the data of references [7, 8]. The program selects at random, by method B, a mean value δ_i in some interval. The new energy, after collision with a heavy element, is [2, p. 97]

$$E' = E(S + T\delta_i), \tag{9}$$

were

$$\begin{cases} S = 1/2\,(1 + \alpha) \\ T = 1/2\,(1 - \alpha) \\ \alpha = \left(\dfrac{A-1}{A+1}\right)^2. \end{cases}$$

In hydrogen, the scattering can be calculated from the formulae [2, p. 98]

$$\begin{cases} \delta = \sqrt{R} \\ E' = ER. \end{cases} \tag{10}$$

For inelastic scattering, method C was applied. The energy E' of an inelastically scattered neutron is assumed according to Weisskopf [9] to have a Maxwell distribution, where

$$p(E,E')\,dE' = KE'\,\exp\left(-\sqrt{\frac{a}{E}}\,E'\right)dE', \tag{10'}$$

in which $p(E,E')$ is the density function and the energies as above, K is a normalizing constant and a is an experimentally determined constant a little dependent on the atomic mass unit [9]. Theoretically equation (10') is applicable when energy levels are dense, but Bjorklund [9] has pointed out experimentally that it applies by many elements as E is so low as 1,5 MeV. On the ground of this all inelastic scattering is dealt with (10'). Function (5), when $x = E'$, becomes

$$y = E'\sqrt{\frac{a}{E}}\,\exp\left(-\sqrt{\frac{a}{E}}\,E' + 1\right), \tag{11}$$

$$0 \leq E' \leq E.$$

Since inelastic scattering is isotropic, then [2, pp. 101 ··· 102]

$$\delta = 2R - 1. \tag{12}$$

In addition to ω before collision and δ, there is needed a cylindrically symmetric angle $\varphi = \pi R$ for calculation of the cosine of the directional angle after collision [2, p. 163]

$$\omega' = -\sqrt{1-\delta^2}\,\cos\varphi\sqrt{1-\omega^2} + \delta\omega. \tag{13}$$

At the end of any neutron history, the resulting values of E, r and W have been reformulated for storage in the memory. Thus, if the final energy is between 0.75 and 0.1 MeV, the result is considered to belong to the first energy category, but if it is below 0.1 MeV, the result falls in the second one. The distance from the origin between 0 and 117 cm has been divided into 44 intervals, which increase in size as the distance grows. Thus there are 45 spherical shells around the source, (the 45th being between 117 cm and infinity), as spatial categories in each energy category. The resulting value for distance r gives the final category, in which the number W is added to the sum of the earlier W numbers in this category. At the end of all computation, the sum number in any category is divided by the total number of computed neutron histories, and by the volume of the corresponding spherical shell. The computation gives as result the spatial neutron distribution in two energy groups. During the calculation, the collision number was also stored for determination of the mean collision number, except when the source energy was 100 keV.

The number of computed neutron histories in this work was about 1000, so that the accuracy of the neutron count in any category was no higher than 10 %. This was because the computer was slow, and the operating time was restricted. To ensure a sufficiently close degree of accuracy more than 10 000 neutron histories would need computation.

3. MULTIGROUP DIFFUSION CALCULATION

From reference [10, p. 157], the slowing down density for heavy elements is given by

$$q(\vec{r},u) = \left(\sum_{k\neq H} \xi_k \mu_{sk}\right) \Phi(\vec{r},u), \tag{14}$$

where μ_{sk} is the scattering cross section of the k'th heavy element, and $\Phi(\vec{r},u)$ the neutron flux. This formula (14) includes the age approximation. The slowing down density for hydrogen is exactly

$$h(\vec{r},u) = \int_0^u \mu_{sH}(u')\,\Phi(\vec{r},u')\,e^{-(u-u')}\,du', \tag{15}$$

where μ_{sH} is the scattering cross section of hydrogen. By the application of these slowing down densities, there is in the Selengut-Goertzel age-diffusion approximation the equation [11, p. 125; 10, p. 157]

$$-D(u)\nabla^2\Phi(\vec{r},u) + \mu_a(u)\,\Phi(\vec{r},u) = -\frac{\partial}{\partial u}q(\vec{r},u) - \frac{\partial}{\partial u}h(\vec{r},u) + S(\vec{r},u), \tag{16}$$

where

$$D(u) = \frac{1}{3\mu_{tr}(u)}, \tag{17}$$

and $S(\vec{r},u)$ is the source term. $\mu_{tr}(u)$ is the macroscopic transport cross section.

The energy interval 0.75 MeV ··· 0.1 eV was divided into 8 lethargy groups (g = 0, 1, 2, ..., 7). Integration of equation (16) over lethargy interval Δu_g yields [11]

$$(-\bar{D}^g\nabla^2\bar{\Phi}^g + \bar{\mu}_a^g\bar{\Phi}^g)\Delta u_g = q^g - q^{g+1} + h^g - h^{g+1} + \bar{S}^g\Delta u_g. \tag{18}$$

An upper bar and the supercript g denote an average value of the relevant quantity in the interval $\Delta u_g = u_{g+1} - u_g$. The supercript g, alone, denotes a value for a quantity at lethargy u_g. In the derivation of equation (18), the mean of a product has been replaced by the product of the means. Differentiating (15), there is found

$$\frac{\partial h}{\partial u} = \mu_{sH}\Phi - h, \tag{19}$$

and this gives approximately [11]

$$h^{g+1} = h^g e^{-\Delta u_g} + (1 - e^{-\Delta u_g})\bar{\mu}^g_{sH}\bar{\Phi}^g. \tag{20}$$

When the division into lethargy groups is sufficiently fine, the inaccuracy of the approximations made above is not serious; this also applies to the approximate formula

$$\Phi^{g+1} = 2\bar{\Phi}^g - \Phi^g. \tag{21}$$

In (14), there can be written

$$q^g = (\xi\mu_s)^g \Phi^g, \tag{22}$$

where the sum quantity $(\xi\mu_s)^g$ is calculated with the contribution from hydrogen ignored. By substituting (20), (21) and (22), equation (18) is transformed into

$$-\bar{D}^g \nabla^2\bar{\Phi}^g + A^g\bar{\Phi}^g = S^g, \tag{23}$$

with the source term

$$S^g = B^g\Phi^g + C^g h^g + \bar{S}^g, \tag{24}$$

in which

$$\begin{cases} A^g = \bar{\mu}^g_a + \dfrac{1 - e^{-\Delta u_g}}{\Delta u_g}\,\bar{\mu}^g_{sH} + \dfrac{2(\xi\mu_s)^{g+1}}{\Delta u_g} \\ B^g = \dfrac{(\xi\mu_s)^{g+1} + (\xi\mu_s)^g}{\Delta u_g} \\ C^g = \dfrac{1 - e^{-\Delta u_g}}{\Delta u_g}. \end{cases} \tag{25}$$

The thermal flux Φ_{th} satisfies

$$D_{th}\nabla^2\Phi_{th} + \mu^{th}_a\Phi_{th} = g_{th} + h_{th}, \tag{26}$$

and thus, in the ninth energy group,

$$A^8 = \mu^{th}_a, \quad B^8 = (\xi\mu_s)^{th} \quad \text{and} \quad C^8 = 1. \tag{27}$$

The microscopic cross sections required have been found in [3, 4].

The next problem is that of finding the spatial solutions of equation (23); this is transformed into spatial difference equations. The radius is accordingly divided as on page 11 into intervals $\Delta r_i = r_i - r_{i-1}$ $(i = 1, 2, \ldots, 44)$, and still $\Delta r_{45} = r_{45} - r_{44} = 137$ cm - 117 cm = 20 cm. In our spherical geometry, we have

$$D\nabla^2\Phi = D\left(\frac{d^2\Phi}{dr^2} + \frac{2}{r}\frac{d\Phi}{dr}\right). \tag{28}$$

Equation (23) is multiplied by r^2, and integration made between $r_{i-\frac{1}{2}} = r_i - \frac{1}{2}\Delta r_i$ and $r_{i+\frac{1}{2}} = r_i + \frac{1}{2}\Delta r_{i+1}$ and get, omitting superscipts g,

$$\int_{r_{i-\frac{1}{2}}}^{r_{i+\frac{1}{2}}} \bar{D} r^2 \frac{d\bar{\Phi}}{dr} + \int_{r_{i-\frac{1}{2}}}^{r_i} \frac{r^3}{3} [A\bar{\Phi}_i - S(r_i^-)] + \int_{r_i}^{r_{i+\frac{1}{2}}} \frac{r^3}{3} [A\bar{\Phi}_i - S(r_i^+)] = 0, \quad (29)$$

where $S(r_i^-)$ and $S(r_i^+)$ are the source values (24) inside and outside the boundary r_i, and $\bar{\Phi}_i$ is the flux at the boundary. From (29) is derived as a fairly good approximation the difference equation

$$\alpha_i^g \bar{\Phi}_{i+1}^g + \beta_i^g \bar{\Phi}_i^g + \gamma_i^g \bar{\Phi}_{i-1}^g + \delta_i^g = 0, \quad (30)$$

$$i = 0, 1, 2, \ldots, 44 \qquad g = 0, 1, 2, \ldots, 8$$

where, without superscripts,

$$\begin{cases} \alpha_i = \gamma_{i+1} = -\bar{D} \dfrac{r_i r_{i+1}}{\Delta r_{i+1}} \\ \beta_i = \bar{D}\left(\dfrac{r_i r_{i+1}}{\Delta r_{i+1}} + \dfrac{r_i r_{i-1}}{\Delta r_i}\right) + Ar_i^2 \left[\dfrac{\Delta r_i}{2}\left(1 - \dfrac{\Delta r_i}{2r_i}\right) + \dfrac{\Delta r_{i+1}}{2}\left(1 + \dfrac{\Delta r_{i+1}}{2r_i}\right)\right] \\ \delta_i = -S(r_i^-) r_i^2 \dfrac{\Delta r_i}{2}\left(1 - \dfrac{\Delta r_i}{2r_i}\right) - S(r_i^+) r_i^2 \dfrac{\Delta r_{i+1}}{2}\left(1 + \dfrac{\Delta r_{i+1}}{2r_i}\right). \end{cases}$$

Near the origin, more exact expressions must be used

$$\begin{cases} \alpha_1 = \gamma_2 = -\bar{D}\left(r_1 + \dfrac{\Delta r_2}{2}\right)^2 / \Delta r_2 \\ \beta_1 = \bar{D}\left[\left(r_1 + \dfrac{\Delta r_2}{2}\right)^2 / \Delta r_2 + \dfrac{\Delta r_1}{4}\right] + A\left[\dfrac{7}{24}(\Delta r_1)^3 + r_1^2 \dfrac{\Delta r_2}{2}\left(1 + \dfrac{\Delta r_2}{2r_1} + \dfrac{(\Delta r_2)^2}{12 r_1^2}\right)\right] \\ \gamma_1 = \alpha_0 = -\bar{D} \dfrac{\Delta r_1}{4} \\ \delta_1 = -S(r_1^-) \dfrac{7}{24}(\Delta r_1)^3 - S(r_1^+) r_1^2 \dfrac{\Delta r_2}{2}\left(1 + \dfrac{\Delta r_2}{2r_1} + \dfrac{(\Delta r_2)^2}{12 r_1^2}\right) \\ \beta_0 = \bar{D} \dfrac{\Delta r_1}{4} + A \dfrac{(\Delta r_1)^3}{24} \\ \gamma_0 = 0 \\ \delta_0 = -S(0^+) \dfrac{(\Delta r_1)^3}{24} - S(0^-) \dfrac{(\Delta r_1)^3}{48}. \end{cases}$$

The solution of equation (30) can be obtained by an algorithm in three steps:

1)

$$\Gamma_i = \frac{-\alpha_i}{\beta_i + \gamma_i \Gamma_{i-1}} \qquad i = 1, 2, \ldots, 43 \tag{31}$$

with starting value $\Gamma_0 = \frac{-\alpha_0}{\beta_0}$

2)

$$\Omega_i = \frac{-(\gamma_i \Omega_{i-1} + \delta_i)}{\beta_i + \gamma_i \Gamma_{i-1}} \qquad i = 1, 2, \ldots, 44 \tag{32}$$

with starting value $\Omega_0 = \frac{-\delta_0}{\beta_0}$

3)

$$\Phi_{i-1} = \Gamma_{i-1} \Phi_i + \Omega_{i-1} \qquad i = 44, 43, \ldots, 1 \tag{33}$$

with starting value $\Phi_{44} = \Omega_{44}$.

The principal idea in this work is that the results of the Monte Carlo calculation should produce the source terms $\bar{S}^0$ and $\bar{S}^1$ in the different spherical shells. The number of neutrons in the 45th spatial categories of the Monte Carlo results was set into the shell between r_{44} and r_{45}. Computation is started in the group corresponding to g = 0, then in equation (24) $S^0 = \bar{S}^0$. In each energy group, the results arrived at are the flux values $\bar{\Phi}_i^g$ (i = 0, 1, 2, ..., 44). For computation in the subsequent energy group, Φ^{g+1} is determined from (21) and h^{g+1} from (20), except

$$\Phi^1 = \frac{(\overline{\xi \mu_s})^0}{(\xi \mu_s)^1} \bar{\Phi}^0, \tag{33'}$$

[10, pp. 127 ··· 129]. However, Φ^{g+1} and h^{g+1} are boundary values, and in (24) auxiliary quantities must be utilized

$$W_i^{g+1} = B^{g+1} \Phi_i^{g+1} + C_i^{g+1} h_i^{g+1} \tag{34}$$

$$Y_i^{g+1} = \tfrac{1}{2}(W_{i-1}^{g+1} + W_i^{g+1}) \tag{35}$$

in order to get

$$S^{g+1}(r_i^-) = S^{g+1}(r_{i-1}^+) = S_i^{g+1} = \bar{S}_i^{g+1} + Y_i^{g+1}. \tag{36}$$

In particular

$$S(0^-) = W_0 + (Y_1 - W_0) + \bar{S}_1, \tag{37}$$

and

$$S(r_{44}^+) = W_{44} - (Y_{44} - W_{44}) + \bar{S}_{45}. \tag{38}$$

Finally, the results $\bar{\Phi}_i^g$ (i = 0, 1, 2, ..., 44) represent the distribution of the thermal flux. The programme also listed the flux values $\bar{\Phi}_i^6$, which give the epithermal flux at an energy of about 1.6 eV.

4. RESULTS OF THE COMPUTATION

The computer used in the numerical calculations was Elliott 803 A.

Most of the calculation results have been illustrated and discussed in reference [12]. Here, in figure 1, there are presented the thermal neutron flux distributions, calculated for two densities of a soil material and for four cases of moisture content. The composition of the soil was taken as: O 48 %, Na 2.3 %, MgAl 9 %, Si 32 %, KCa 5.4 % and Fe 3.3 % by weight. Elements Mg and Al, and similarly K and Ca, were taken to be identical in the treatment by virtue of the similarity of their neutron-physical properties. The theoretical curves, ignoring the uncertainty near the origin at low moisture content appearing as oscillations in the multigroup calculations, are in close agreement with experimental results.

From figure 1 can be calculated that for the moisture of 20 % by volume the relative change in the thermal flux in the origin arising from a density difference of 0.1 g/cm^3 is at least 3.3 % corresponding to the change of about 0.5 % by volume in moisture. In [12] there has been reported that in the soil with a density of 2.0 g/cm^3 and a moisture of 20 % the boron content of 50 ppm causes the relative change in the thermal flux of 17.5 % corresponding to 2.6 % by volume in water content. These results agree well with recent Danish investigations [13].

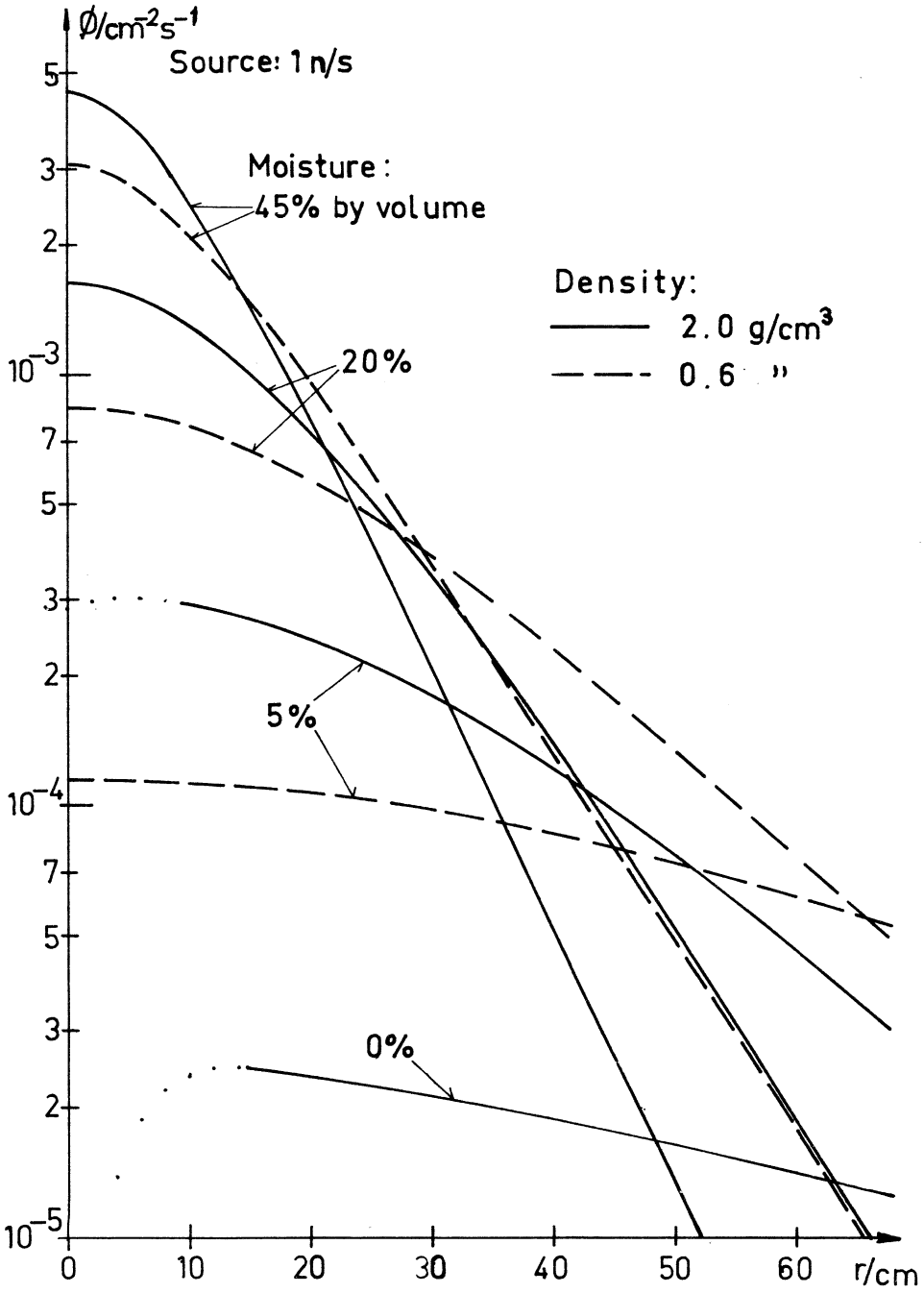

Figure 1. Thermal flux.

ACKNOWLEDGEMENTS

I am grateful to Professor Erkki Laurila, Director of the Laboratory of Technical Physics in the State Institute for Technical Research, where this work has been made, for support, and for encouragement he gave by many discussions, to Professor Pekka Jauho and Heikki Koskinen, Tech. Lic., for valuable criticism, and to Mrs. Lorna Sundström and Mr. F. Fewster for the final linguistic revision.

REFERENCES

[1] Dixon, W.R., Bielesch, A. & Geiger, K.W., Neutron spectrum of an actinium-beryllium source. Can. J. of Physics 35 (1957):6, pp. 699 ··· 702.

[2] Cashwell, E.D. & Everett, C.J., A practical manual on the Monte Carlo method for random walk problems. Washington 1957. [Los Alamos Scientific Laboratory, LA-2120]. (Also, Pergamon Press, 1959).

[3] Reactor physics constants. 2 ed. Washington 1963. [Argonne National Laboratory, ANL-5800].

[4] Hughes, D.J. & Schwartz, R.B., Neutron cross sections. Washington 1958. [Brookhaven National Laboratory, BNL-325].

[5] Howerton, R.J., Semi-empirical neutron cross sections. Washington 1958. [University of California, Lawrence Radiation Laboratory, UCRL-5351].

[6] Howerton, R.J., Tabulated neutron cross sections. Washington 1959. [University of California, Lawrence Radiation Laboratory, UCRL-5226].

[7] Howerton, R.J., Tabulated differential neutron cross section. Washington 1961. [University of California, Lawrence Radiation Laboratory, UCRL-5573].

[8] Coldberg, M.D., May, V. & Stehn, J.R., Angular distributions in neutron-induced reactions. Washington 1962. [Brookhaven National Laboratory, BNL-400].

[9] Soodak, H., Reactor handbook, Vol. III, part A, Physics. New York, John Wiley & Sons, 1962, pp. 46 ··· 47.

[10] Beckurts, K.H. & Wirtz, K., Neutron physics. Würzburg, Springer-Verlag, 1964.

[11] Sangren, W.C., Digital computers and nuclear reactor calculations. New York, John Wiley & Sons, 1960, pp. 125 ··· 135.

[12] Kasi, S. & Koskinen, H., Analysis, calculations and measurements concerning the moisture measuring by the neutron method. RILEM/CIB Symposium: Moisture problems in buildings, Helsinki 1965. Report 6-14, 17 p. Also, Nuclear Engineering and Design 3 (1966):1, pp. 74 ··· 82.

[13] Ølgaard, P.L., On the theory of the neutronic method for measuring the water content in soil. Copenhagen 1965. [Danish Atomic Energy Commission, Risö Report No. 97].

Text III

Int. J. Appl. Radiat. Isot. Vol. 33, pp. 667 to 671, 1982
Printed in Great Britain.

0020-708X/82/080667-05$03.00/0

An Attempt to Calculate Correctly the Region of Influence in Gauging Moisture with Neutrons

S. S. H. KASI

Laboratory of Physics, Helsinki University of Technology, SF-02150 Espoo 15, Finland

(*Received* 11 *June* 1981)

A neutron device, when employed for moisture gauging, samples only part of bulk material having dimensions large compared with the neutron range. In this paper, firstly, a new method is presented for calculating the size of this sample, i.e. the region of influence of the gauge. The method is not distorted by the neutron leakage (the large value of such an effect in the method availed by finite spheres is also pointed out here). In the present method the relative influence of a sample point, i.e. its weight, is calculated. For this the neutron flux and neutron importance (or, possibly, slowing-down density) can be used. The region of influence is then inside a surface of equiweight points and it has the total weight of a certain percentage, e.g. 99%. Secondly, this method was applied to the subsurface gauge based on neutron slowing down. Three simple diffusion approximations of the neutron transport were then used, though the reliability of these approximations is in doubt. Values for the radius of a sphere as the region of 99% influence were calculated for a certain soil. Among these results those obtained by means of the 3-group diffusion are, especially at larger moisture values, preferred by the author. The age theory may be useful for nearly-dry substances.

1. Introduction

CERTAIN devices for moisture measurement, widely used in hydrology and engineering, comprise a source of fast (MeV, keV) neutrons and a detector of usually slower neutrons. These moisture gauges are based on the fact that the distribution of neutrons in a substance is strongly dependent on its hydrogen content, because the main slowing-down of neutrons is caused by hydrogen. Also the methods using only fast or only thermal neutrons have been investigated. In the following text a general method is presented for calculating the region of influence of any neutron device. A few diffusion approximations of it are then applied to that backscattering type of gauge in which a probe, having the source and detector close to one another, is inserted into a material, usually in an access tube (the so-called subsurface gauge).[1]

The calibration of a neutron gauge for materials of different volumes, as encountered operationally, can be calculated. For this the sphere of material in empty space having the probe at its centre can be calculated in which the response of gauge, a counting rate, is 99% of that in infinite substance.[1,2,3] The subsurface gauge in a large volume of a material, however, measures only a sample of it located in a region around the probe. The different parts of the sample have various degrees of influence on the counting rate. In hydrology the resolution of a subsurface gauge is an important question, and a rather accurate description of the sample of soil gauged by a probe is needed for determination of the relevant quantities. The determination of ranges of measurement in different directions, etc. is also useful for other, e.g. industrial, applications. For such illustrations the 99% sphere defined above or a more adequate and complicated corresponding body, determined by any appropriate calculation with empty space outside the body, is too large, because of neutron leakage from the body. That is, the body for calibration is larger than the real sample of measurement. The generalized concept of the 99% sphere where the material of the outer space varies, has led to a theoretically still rather arbitrary estimate of the measured region.[4]

Naturally, the sample is elongated in the direction of an access tube, not containing water. A relevant calculation of the fluxes for determination of the sample would, in most cases, have two spatial coordinates, and would include several regions of different media.[5] The approximate methods of neutron diffusion in three energy groups have been rewarding in calculations of calibration curves for neutron gauges, except for some uncertainty as to the adequacy of these methods at rather low moisture contents.[1] The effect of the access tube has been investigated successfully even with a multi-region two-group diffusion calculation.[6]

2. A Way to Illustrate the Sample

The scattering of a neutron at some place from a hydrogen atom of moisture is an event giving moisture information from this place. In addition

both matrix substance and moisture influence the neutron transport before and after this collision.

Let the angular flux $\phi(\mathbf{r}, \mathbf{\Omega}, E)$ be the solution of the neutron transport equation in the case of a moisture measurement. $\mathbf{r}$ is the position, $\mathbf{\Omega}$ a unit vector in the direction of the velocity, and E the energy of a neutron. The counting rate of the detector

$$C = \int_0^\infty \int_{V_d} \Sigma_d(\mathbf{r}, E)\phi(\mathbf{r}, E)\,\mathrm{d}V\,\mathrm{d}E$$
$$= \int_0^\infty \int_{4\pi} \int_{\text{all space}} S(\mathbf{r}, \mathbf{\Omega}, E)\phi\dagger(\mathbf{r}, \mathbf{\Omega}, E)\,\mathrm{d}V\,\mathrm{d}\Omega\,\mathrm{d}E \tag{1}$$

is presented in the first formula in the usual way. $\Sigma_d(\mathbf{r}, E)$ is the cross section of the reaction in detection,

$$\phi(\mathbf{r}, E) = \int_{4\pi} \phi(\mathbf{r}, \mathbf{\Omega}, E)\,\mathrm{d}\Omega$$

$\mathrm{d}\Omega$ is a differential solid angle around $\mathbf{\Omega}$, and V_d is the volume of the detector. In the second formula $\phi\dagger(\mathbf{r}, \mathbf{\Omega}, E)$, the "neutron importance", is the solution of the adjoint of the transport equation with the "source" $\Sigma_d(\mathbf{r}, E)$.[7] $S(\mathbf{r}, \mathbf{\Omega}, E)$ can be a real neutron source, or the distribution of the neutrons slowed down through an energy E', or a combination of these. In the second one of these cases we have the slowing-down density

$$q(\mathbf{r}, E') = \int_0^{E'} \int_{4\pi} S(\mathbf{r}, \mathbf{\Omega}, E)\,\mathrm{d}\Omega\,\mathrm{d}E\,. \tag{2}$$

The source $S(\mathbf{r}, \mathbf{\Omega}, E)\mathrm{d}V$ in $\mathrm{d}V$ with certain $\mathbf{\Omega}$ and E distributions causes the flux field $\mathrm{d}\phi(\mathbf{r}, E)$ over the whole space and it has the contribution

$$\mathrm{d}C = \int_0^\infty \int_{V_d} \Sigma_d(\mathbf{r}, E)\,\mathrm{d}\phi(\mathbf{r}, E)\,\mathrm{d}V_d\,\mathrm{d}E$$
$$= \mathrm{d}V \int_0^{E'} \int_{4\pi} S(\mathbf{r}, \mathbf{\Omega}, E)\phi\dagger(\mathbf{r}, \mathbf{\Omega}, E)\,\mathrm{d}\Omega\,\mathrm{d}E \tag{3}$$

to C. In many cases of real geometries the determination of $\phi\dagger$ is an easier way than the calculations of $\mathrm{d}\phi$ for all necessary $S(\mathbf{r}, \mathbf{\Omega}, E)\,\mathrm{d}V$. The spatial distribution (E' above denoted by E)

$$p_E(\mathbf{r}) = \frac{\mathrm{d}C/\mathrm{d}V}{C} \tag{4}$$

expresses the portion of the counting rate per unit volume that is caused by the neutrons slowed down through E at $\mathbf{r}$. The energy E here is arbitrary. One should select many E, which are distributed between the source energies and the detection energies in an appropriate way, or, if the distribution of these energies is arbitrary one should weight different $p_E(\mathbf{r})$ correctly. In these procedures one should consider the hydrogen interactions in relation to those of the whole substance, and the influence of the regions not occupied by the substance gauged. The averaged value of $p_E(\mathbf{r})$, denoted by $p(\mathbf{r})$, then illustrates the weight of the moisture at $\mathbf{r}$ in the response of gauge, i.e. what is the sample like. The function $p(\mathbf{r})$, can be used for the estimation of the ranges of measurements. The region of influence then has the boundary surface at which $p(\mathbf{r})$ has a certain constant value and the integral of $p(\mathbf{r})$ for instance over the region of the 99% influence has the value 0.99, cf. equation (10) in the following chapter.

In calculation of $\phi(\mathbf{r}, \mathbf{\Omega}, E)$ and $\phi\dagger(\mathbf{r}, \mathbf{\Omega}, E)$ many methods can be used. The calculations of $\phi\dagger(\mathbf{r}, \mathbf{\Omega}, E)$, e.g. those by Monte Carlo, start from the "source" $\Sigma_d(\mathbf{r}, E)$ and proceed in the opposite direction to the course of the neutrons to be detected, i.e. the principal of reciprocity[8] in its general form.[7] In the rather common P_1 approximations the conventional $\mathbf{\Omega}$ expansions of flux and importance are truncated after the first two terms. The diffusion equations are then obtained when, further, the source is isotropic, and the product of the neutron (or importance) current and the second term in the spherical expansion of the scattering cross section can be assumed to be constant over at least two scatterings.[9] For the energy coordinate its division into several intervals and integration of the transport equations over them leads to the popular multigroup picture. When the number of the groups is very small the transfers other than those from any group to the lower one can be neglected.

In this paper only some simple diffusion and age calculations are treated in detail. In them a point detector is used, and then the corresponding formulae of $\mathrm{d}\phi$ and $\phi\dagger$ are proportional to each other. In these calculations the source S of equation (2), when q means a group transfer, has been approximated to isotropic.

3. Diffusion and Age Theory Calculations

We search for the sample measured by the subsurface gauge with 2- and 3-group diffusion calculations and also, at low moistures, with the age theory. We have the rough approximation of a "point probe" in an infinite homogeneous substance. At that "point" we have a source of 4,5 MeV($=E_0$) neutrons and the coexisting detector of lower energy neutrons. The detector is assumed to be so weak that it does not depress the fluxes. The slowing-down power of hydrogen and the other common elements can, as to the accuracy of this treatment, be taken as constant below about 50 keV until the thermal energies. This means that the slowing-down density q at these energies has, in the homogeneous medium, a certain relative part caused by hydrogen.

2-group diffusion

e.g. The neutrons under slowing-down form the first, and the thermal neutrons the second energy

group. If the neutron source emits S neutrons per time unit and L_s is the slowing-down length from the source energy E_0 to the thermal energies, then, omitting epithermal absorption,

$$q(r) = \frac{Se^{-r/L_s}}{4\pi L_s^2 r} \tag{5}$$

is the slowing-down density from the first group to the second one at a distance r from the source. The neutrons which are slowing down (at a certain approximation-technical energy E_2) to the thermal group form the source of thermal neutrons. The point source $q(r)\mathrm{d}V$ causes {in (3) suppose $\Sigma_r = \delta(\mathbf{r})$} at the detector the thermal neutron flux

$$\{\mathrm{d}C = q(r)\phi\dagger(r)\,\mathrm{d}V = \}\ \mathrm{d}\phi(0;r) = q(r)\,\mathrm{d}V\,\frac{e^{-r/L}}{4\pi\Sigma_a L^2 r} \tag{6}$$

where L is the thermal diffusion length and Σ_a the thermal absorption cross section. Integration of (6) over the whole space gives the thermal flux

$$\phi(0) = \frac{S}{4\pi\Sigma_a L_s L(L_s + L)}. \tag{7}$$

We can now write the distribution function of the moisture weight as (4) with

$$p(r) = \frac{\mathrm{d}\phi(0;r)/\mathrm{d}V}{\phi(0)}. \tag{8}$$

Equations (8), (6), (5) and (7) give

$$p(r) = \frac{e^{-(1/L_s + 1/L)r}(L_s + L)}{4\pi r^2 L_s L}. \tag{9}$$

We see from (9) that $p(r)$ decreases rapidly with r. Because

$$\int_0^\infty p(r)4\pi r^2\,\mathrm{d}r = 1$$

we define the *radius R of a 99% sphere* according to

$$\int_0^R p(r)4\pi r^2\,\mathrm{d}r = 0.99 \tag{10}$$

The weight function (9) leads by (10) to the radius

$$R = \frac{\ln 100}{L_s^{-1} + L^{-1}} \tag{11}$$

of this 99% sphere.

3-group diffusion

We divide the energy interval $E_0 \ldots E_2$ into the first energy group $E_0 \ldots E_1$ with the slowing-down length L_1 and the second one $E_1 \ldots E_2$ with L_2. Then

$$L_s^2 = L_1^2 + L_2^2. \tag{12}$$

We suppose $E_1 \lesssim 50\,\mathrm{keV}$. Equation (5) gives for the slowing-down density from the first energy group, as can in practice be assumed, to the second one:

$$q_1(r) = \frac{Se^{-r/L_1}}{4\pi L_1^2 r}. \tag{13}$$

For the slowing-down density from the second group we have

$$q_2(r) = \frac{S}{4\pi r}\,\frac{e^{-r/L_1} - e^{-r/L_2}}{L_1^2 - L_2^2}. \tag{14}$$

In this case the thermal flux at the detector can be calculated in two ways:

1. Equation (13) gives the source $q_1(r)\,\mathrm{d}V$ of a two-group diffusion. The formula for the calculation of the differential thermal flux at the detector point {as well as the corresponding $\phi\dagger$} is similar to (14).
2. $q_2(r)$ of (14) serves for the source of diffusion of thermal neutrons and the thermal flux is obtained as in the case of two groups.

Setting the weight of both group transfers as equal, we thus multiply both of the differential fluxes, calculated in the ways above, by a half, and sum them up:

$$\mathrm{d}\phi(0;r) = \frac{1}{2}\,\frac{q_1(r)\,\mathrm{d}V(e^{-r/L_2} - e^{-r/L})}{4\pi r\,\Sigma_a(L_2^2 - L^2)} + \frac{1}{2}\,\frac{q_2(r)\,\mathrm{d}V e^{-r/L}}{4\pi r\Sigma_a L^2}.$$

By integration the well-known

$$\phi(0) = \frac{S}{4\pi\Sigma_a(L_1 + L_2)(L_1 + L)(L_2 + L)} \tag{15}$$

is obtained. The definition (8) then gives

$$p(r) = \frac{(L_1 + L_2)(L_2 + L)(L + L_1)}{8\pi r^2} \times \left[\frac{e^{-r/L}}{L^2}\,\frac{e^{-r/L_1} - e^{-r/L_2}}{L_1^2 - L_2^2} + \frac{e^{-r/L_1}}{L_1^2}\,\frac{e^{-r/L_2} - e^{-r/L}}{L_2^2 - L^2}\right]. \tag{16}$$

By using (16) and the definition (10) we derive the equation

$$\frac{L_2}{L_1}\,\frac{L_1 + L}{L_2 - L}\exp(-R/L_1 - R/L_2) + \frac{L_2}{L}\,\frac{L + L_1}{L_2 - L_1}\exp(-R/L_2 - R/L) + \left(\frac{L_1}{L}\,\frac{L + L_2}{L_1 - L_2} + \frac{L}{L_1}\,\frac{L_1 + L_2}{L - L_2}\right) \times \exp(-R/L_1 - R/L) = 0.02 \tag{17}$$

for the calculation of the radius R of the 99% sphere. The solution of (17) is easily found by iteration.

Age theory formulae

In the age theory, i.e. in the model of continuous slowing-down, the slowing-down density at the energy E becomes

$$q_E(r) = \frac{S \exp(-r^2/4L_1^2)}{(2\sqrt{\pi}L_1)^3}, \tag{18}$$

where $L_1^2 = \tau(E)$ is the Fermi age from E_0 to E. The source $q_E(r)$, (18), causes at the detector the thermal flux per volume unit

$$\frac{d\phi_E(0;r)}{dV} = \frac{S}{4\pi D} \frac{\exp(-r^2/4L_1^2 + L_2^2/L^2)}{16r(\sqrt{\pi}L_1)^3} \times \{e^{-r/L}[1 + \mathrm{erf}(r/2L_2 - L_2/L)] - e^{r/L}[1 - \mathrm{erf}(r/2L_2 + L_2/L)]\}. \tag{19}$$

In (19) D is the thermal diffusion coefficient and L_2^2 is the Fermi age from the energy E to the thermal energies. In this case[10]

$$\phi(0) = \frac{S}{4\pi D}\left[\frac{1}{\sqrt{\pi}L_s} - \exp(L_s^2/L^2)\frac{1 - \mathrm{erf}(L_s/L)}{L}\right] \tag{20}$$

can be verified to result by the integration of (19) over the whole space. Equation (12) is still valid. The relation of (19) and (20)

$$p_E(r) = \frac{d\phi_E(0;r)/dV}{\phi(0)} \tag{21}$$

corresponds to (4) and (8). In this case the adequate function $p(r)$ is best achieved by integrating $p_E(r)$ of (21) over E when weighting it at first by an appropriate function of E.

4. An Example

We consider the same substance, Risø soil, as in the earlier, Danish investigation.[4] The density of this mineral soil is then 1400 kg/m^3 and the composition as measured.[11] In the calculation of the slowing-down lengths and thermal diffusion length an earlier programme[12] including some additional approximations was used. It was $E_1 = 45$ keV. The radii of 99% spheres with diffusion theory: the solution of the 3-group equation (17) and the value of the 2-group equation (11), are presented in Fig. 1 as functions of moisture. The 3-group radius is c_a 4/3 times the 2-group radius. The former 3-group estimate[4] for the 99% sphere has also been presented in Fig. 1.

The parameters from the earlier programme[12] have also been used for the diffusion determination of the soil sphere[13] in empty space in which the thermal flux at the "point probe" is 99% of that in infinite soil, see Fig. 1.

The density-corrected value of L by Olgaard[13] was 1 . . . 6% larger, that of L_s by means of the corresponding L_1 and L_2[13] even 17 . . . 10%, the value of the 3-group radius (17) by means of these L, L_1 and L_2 8 . . . 15%, and that of the 2-group radius (11) 5 . . . 8% larger than my values for them at moistures 0 . . . 400 kg/m^3, respectively. Also the 3-group radius of the finite medium 99% sphere by Olgaard and Haahr[4] was noticeably larger, 12 . . . 7%, than that, the broken curve, in Fig. 1. However, the 3-group diffusion models[2,12] used gave almost equal and correct diffusion parameters for water (L_s by Olgaard was even 5% smaller than mine). The difference of the energy boundary E_1, 2 MeV of Olgaard[2] and the differences in the procedures of the parameter calculations, obviously are the reasons for the discrepancies above. The differences of the 99% spheres when using a point detector or the line detector with a length 12 cm[4,13] are rather small. The radius of the finite medium 99% sphere with the line detector is[13] at zero moisture 0.2% and, at 400 kg H_2O/m^3 2.0% larger than that with the point detector. However, when the length of the line detector grows from 11.8 to 26.6 cm then this radius even has[13] the increase of 11% at 400 kg H_2O/m^3.

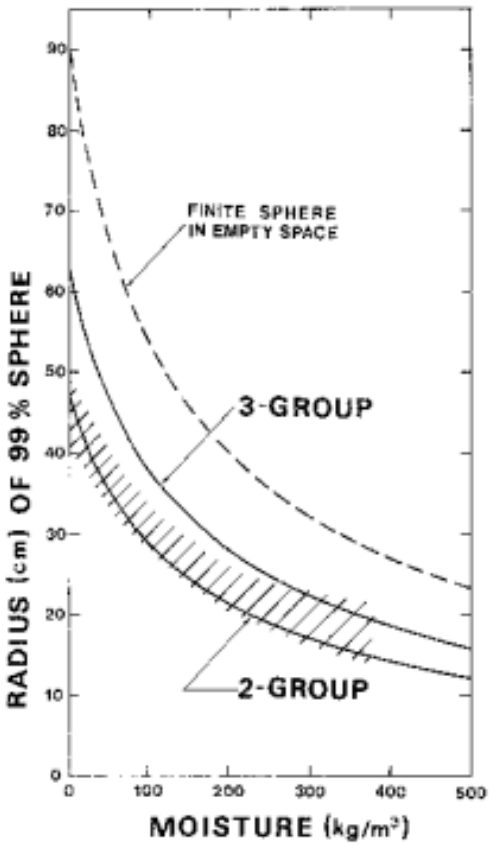

FIG. 1. Radii of 99% spheres for a mineral soil by means of diffusion calculations with a "point probe". The solid curves for the case of homogeneous infinite medium have been determined by means of the 3-group equation (17) and 2-group equation (11) of the present theory. The diagonalized area shows the former 3-group estimate. The broken curve concerns the 3-group calculation of the soil sphere in empty space in which the counting rate is 99% of that in infinite soil.

The age theory calculation in the case of dry Risø soil gave the radius 77 cm for the 99% sphere from (10); $p(r)$ was then averaged from the functions (21) where E had the values 45 keV, 80.2 eV and 0.143 eV ($E_2 = 0.139$ eV). Each $p_E(r)$ had the same weight. The low highest energy, 45 keV, is justified since hydrogen contributes less to the slowing-down at high energies.

5. Value of the Methods

We must remember that the diffusion theory and the age theory in particular are incompatible with neutron transport in hydrogeneous substances. The radius R of the spherical 99%-sample obtained with such a 3-group calculation as above can be more reliable than the 2-group R. The distributions of the thermal flux calculated with the 3-group diffusion method have, e.g. in water,[2] the same form as the experimental results have, but any corresponding distribution of the 2-group diffusion calculation is unrealistically peaked at the point source. Figure 2 presents $4\pi r^2 p(r)$ distributions at zero moisture. The 3-group $4\pi r^2 p(r)$ has, according to (16), the value zero at $r = 0$. The relations of the $4\pi r^2 p(r)$ distributions at larger moistures are of the same kind as in Fig. 2. It seems that the $4\pi r^2 p(r)$ distributions from the 3-group diffusion calculations have an adequate resemblance to the slowing-down density distributions of the literature.

However, the physical (e.g. E_0) and geometrical simplifications in section 3 are drastic. Also the inaccuracy of the parameters, see section 4, causes uncertainty about the results of diffusion and age calculations.

The age theory is applicable for SiO_2, $CaCO_3$, and other hydrogenless substances when the energy of source neutrons is low.[14] However, in graphite near a Ra–Be source (with the broad spectrum of energies) the correct formula of the slowing-down density at an epithermal energy has three terms like equation (18).[15] From the P_1 approximation of the age theory there follows a spatial confinement for its applicability.[16] In the age calculation of section 4 for a dry soil this condition of applicability, i.e. the distance from source $r \ll 2L_s^2/D_2 = 8.3$ m,[12] is sufficiently well satisfied.

The simple diffusion methods of section 3 are most applicable when the source–detector distance is small, the access tube is narrow and thin, and the neutron absorption of the probe is weak. The diffusion methods may be of a general value. However, their usefulness for calculation of the sample around a certain gauge must be tested by means of some accurate method referred in section 2. The importance

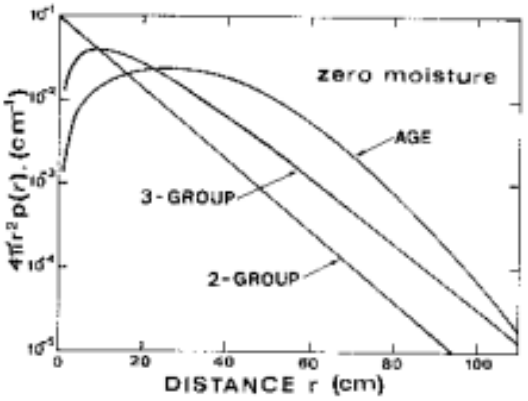

FIG. 2. Distributions $4\pi r^2 p(r)$ for infinite dry mineral soil (r the distance from a "point probe") when the moisture weight, in the thermal flux at the probe, $p(r)$ has been calculated by means of the 2-, and 3-group diffusion, and age theory.

technique introduced is then very useful when dC/dV of equation (3) is calculated. Naturally, the perfect illustration of the sample can directly be obtained by means of the accurate methods. However, in the use of any method the gauge, access tube, and medium must often have an idealized configuration and averaged compositions. It is an important question, treated above incompletely, to find the appropriate weighting of $p_E(\mathbf{r})$, (4), for determination of the averaged function $p(\mathbf{r})$ presenting the contribution of moisture at $\mathbf{r}$ to the response of the gauge.

References

1. Neutron Moisture Gauges, *Tech. Rep. Ser. No.* 112 (IAEA, Vienna, 1970).
2. OLGAARD P. L. *Risø Rep. No.* 97 (1965).
3. LAKSHMIPATHY A. V. and GANGADHARAN P. *Nucl. Instrum. Methods* **142**, 577 (1977).
4. OLGAARD P. L. and HAAHR V. *Riso Rep. No.* 256, 99 (1972).
5. COUCHAT P. *Report FRNC-TH-566* (1974).
6. MORSTIN K. and WOŹNIAK J. In *Nuclear Techniques and Mineral Resources* 1977, p. 119 (IAEA, Vienna, 1977).
7. BELL G. I. and GLASSTONE S. *Nuclear Reactor Theory*, p. 256–273 (Van Nostrand Reinhold, New York, 1970).
8. KIRKEGAARD P. *Report Riso-M-896* (1969).
9. BELL G. I. and GLASSTONE S. Ref. 7, pp. 178–180.
10. Ref. 1, pp. 38–39.
11. HAAHR V. and OLGAARD P. L. In *Isotopes and Radiation in Soil-Plant Nutrition Studies*, p. 129 (IAEA, Vienna, 1965).
12. KASI S. S. H. *Rep. TKK-F-A190* (1972).
13. OLGAARD P. L. *Report Riso-M-637* (1967).
14. TITTMAN J. *J. Appl. Phys.* **26**, 394 (1955).
15. BECKURTZ K. H. and WIRTZ K. *Neutron Physics*, p. 349 (Springer-Verlag, Berlin, 1964).
16. *Ibid.*, pp. 148–149.

Text IV

Reprint from

"ISOTOPE AND RADIATION TECHNIQUES
IN SOIL PHYSICS
AND IRRIGATION STUDIES 1983"

INTERNATIONAL ATOMIC ENERGY AGENCY
VIENNA, 1983

IAEA-SM-267/17

SOME CONSIDERATIONS FOR SOIL MOISTURE GAUGING WITH NEUTRONS

S. KASI, J. IMMONEN, K. SAIKKU
Physics Laboratory,
Helsinki University of Technology,
Espoo, Finland

Abstract

SOME CONSIDERATIONS FOR SOIL MOISTURE GAUGING WITH NEUTRONS.

The sensitivity of the moisture gauge, especially the neutron gauge, is discussed. The neutron gauge is very sensitive to hydrogen content. The interference of other elements including the most significant absorbers of thermal neutrons is computed. The so-called composition effect is made quantitative. Normally it is not very significant. A calculation of the weight function of the neutron gauge is reported, and a simple formula given for the 95% "sphere" of influence. To simulate the subsurface gauge a procedure is presented and applied by using available experimental data. The procedure is not a very good approximation of the transport theory:diffusion theory with a neutron absorbing sphere. The position and size of this sphere were two fitting parameters; altogether five gauge parameters were used for a fitting.

1. SENSITIVITY OF THE MOISTURE GAUGE

In agricultural use of soil its moisture content should not remain long below wilting-moisture content and above field capacity. Irrigation or drainage is needed to keep water within this range. On the other hand, the soil may have pores for relatively large amounts of gravitational water. All these moisture quantities — wilting moisture, available water, moisture deficit, field capacity, saturating water content etc. [1], can be presented as density quantities which have the unit kg/m^3. Let us denote this quantity by w.

The user of a moisture gauge can have a requirement Δw for its accuracy. Roughly a constant absolute accuracy of moisture determination is often appropriate. Then the sensitivity quantity

$$S = \frac{1}{R}\frac{dR}{dw} \qquad (1)$$

where R is the response of the moisture gauge, offers a good basis for comparing instruments which have a response function of the type $R = R(w)$. In some such comparisons it is better to use[2] the relative sensitivity $S_r = (dR/R)/(dw/w)$.

For neutron gauges many types of sensitivity evaluation have been proposed. S of Eq. (1) has been used, e.g. in Ref. [3]; the relative sensitivity, see Ref. [4], is best when a constant $\Delta w/w$ is demanded (as in many mass gaugings); the sensitivity quantity dR/dw [5] has the advantage of being proportional to source strength, but these sensitivity evaluators have no basis in the statistical error of radioactivity such as the quantity

$$E = \frac{1}{R^{1/2}} \frac{dR}{dw} \tag{2}$$

presented in Ref. [6] has (see Ref. [7:a]). The higher E is, the smaller is the statistical error in the moisture w measured. The modifications of E in the cases of measured background or standard count-rate comparison have been given in Ref. [6].

A requisite for a nuclear gauge is that radiation risk must be at a minimum. This certainly has been achieved when natural radiation is used. Relatively slow moisture processes near the soil surface can be followed by cosmic radiation [8].

The neutron measurement used for moisture determination is in first place the protium (^1H) density determination. Therefore, the hydrogen content of the matrix must be very accurately known. Consider gaugings with a "point probe", i.e. with the probe where the source and detector are close. When you measure very organic soil matter, e.g. peat, and when its dry density $\rho = \rho_t \cdot w$ does not vary (ρ_t is the total density), then $R \propto \rho_t$, and thus $S \simeq 1/\rho_t$. In this matter the point neutron and gamma probes gauge similarly [9]. For neutron gauging in mineral soil, where the matrix includes little hydrogen, the effect of density is relatively weak and the counting rates, at least without background, are small for a point in dry substance. Thus, $S \simeq 1/w$.

2. BASIC CALIBRATIONS

For a neutron moisture gauge the dependence of calibration on matrix density is minimal when the substance is free from hydrogen. When the hydrogen content of the matrix is known, the equivalent moisture content can be used [10], and the calibration which was done for a substance which has no hydrogen in its composition.

The hydrogen content of the soil matrix should be determined accurately. For this, thermogravimetric methods can be useful. Many other soil elements that considerably interfere with the neutron measurement cannot be analysed easily. Fortunately, the effect of composition is not usually very significant, (see Section 4). For calibration, a basic composition can be selected which is most representative for the tasks of the gauge. For soil studies the best basic matrix composition is

TABLE I. INTERFERING POWER S_i (kg/m³)/(kg/m³) OF THE ELEMENT i CALCULATED FOR A NEUTRON MOISTURE GAUGE WHEN THE DETECTOR, BLACK FOR THERMAL OR EPITHERMAL NEUTRONS, IS A CONCENTRIC SPHERE WITH A POINT AmBe SOURCE.

The free density of the matrice substance is 1500 kg/m³ and it has the averaged composition of the earth's crust, except the hydrogen content $p_H = 0$. The moisture content w = 100 kg H_2O/m³

Element i	Content p_i value ± SD	Interfering power S_i in thermal	epithermal
O	464 ± 30 g/kg	0.11	0.36
H	0 ± 0	8.0	6.0
Si	282 ± 100 g/kg	0.04	0.22
Al	82 ± 30 g/kg	0.025	0.19
Fe	56 ± 30 g/kg	−0.08	0.20
Ca	41 ± 20 g/kg	0.005	0.14
Na	24 ± 10 g/kg	0.06	0.4
Mg	23 ± 10 g/kg	0.07	0.27
K	21 ± 10 g/kg	−0.13	0.13
Ti	5.7 ± 3 g/kg	−0.3	0.24
P	1050 ± 500 mg/kg	0.04	0.20
Mn	950 ± 450 mg/kg	−0.6	0.27
S	260 ± 120 mg/kg	−0.004	0.17
C	200 ± 90 mg/kg	0.17	0.5
Cl	130 ± 60 mg/kg	−2.6	0.15
N	20 ± 9 mg/kg	−0.23	0.5
Li	20 ± 9 mg/kg	−32	−0.3
B	10 ± 5 mg/kg	219	−6.6
Gd	7.3 ± 3.6 mg/kg	−708	−1.0
Sm	7.3 ± 3.6 mg/kg	−187	−2.3
Eu	1.2 ± 0.6 mg/kg	−115	−4.0
Cd	200 ± 100 μg/kg	−84	0.07
In	100 ± 50 μg/kg	−5	−0.08
		measurement	

that of the earth's crust, but even for some mineral soils it must be modified, e.g. for $CaCO_3$ [11].

For light organic soils, which usually include a high water content, a good basic calibration is that which has been determined for H_2O.

3. INTERFERENCE OF ELEMENT

An increase of density ρ_i of an element i in a substance causes a change of gauge counting rate. A certain change of water density will cause the same counting rate change. We can define the ratio of this water density change (increasing or decreasing) to the increase of the element density, i.e.

$$S_i = -(\partial w/\partial \rho_i)_R \tag{3}$$

as the interfering power of this element, or as the sensitivity of the gauge to the density of this element.

To make calculational investigations concerning the basic calibration for mineral soils, the composition of the earth's crust was taken from Krauskopf [12]. For hydrogen the content zero was selected. The composition and the result of a calculation are presented in Table I. The first elements up to manganese are the most common in the earth's crust. The last seven elements have a very high absorption cross-section for thermal neutrons. They absorb 30% of thermal neutrons in the soil when it is dry. One can calculate, when w = 10% by volume, that an increase of 3.6 ppm in gadolinium content causes $\Delta w = -3.8$, and that a 5 ppm increase in boron content gives $\Delta w = -1.6$ kg H_2O/m^3 as the error of moisture reading.

The hydrogen sensitivity is generally higher in gauges that detect thermal than in those that detect epithermal neutrons – see Table I [7:b, 13]. In calculations with models of different "point" gauges we found that in the thermal measurements S_i for hydrogen varies between 6–9 for rather mineralized soil, and decreases with moisture. In the case of epithermal detection S_i may in such cases be below the value of 4. The reason for the low epithermal sensitivity is that the increase of slowing-down power decreases flux with respect to the slowing-down density at the same energy; the growth in the response is due to the decrease of diffusion. Otherwise, when the detector is a very strong absorber of even epithermal neutrons, the spectrum of detectable neutrons is to be hardened considerably. For this case, our 3-group diffusion calculations (though comprising flux depression treatment) may be misleading.

Now we also define, by the same means as S_i,

$$S_\rho = -(\partial w/\partial \rho)_R \tag{4}$$

TABLE II. THE INTERFERING POWER OF DENSITY S_ρ, ITS VARIANCE D_c AND THEIR RATIO E_c
The type of gauge, matter and moisture as in Table I. The used estimates of $\sigma(p_i)$ are also presented there

Neutron detector	$S_\rho \pm D_c$	E_c
Thermal	0.0500 ± 0.0069	13.8%
Epithermal	0.283 ± 0.026	9.4%

to be the interfering power of dry density ρ. The values of this are given in Table II for the same cases as in Table I. The increase $\Delta\rho = 100$ kg/m^3 is eliminated with $\Delta w \simeq -5$, or $\simeq -28$ kg H_2O/m^3 in thermal or epithermal detection, respectively.

Change of density does not generally cause a unique S_ρ. We define it to be the change of dry density without any change of composition, i.e. $d\rho_i = p_i d\rho$. Thus,

$$S_\rho = \sum_i p_i S_i. \tag{5}$$

4. EFFECT OF COMPOSITION

It is supposed that the variance of the content of each element i is known. $\sigma(p_i)$ is the standard deviation. If we suppose that the p_i are independent – though their sum must be 1 and they co-exist in many minerals – then Eq. (5) gives the variance

$$\sigma^2(S_\rho) = \sum_i S_i^2 \sigma^2(p_i) \tag{6}$$

Thus, the composition causes in S_ρ the standard deviation

$$D_c = \sigma(S_\rho) \tag{7}$$

The interfering effect of composition is properly defined, we consider, with the measure

$$E_c = D_c/S_\rho \tag{8}$$

D_c and E_c, in addition to S_ρ, have been calculated in Table II for the case we have been using as an example.

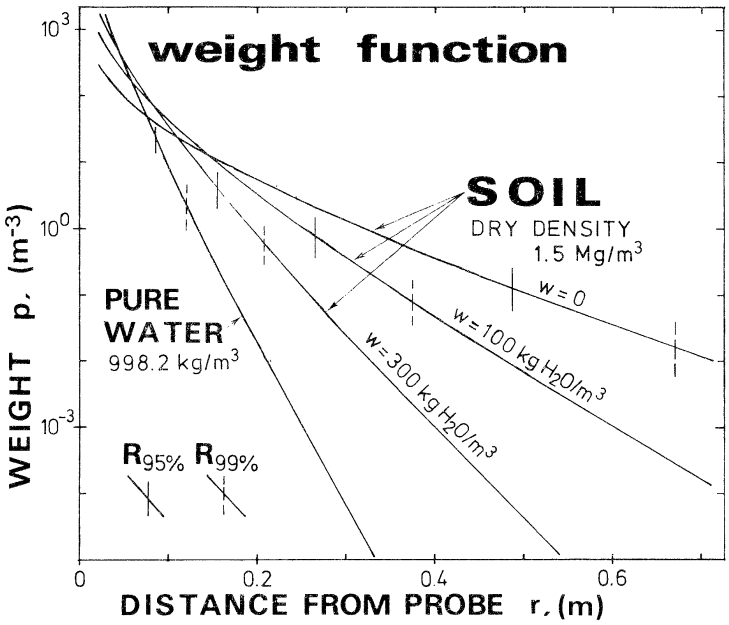

FIG.1. The weight function p(r) calculated with the model of a "point" probe in homogeneous media: water and a soil with three values of moisture. The soil has the composition of the earth's crust – see Table I – with an H content of 1400 mg/kg. The radii of the 95% and 99% influence spheres around the probe are shown.

5. ILLUSTRATION OF SAMPLE VIRTUALLY GAUGED

The region measured by a neutron gauge is often represented as a sphere [14]. A soil hole, surface, etc., however, considerably deforms this picture [13], even for a "point" probe. There have been few attempts to determine a weight function [15] appropriate for the real geometry of measurement, while the subsurface gauge calculations with a finite sphere, in which the probe is in the centre, have been common.

For our basic soil composition with w = 100 kg H_2O/m^3 the slowing-down effect of water below 100 keV represents about 90% of the total slowing-down power. We can rather definitely define the weight function p by considering the number of hydrogen scatterings during the slowing-down of the detected neutrons: we establish that the ratio of the number of these scatterings in a small soil element dV to their total number is given by pdV [14]. In the model of a point source in homogeneous medium we have

$$\int_0^{R_t} p 4\pi r^2 \, dr = t \qquad (9)$$

where t = 1 when $R_t = \infty$. The solution R_t of Eq. (9) is the radius of the 100 t% influence sphere in moisture gauging.

The weight function p decreases very rapidly with the distance from the point probe – see Fig. 1. In the calculations, a 3-group diffusion model has been used [14].

In Fig. 1 the radii of the spheres that have an influence of 95% and 99% in the counting rate are presented. For the radius of the 95% region of influence, in the case of a point probe in a Danish soil (composition near that of the earth's crust) which has a hydrogen content 0.326%, we have the formula

$$R_{95\%} = \frac{4.3}{L_1^{-1} + L_2^{-1}} \qquad (10)$$

Eq. (10) is based on the observation presented in Ref. [14] concerning the relation between 3-group and 2-group diffusion results. L_1 and L_2 are the slowing-down length and thermal diffusion length, respectively. Their formulae can be found in the references.

6. SIMULATIONS OF GAUGE

The exact theory of a neutron gauge is the transport theory [16]. Its normal form and the combined one [16] can be used. The latter gives the probability of detecting a neutron. Both are needed for exact determination of the weight function – Section 5 and Ref. [14].

We have found such a model to calculate the fitting to any measured data which seem to be useful. The rather poor data that must be used in calibration today are presented in Fig. 2. The data were neasured with the Danish subsurface probe BASC and a Miniscaler in an access iron tube.

In our model we use a point source in an infinite medium and calculate with a 3-group diffusion model. The detector is a sphere at a certain distance from the source and it absorbs all incoming thermal neutrons and part of the epithermal ones. The effect of the detector is taken into account by depressing the fluxes calculated in a homogeneous medium.

As soil parameters in our data we have had to use: (1) moisture, (2) heating loss, and (3) bulk density, but not the absorption of thermal neutrons, although we have made a certain effort with our facilities to measure the absorption cross-section, as has been determined elsewhere, e.g. Ref. [11]. As instrumental fitting parameters we had: (1) distance between source and detector; (2) radius of detector sphere; (3) multiplier for the calculated counting rate; (4) fraction of the detected epithermal neutrons; and (5) an additional constant term (it made fitting better).

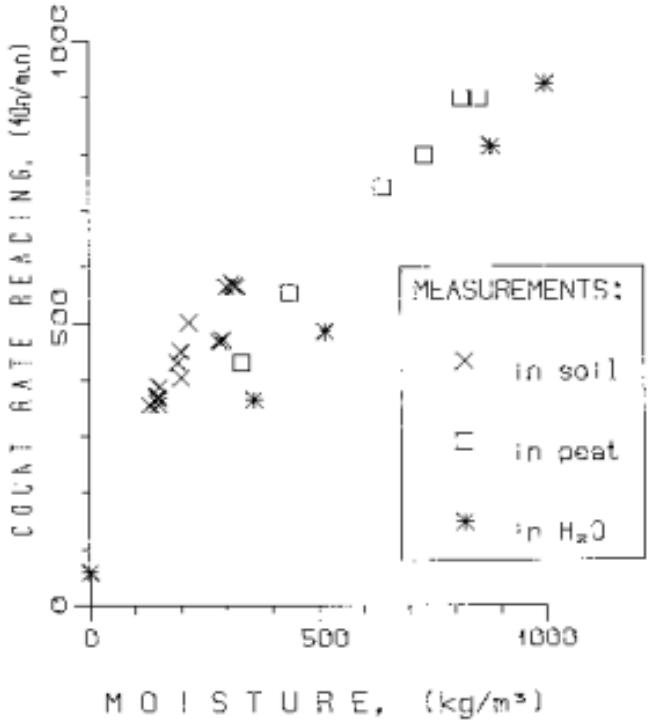

FIG.2. The present experimental data of subsurface gaugings using an iron access tube. The soil data were measured in the lysimeter of Helsinki university [17], at least 0.5 m below the surface of each soil column. The dry densities of these sandy soils are about 1500 kg/m³ and they have hydrogen contents from 0.3 to 0.5%. The samples for weighing were taken 0.5 m from the access tube. Peat measurements in field (dry density ≃73 kg/m³ and ash content ≃3%) may have suffered from moisture inhomogeneity. The samples were taken just around the access tube. In H_2O measurements in ice and snow it required a considerable effort to make the gauge function in the cold. The zero moisture value was obtained with the probe in air.

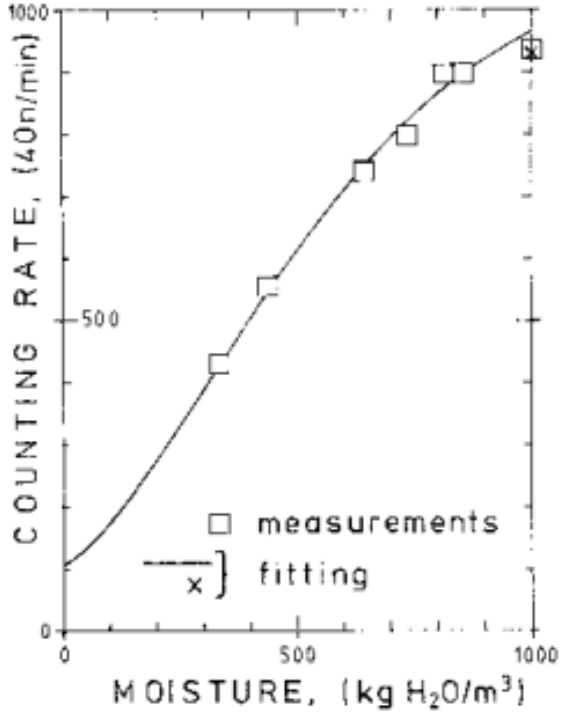

FIG.3. The optimized calibration to the peat and water data of FIG.2. The computer model and parameters are described in the text.

A fitting with our model is shown in Fig. 3. For the geometric fitting parameters this gave the value 6.2 cm for the distance between source and detector sphere, and 1.38 cm for the radius of the sphere; these values are in accordance with the probe measurements.

The trivial geometry and incompatible theory need improvements in our simulation. The best experimental data for the calibration can be achieved by making measurements in a laboratory with homogeneous materials which have certain elemental compositions. We prefer to get different "moisture" contents by mixing materials which possibly contain water of crystallization.

The simulation depends considerably on gauge type, and on special features in the soil geometry (surface against air, etc.).

ACKNOWLEDGEMENT

In preparing the fitting program we received considerable help from the Institute of Mathematics of Helsinki University, who allowed us to use a program they had developed for searching for the maximum of a non-linear parametric representation, see e.g. Ref. [18].

REFERENCES

[1] LINSLAY, R.K., Jr., KOHLER, M.A., PAULUS, J.L.H., Hydrology for Engineers, McGraw-Hill Kogakusha, Ltd., Tokyo (1975) 192.

[2] SEGAL, Y., NOTEA, A., SEGAL, E., "A systematic evaluation of nondestructive testing methods", Research Techniques in Nondestructive Testing (SHARPE, R.S., Ed.) Vol. 3, Academic Press (1977) 293.

[3] ARTSYBASHEV, V.A., Yaderno-Geofizicheskaya Razvedka, Atomizdat, Moscow (1980) 146.

[4] INTERNATIONAL ATOMIC ENERGY AGENCY, Neutron Moisture Gauges, Technical Reports Series No. 112, IAEA, Vienna (1970).

[5] GARDNER, R.P., ELY, R.L., Jr., Radioisotope Measurement Applications in Engineering, Reinhold Publishing Corp., New York (1967) 254.

[6] KASI, S.S.H., Consideration for evaluation and design of radiation gauges, Isotopenpraxis, to be published.

[7] FILIPPOV, E.M., Yadernaja Geofizika, Vols 1 and 2, Izdatelstvo "Nauka", Sibirskoe otdelenie, Novosibirsk (1973). [a] Vol. I, p.173; [b] Vol. II, p. 21.

[8] KASTNER, J., "Effects of soil and water on cosmic ray", Extra-Terrestrial Matter, Northern Illinois Univ. Press (1969) 265.

[9] ØLGAARD, P.L., "Neutron and gamma gauges, their design and application", Radiation Engineering in Academic Curriculum (Proc. Study Group, Haifa, 1973), IAEA, Vienna (1975) 147.

[10] CAMERON, J.F., "Nucleonic soil density and moisture gauges", Nucleonic Techniques and Mineral Resources (Proc. Symp. Buenos Aires, 1968), IAEA, Vienna (1969) 81.

[11] COUCHAT, Ph., et al., "The measurement of thermal neutron constants of the soil; Application to the calibration of neutron moisture gauges and to the pedological study of soil", Proc. 4th Conf. Nuclear Cross Sections and Technology, CEA-CONF-3167, USA, 3– 7 March 1975.
[12] KRAUSKOPF, K., Introduction to Geochemistry, McGraw Hill Book Co. (1967) 639.
[13] COUCHAT, Ph., Mesure Neutronique de l'Humidité des Sols, Rep. FRNC-TH-566, Toulouse (1974).
[14] KASI, S.S.H., An attempt to calculate correctly the region of influence in gauging moisture with neutrons, Int. J. Appl. Radiat. Isot. 33 8 (1982) 667.
[15] FEARON, R.E., Neutron well logging, Nucleonics 4 6 (1949) 32.
[16] BELL, G.I., GLASSTONE, S., Nuclear Reactor Theory, New York (1970).
[17] VAKKILAINEN, P., Maa-alueelta Tapahtuvan Haihdunnan Arvioinnista, Acta Univ. Oul. C 20.1981, Oulu (1982) 24.
[18] VIRKKUNEN, J., A Cyclic Coordinate Ascent Algorithm in Linearly Constrained Nonlinear Optimization, Rep. HTKK-MAT-A57, Espoo (1974).

Text V

NHP-SEMINAR ON WATER IN THE UNSATURATED ZONE — SPATIAL VARIABILITY

29-31.1.1986, Agricultural University of Norway, As, Norway

SPATIAL CORRELATIONS OF THE SOIL QUANTITIES RELATED WITH THE NEUTRON GAGE OF SOIL MOISTURE

Servo Kasi
Helsinki University of Technology
Otakaari 1, SF-02150 Espoo, Finland

Determination of the soil moisture content quantities (parameters), those that absolute and permanent (porosity, field capacity, wilting point) especially, require the accurate calibration of their gages. The soil moisture content (the loose water per volume unit) can be determined accurately by nuclear gages. — In addition of soil moisture parameters we have the neutron gage soil parameters. We are using three in a good calibration. The spatial variability of a quantity is proposed to be analyzed by its correlation (or autocorrelation) function. This measure of the spatial dependence between the values of the parameter is useful.

1. Introduction

Soil is a porous matter. It varies considerably in porosity, in texture and chemically. Except mineral as rock it may be organic, or it has an organic matter content. Soils usually comprise water. It may be even strongly chemically bound or loose.

Soil moisture, movable water of soil, has parameters:

PARAMETER	ITS FIELD GA(U)GE
Moisture content	Neutron gage
Binding of water	Tensiometer

The second column above tells the means by which we can measure the parameters accurately in field. Sometimes it is argued that these gages can

be replaced with each others. However, dependence of water content on the binding (presented, e.g., as the pF value) is not at all unique.

Table 2. **Permanent parameters in soil profile. Moisture contents, measured by neutron gaging**

Parameter	Auxiliary gaging
Porosity	
Field capacity	
Wilting point	tensiometer use

The parameter porosity is the moisture content of saturated soil. The field capacity and wilting point often mean the moisture contents of these soil moisture states (the binding — a pressure quantity — is then fixed). These three quantities of soil moisture: porosity, field capacity and wilting point moisture contents are all permanent soil parameters. They are also all absolute values of soil moisture.

The soil moisture contents of table 2 are necessary in order to determine proper actual soil moisture quantities (e.g. SMD) from temporally varying soil profile moisture content data.

2. Good calibrations for n and γ gages

The author has material for these both, but a lot of works is to be done in this important task. For both the gages I have theoretical models. The gage parameters of the models are to be determined. They are probe and access tube dependent. A n method and fitting to data, that of *Kasi, Immonen and Saikku, 1983*, has been described in the FAO/IAEA symposium. The γ calibration curve given by a Nordic factory is a falling straight line. The response function of *Czubek, 1983* still accepted, has been used to fit to the results of water, a sand and clay. The calibration curve obtained is clearly curved. The soil moisture and density values by weighing were determined from nondestructive, but not very representative samples. In Appendix,

there we have some substances to use in accurate measurements. When doing those we are gaging moisture (or H content) in chemically known and, should be, homogeneous matters.

For the use of the good calibrations we should have the following neutron gage soil parameters (*Hooli and Kasi, 1975*):

1. bound hydrogen content,

2. thermal n absorption cross section Σ_a — *Couchat et al., 1975*, *McCulloch and Wall, 1976*, and *Czubek et al., 1983*, show three different methods for its determination,

3. soil density.

The two first should be measured from soil samples extracted when the access tube is inserted in soil. Σ_d by *Couchat, 1983*, is less preliminary a quantity than the hydrogen content. The density can be gaged by the γ probe. When a parameter is lacking, it is to be estimated. The estimation may be done by using results from nearby places or known value of the same type soil.

3. Spatial correlation of parameter

How does a quantity vary in field? E.g. the water content of field capacity is different in clay, sandy soils and peat. *Webster, 1983*, has represented a review of the correlation measurements in soil, a lot of which he has been measuring with. We know that the soil types make combined areas, but also vertical layers. The soil types have subtypes. The hydrological nature of soil is described by means of adequate parameters. The soil moisture contents of table 2 are such.

Set x to be a soil parameter. The spatial fluctuations of x can be analyzed by the correlation C and variation V functions, *Journel and Huijbregts, 1978*, *Yevjevich, 1972*, illustrating them with the correlograms and variograms. Along a straight line, having equally separated sites of samples, for the correlation function C we have the estimate

$$C_k = \frac{s_k^2}{\sigma_E^2}, \quad s_k^2 = \frac{1}{n-k-1}\sum_{i=1}^{n-k}(x_i - \bar{x})(x_{i+k} - \bar{x}), \quad \bar{x} = \frac{1}{n}\sum_{i=1}^{n} x_i. \quad C_0 = 1,$$

where n is the number of samples, taken or direct gaged. $\sigma_E^2 = s_0^2$ is the value of the nonbiased estimate of the variance as well as $\bar{x}$ is the estimate of the mean value of the statistical distribution of x. The function V is estimated by

$$V_k = \frac{1}{2(n-k)} \sum_{i=1}^{n-k} (x_{i+k} - x_i)^2.$$

x is a continuous variable on its line. It can then, too, be integrated over its line when we know the distribution.

In the literature concerning the unsaturated horizon I have found few examples of use of the C_k formular above: the analysis by *Warrick and Nielsen, 1980*, from the data of Gajem and Warrick, and the application of *Moutonnet, Perrochet and Couchat, 1983*. In the former $C_k \neq 0$ when k covers not more than 4 m. In the latter example three hosts in Aix find no horizontal correlations in the two n gage soil parameters investigated. These were Σ_a and Σ_d. Their soil was too homogeneous and the accuracy of the neutron data device of *Couchat, et al., 1975*, too poor. It is so poor and the device so slow, that this result does not recommend dense determinations of the n gage soil parameters. Their measurements, in the 100 m × 100 m square area along two crossing lines, only faintly tell that in the surface layer 0...30 cm the bound hydrogen content is larger than in the layer 30...60 cm. This is seen from the values of Σ_d.

The parameters can vary in large. E.g., the diffusion cross section Σ_d of peat is about 3 times bigger than in the Cadarache arable land we circulated. In Cadarache the hasty French should have measured the neutron soil parameters more widely, — or perhaps more densely than at 2 m intervals.

Below I have a fictive example of a sample line in Nordic uncultivated soils. I have selected as a parameter the loss of mass when the soil piece is heated to 900 °C and hold there since its mass remains constant. Sample places have the interval of 10 m (and because n = 35, the line does not extend, e.g., over our countries).

clay sand peat sand

7 9 8 10 7 4 5 3 4 7 50 75 80 90 82 50 6 3 7 4 0 100 10 4 3 3 0 5 2 3 4 11 15 60 2

This is an exercise, please; the unit is % by weight. The correlation function, you then obtain, has both positive and negative values intervals. The nugget value of the function V is large.

The simple variation function V has the advantage that the unexplained zero variance the nugget is found out. Also the range of the positive correlation is clearly seen. The correlation function C tells well at which distances the positive or negative correlations occur and which are their strengths.

Instead of the preceding presentation, where the formulas are along a line, we generally, and often, have a quantity $x(\mathbf{r})$, where $\mathbf{r}$ is the space vector, two- or three-dimensional. x is a scaler. $C = C(\mathbf{r})$ (and $V = V(\mathbf{r})$) may be at best a tensor, but its vector components seem to be most informative. In many cases the tensor is isotropic, but mostly in horizontal planes. A horizontal plane is the "projection" of the unsaturated soil layer. We have the area quantities and the spatial ones.

References

Couchat, Ph., 1983, Les applications de la methode neutronique dans la recherce agronomique, "Isotope and Radiation Techniques in Soil Physics and Irrigation Studies 1983", IAEA, p. 509

Couchat, Ph., C. Carre, J. Marcesse, J. Le Ho, 1975, 4. Conference on nuclear cross section and technology, CEA-CONF-3167, p. 516

Czubek, J. A., 1983, Advances in gamma-gamma logging, Int. J. Appl. Radiat. Isot. **34**(1), p. 153

Czubek, J. A. et al., 1983, Measurement of thermal neutron absorption cross section, Int. J. Appl. Radiat. Isot. **34**(1), p. 143

Hooli, J., S. Kasi, 1975, Field measuring techniques, Nordic IHD Report No. 9, p. 64

Journal, A. G., Ch. J. Huijbregts, 1978, "Mining Geostatistics", Academic Press, N.Y.

Kasi, S., J. Immonen, K. Saikku, 1983, Some consideration for soil moisture gauging with neutrons, "Isotope and Radiation Techniques in Soil Physics and Irrigation Studies 1983", IAEA, p. 479

McCulloch, D. B., T. Wall, 1976, Nucl. Instr. Methods **137**, p. 577

Moutonnet, P., P. Perrochet, Ph. Couchat, 1983, Variabilite spatiale caracteristiques neutroniques d'un sol: incidence sur la determination des courbes d'etalonnage des humidimetres a neutrons, "Isotope and Radiation Techniques in Soil Physics and Irrigation Studies 1983", IAEA, p. 41

Warrick, A. W., D. R. Nielsen, 1980, Autocorrelation and Spatial Analysis, Ch. G, in Applications of Soil Physics, ed. *D. Hillel*, Academic Press, p. 319

Webster, R., 1983, Elucidation and characterization of spatial variation in soil using regionalized variable theory, "Geostatistics for Natural Resources Characterization", ed. *Verly, G.*, et. al., Part 2, D. Reidel Publ. Co., p. 903

Yevjevich, V., 1972, "Stochastic Processes in Hydrology", Water Resources Publications, Colorado

Appendix. Substances for calibration

Substance	Density kg/m³	Phase changes °C
$MgSO_4 \cdot 7\,H_2O$	1677	150 ($\Rightarrow MgSO_4 \cdot H_2O$)
$Na_2SO_4 \cdot 10\,H_2O$	1464	32,4 and 100 ($\Rightarrow Na_2SO_4$)
$KAl(SO_4)_2 \cdot 12\,H_2O$	1757	92,5 ($\Rightarrow KAl(SO_4)_2 \cdot 3\,H_2O$)
$NaAl(SO_4)_2 \cdot 12\,H_2O$	1675	61
$Na_2CO_3 \cdot 10\,H_2O$	1440	33.5 ($\Rightarrow Na_2CO_3 \cdot 9\,H_2O$)

Except measuring in these substances, when pure, we can combine:

CRYSTAL WATER SUBSTANCE + QUARTZ
(or)+ any FELDSPAR

And we can also make mixtures:

SUGAR + pure QUARTZ (or FELDSPAR)

Text VI

SOIL WATER CONTENT MORE ACCURATELY BY NUCLEAR METHODS

Servo S. H. KASI
FIN-04230 Kajavankatu 6 B 45, Kerava, Finland

ABSTRACT

TDR (Time domain reflectometry) is — very popular today — a useful instrument to determine e.g. liquid water content in soil and snow, as also other capasitive measurements are in many cases. Many years neutron measurements have been used to determine the total water content. TDR depends on temperature and chemical bindings of matter, but neutron and gamma measurements almost not at all. Precision of neutron gage result is excellent. Uncorrect calibration can, however, cause remarkable systematic errors. Hydrogen content of dry soil, density (gamma gage determined) and thermal absorption cross section must be known in calibration. Gamma measurement can be used to determine water content, when density changes are caused by moisture. Narrow horizontal gamma beam gives vertical resolution in mm...cm class. Snow attenuates today, in addition to the natural gamma-radiation, also that of cesium in soil. Using both the radiations we measure the water equivalent and soil water content. The narrow beam attenuation ($E_\gamma > 90$ keV) and the last ray measurements depend on temperature and chemical bindings not at all.

DIELECTRIC CONTRA NUCLEAR METHODS

Materials consist of nuclii and electrons; the latter mainly are around the nuclii. The free electrons or mobile charged atoms (positive or negative ions) influence electric conductivity. Dielectricity of matter is determined by polarizability of the charges of atom or molecule. The positive charge of nucleus and the negative charge of electron cloud only around in the noble gases remain cocentric in any practical conditions. Variability of polarizations of matter is seen in variation of dielectric constant. Except of chemical composition it depends on temperature. In dry soils the dielectric constant varies 4...8 (Carlsson, 1998). Dielectric constant of water liquid is clearly higher, i.e. 82.19 at the temperature 15 °C and decreases with increasing temperature, 78.48 at 25 °C (Lück, 1964), see also Persson and Berndtsson (1998). However, for ice the dielectric constant is 3.2 (as well as it is low for with matrix bound water). Del Río and Whitaker (2000) consider the influence of porosity in electromagnetic operations as TDR in rigorous manner.

Neutron and gamma gages have been used for measurement of soil moisture, its water content. The displayed result of these meters may depend only on the atom composition of soil. In neutron and gamma gages the source

of radiation has been capsulated in two-layer steel shelter relatively small in size.

Chemical bindings in matter and such conditions as temperature do not influence neutron and gamma measurements almost not at all. On the contrary they influence essentially electronic soil meters as TDR (Time Domain Reflectrometry), e.g. Carlsson (1998), Persson (1999) and Petersen et al. (1995).

Neutron and gamma used in the meters of water content have the energies 100 keV - 10 MeV; also smaller-energy photon sources can be used. Chemical binding energy is seldom above 10 eV. The binding energies of outer shell electrons or the ionisation energy of atom are in the same order. The binding energy of inner shell K-shell electron is larger (13.6 eV for hydrogen, 7 keV for iron, 9 10^4 eV for lead), but the iron atom is largest among common elements and the number of K-shell electrons is only 2.

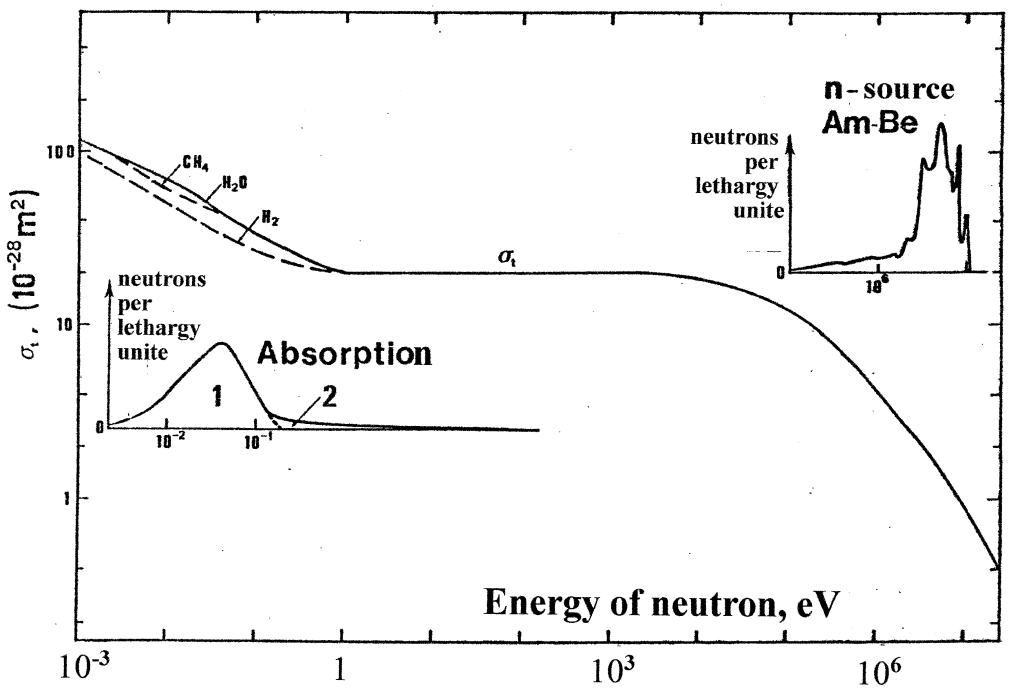

Fig. 1. Total cross section $\sigma_t(E)$ of hydrogen in H_2O and two other molecules over all neutron energies, E. On the right above the spectrum of source neutrons. On the left the energy distribution of absorption of thermal neutrons in the Maxwell presentation (1) and of epithermal neutrons (2) in homogeneous infinite mineral soil. Lethargy $u = ln\ E + u_0$.

Fig. 1 illustrates certain essential features of neutron measurements. The main curve σ_t is the cross section with which a hydrogen atom catches neutrons. The Am-Be source of neutrons is mainly used today, though the neutrons of the relatively expensive AmLi source had more appropriate energy for many moisture gagings and those of Cf source also, but less appropriate. Hydrogen atom mainly scatters neutrons and the source neutrons slow down just in the hydrogen scatterings. For AmBe-source about 19 hydrogen scatterings slow

down neutrons to be thermal. The detector of thermal neutrons or of a little higher energy epithermal neutrons has been set near the neutron source. The hydrogen atoms, when slowing down neutrons, keep them near the source and detector.

CALIBRATION OF GAGES

Calibration of soil moisture meters (and any meter) demands very accura-

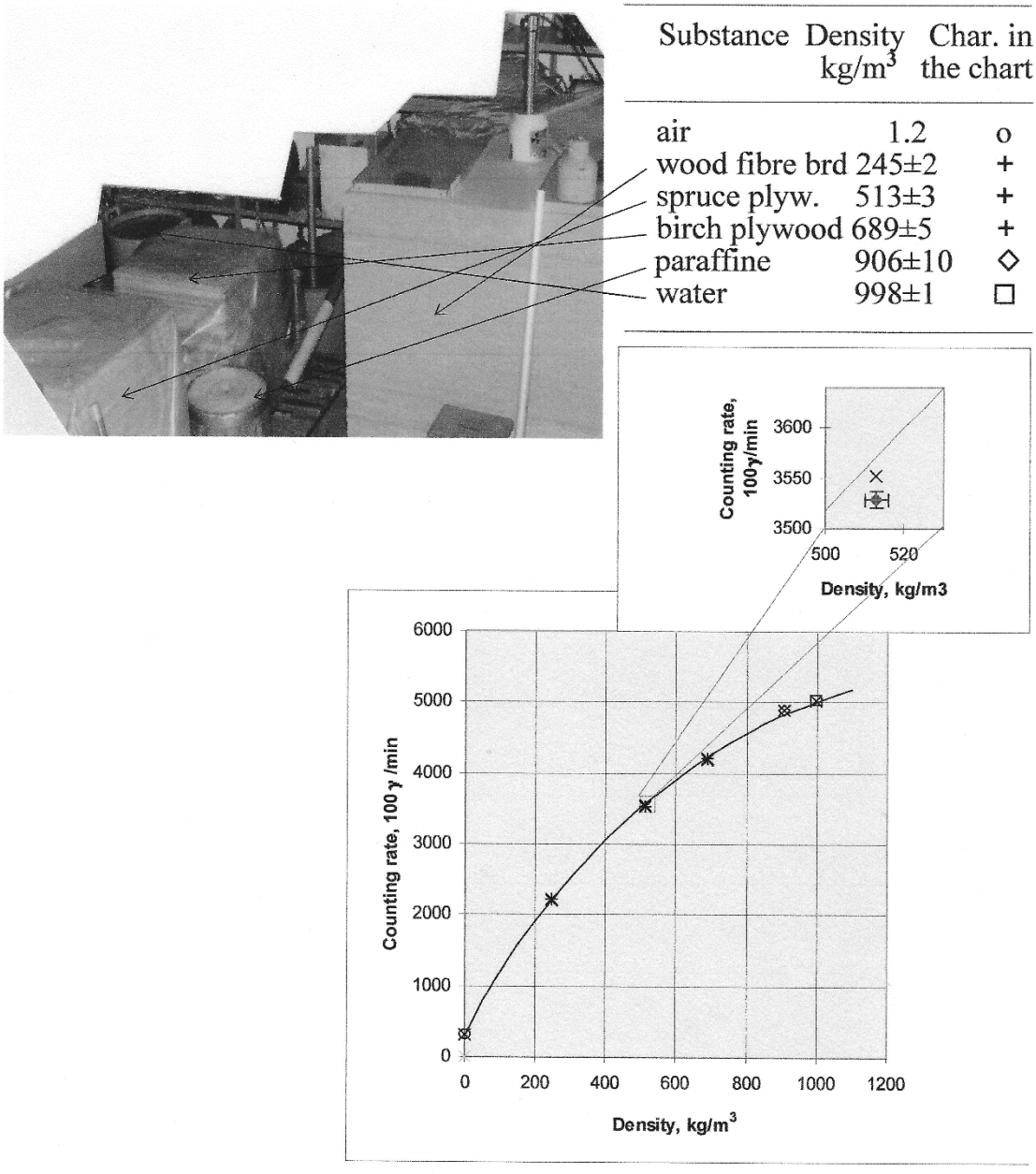

Fig. 2. Calibration of small-density cesium-137 gage. x are results of fitting calculation (Kasi, 1988) for the calibration substances used. Curve is for peat.

tely fulfilled conditions. They generally can be achieved only in laboratory. Kasi (1988) tried to show the results of good calibration of a gamma meter using capsulated cesium-137 source and homogeneous materials, Fig. 2, which cover the whole range to be measured with the gage. The accuracy is better than 1 %. That the fitting in the extraction of Fig. 2 is not in the error limits of measurement, shows that the calibration can be improved. The inaccuracy is probably caused by rough theoretical model.

The instrument above is applicable for peat soils and also for snow density measuring. It can be used for all substances, in which the density is below 1200 kg/m^3. In 1984 during the field excursion of the Fifth Nothern Research Basins Symposium a similar gauge was presented by Kasi for snow density gaging, but it has a smaller probe than the peat instrument.

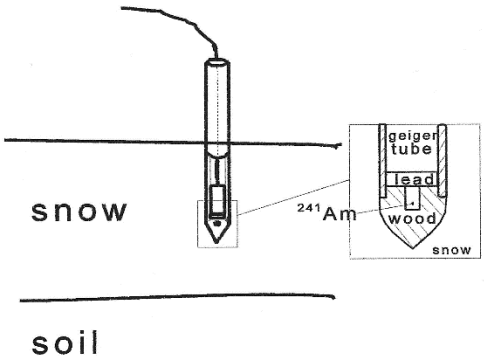

Fig. 3. Cheap snow density gage using 60 keV americium-241 gamma source.

Gamma measurement can be used to determine water content, when density changes are caused by moisture. Narrow horizontal gamma beam gives vertical resolution even below 1 cm (Hooli and Kasi, 1975). When the photon energy $E_\gamma > 90$ keV then even lead cannot cause any chemical effects in γ-photon interactions. In the interesting work (1986) Touma and Vauclin determined water content by the ^{241}Am photon attenuation.

The method for the good calibration of neutron gage of moisture has been described e.g. by Kasi (1986, 1988). Hydrogen content of dry soil, density (gamma gage determined) and thermal absorption cross section must be known. These quantities can be determined when the access tube for measurements is installed, from soil samples, or using auxliary gagings in the access tube, e.g. gamma-gaging for density profile determination. The theory of n-measuring is more complicated than that of γ-measuring, because the number of scatterings is much bigger. However the rough three-group diffusion calculation is probably as good as the gamma-theory used in the example above. The parameters of the theoretical model of the gage can be determined with the same kind of method as in the figure 2. I have tried to perform such accurate laboratory measurements but the proposals for good calibration materials are the only steps in the way to progress. The practical use of neutron gages of soil moisture has already many decades. I state that the results of these moisture measurements have unnecessary systematic errors.

RADIATION SAFETY

The permissible dose rate for a person in the radioactive work (in the nuclear reactors, hospitals, industries, etc.) is 20 mSv/a (maximum mean in 5 years) and for a member of population it is 1 mSv/a. The radiation sources of the soil moisture and density measurements are so strong that their users and, of course, their preparers, must be under radiation dose control. However, these sources are so small that the dose of the user is easily at the level of the common person and therefore almost not at all above the level caused by natural background radiation.

ACTUAL MEASUREMENTS

Kasi (1998) shows how deposition of cesium-137 after Chernobyl catastrophy is possible to utilize, because it forms a gamma plane source close to soil surface. About in half of the Nordic countries the intensity of cesium radiation is in the order or above the higher-energy radiation of potassium-40. With these two types of radiation (measured in airplanes, terrain tops with sight onto ground below, on snow moving vehicles or in certain points just above snow) snow water equivalent and moisture content near soil surface can be measured repeatably in any time during winter. These measurements depend not at all on temperature and chemical bindings of atoms, because the 662 keV of cesium and 1460 keV of potassium sources are also the energies to be detected in these measurements, and because the contribution of scattered photons is itself very small.

The theoretical consideration of Kasi (1998) used the form $D=D_0 \cos\theta$ of the so-called detector function for the 6 Na(Tl) scintillators. Recently Allyson and Sanderson (1998) have the result which shows that the form $D=D_0 \cos\theta + D_1$ is more appropriate. However $D_1 < D_0$. This improvement of Kasi (1998) treatment does not change any essential in the considerations above and in Kasi (1998). Earlier also the case of the constant detector function has been treated, because it is a rough theory in the cases of small cylinderical detectors.

CONCLUSION

Temperature and chemical bindings have less effects in n- and γ-gages. Certain n- and γ-arrangements have these effects not at all. Their possible small effects in n-gages are eliminated when epithermal neutrons are gaged. In the horizontal-beam γ-measurements and when surveying and utilizing γ-radiation which without scatterings comes from radioactive nuclides in soil, the temperature and chemical bindings have no disturbing and deteriorating effects.

γ-gaging with terrestrial ^{137}Cs 662 keV radiation transmission technique, hopefully only in these years applicable, is useful in snow and probably in, generally problematic, surface soil moisture surveying.

REFERENCES:

Allyson, J. D. and Sanderson, D. C. W. 1998. Monte Carlo simulation of environmental airborne gamma-spectrometry. *J. Environ. Radioactivity 38*, 259-282.

Carlsson, M. 1998. *Sources of errors in time domain reflectometry measurements of soil moisture*. SLU (Sveriges landbruksuniversitet), avdelningen för lantbrukets hydroteknik, avd.medd. 98:5

del Río, J. A. and Whitaker, S. 2000. Maxwell's equations in two-phase systems I: Local electrodynamic equilibrium, *Transport in Porous Media 39*(2), 159-186

Hooli, J. and Kasi, S. 1975. Field measuring techniques. In: *Soil water distribution --- a state of art report*. Danfors, E. (ed.). Nordic IHD report No. 9, Oslo 1975, 64-96

Kasi, S. 1986. Spatial correlations of the soil quantities related with the neutron gage of soil moisture, In: *Water in the Unsaturated Zone*, NHP-Seminar, Ås 1986, NHP-15, 113-118.

Kasi, S. 1988. Kalibrering av neutron- och gammamätare (Calibration of neutron and gamma gages, in Swedish). *Nordisk Hydrologisk Konferens*-88, Rovaniemi, NHP-22, Vol. 2, 278-282

Kasi, S. S. H. 1998. Determination of water content in soil below the ground surface using radioactive cesium and potassium. *XX Nordic Hydrological Conference,* Helsinki, NHP-44, Vol. II, 413-422

Lück, W. 1964. *Feuchtigkeit: Grundlagen, Messen, Regeln* (Moisture: basics, measuring, control, in German). R. Oldenbourg, 296 pp.

Persson, M. 1999. *Conceptualization of solute transport using time domain reflectometry, Department of Water Resources Engineering*, Lund Institute of Technology, Lund University, Coden: LUTVDG/(TVVR-1025)/(1999).

Persson, M. and Berndtsson, R. 1998. Texture and electrical conductivity effects on temperature dependency in time domain reflectometry. *Soil Sci. Soc. Am. J. 62*, 887-893.

Petersen, L.W., Thomsen, A., Moldrup, P., Jacobsen, O.H. and Rolston, D.E. 1995. High-resolution time domain reflectrometry: sensitivity dependency on probe-design, *Soil Sci. 159*(3), 149-154

Touma, J. and Vauclin, M. 1986. Experimental and numerical analysis of two-phase infiltration in a partially saturated soil. *Transport in Porous Media 1*, 27-55

Text VII

FIRST RADIOCESIUM PROFILE AND SNOW COVER MASS MEASUREMENTS

S.S.H. Kasi

Hydrological Office
Water and Environment Research Institute
P.O. Box 436, SF-00101 Helsinki, Finland

ABSTRACT

The profile of cesium-137 in soil can be gauged nondestructively. In the measurements a scintillation detector has been set in tube or hole in soil (peaty incl.) at different depths from the ground. Radiocesium of Chernobyl (and also the earlier) makes almost a plane at the surface of any soil. – A scintillator or semiconduction detector can be set above the snow cover and the snow attenuation of cesium gamma can be measured. This method is very sensitive to the snow cover mass thickness, i.e., to its water equivalent. The results of the first measurements and evaluations are presented. In relatively large regions some decades the cesium method is more sensitive than its traditional counterpart which have been the most effective when the radiation of potassium-40 is used. The very thick snow covers may attenuate too much. The cesium-137 layer is also at the surface of any swamp.

KEYWORD

Radiocesium; Chernobyl; soil; cesium-137 profile; swamp; peatland; snow; water equivalent.

INTRODUCTION

The distribution and behaviour of cesium-137 from atom bomb experiments in the 50's and 60's have been examined by taking samples and analyzing them, reviewed by Coughtrey and Thorne (1983). Similar works have been done after the catastrophe in Chernobyl. Its fallout had, in addition of ^{137}Cs, also the shorter living cesium isotope ^{134}Cs. The ratio of the activities of these isotopes of the fallout (7.6.1988 the activity of ^{134}Cs is 31 % of that of ^{137}Cs) have been used to separate the old (2 kBq/m^2) and new contamination from each others. Arvela, *et al.* (1987) have determined the areal distribution of the excess (in 1.10.1986) of external dose rate and estimated ^{137}Cs activity. The maximal excess of the external dose rate was 0.35 µSv/h, estimated ^{137}Cs-activity 100 kBq/m^2, and 52 kBq/m^2 that of ^{134}Cs, then.

The vertical distribution (profile) of cesium-137 can be determined by the nondestructive measurements. In this work a scintillation probe measures it from a tube or a hole of soil or bog. Because radiocesium seems to be very close to the surface of any soil, it can be used as a gamma source for the measurement of snow cover mass. The first experimental results to determine the water equivalent with this actual method are the second subject of this paper.

PROFILES

The scintillation probe B in Fig. 1 in the tube or hole is transferred through the soil surface in small intervals. The counting rate of the photons arriving directly from ^{137}Cs atoms is counted. The photons are catched by the scintillation crystal (at the depth d in Fig. 1). The counting rate depends mainly of the vertical profiles of the ^{137}Cs atoms and that of soil density. For the present only some rough calculations of the cesium profile, using very approximate density profiles, are performed. However, the profiles, already calculated, seem to represent that of the ^{137}Cs atoms rather accurately.

The good accuracy of the cesium-137 profile is obtained, when the accurate density profile (that usually is continuous) is in use. The solution of the inversion problem: seeking the ^{137}Cs profile, is found by minimizing the difference between the measured distribution and simulated distribution of the counting rate. Today I do this optimization manually. It is cumbersome. The same is automized easily. It seems, that the development of the counting rate and density (profiles) according to the polynomials of Laguerre is for help when the solution is sought.

Schell and Massey, in IAEA Symposium 1987, shew that the bomb cesium (over 20 years old) in the three bogs in USA is in the first 15-20 cm from the surface. One of the bogs has the ^{137}Cs profile differing from the others. In this bog the ^{137}Cs atoms have diffused, except down, in so high portions up, that in the uppermost new layers and in those, born during the fallout, the concentrations are equal. I have made a relatively rough measurement in a hole of a fresh swamp. There and in the other soils the calculation gives a sharp peak at the depth 0...2 cm. According to my very uncertain results, in the fresh swamp in the depths 2...25 cm there is a tail of over 50 % of ^{137}Cs atoms. The most accurate measurement I made in soil moisture tubes which are in mineral soil. There is 80 % of the atoms in the peak (0...2 cm) and maybe all the atoms above the depth 12 cm.

Using a good instrument and long measuring times the very accurate ^{137}Cs profiles can be achieved. Using the multichannel analyzer the accurate ^{134}Cs profiles can be obtained, as well, and the old ^{137}Cs can then be separated from the new one.

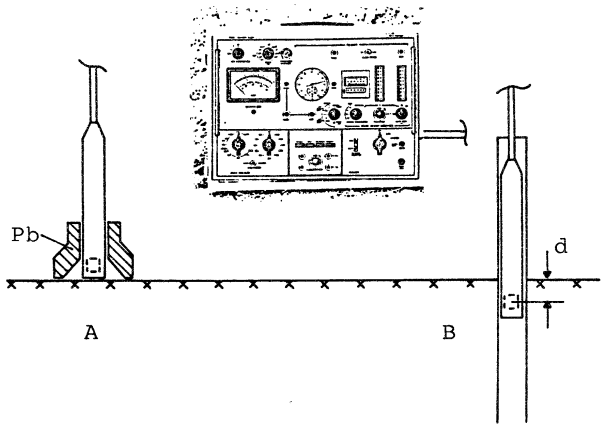

Fig. 1. Radiocesium measurements of the author.

SNOW COVER MASS

The radiocesium of Chernobyl (and also the earlier) makes almost a plane on the surface of any soil. The attenuation of the radiation is very sensitive to the snow cover mass, i.e., to its water equivalent, z in Fig. 2. Then

$$m = t_w z = t_s z_s \tag{1}$$

is the areal mass density of snow. t_w = 1000 kg/m^3. t_s is the mean density and z_s the thickness of snow.

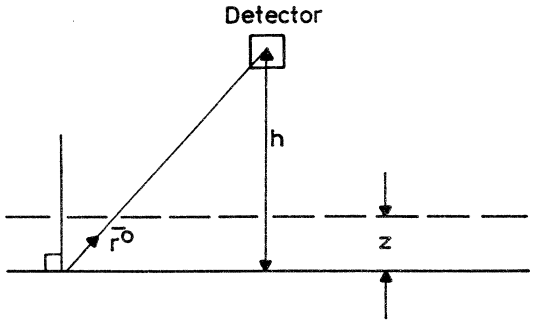

Fig. 2. The gamma measurement of snow cover mass distribution.

In the gamma measurement we have the counting rate

$$R = 2\pi \int_h^\infty D(\bar{r}^\circ) I(\bar{r}^\circ) \exp(-\mu t_a r) dr/r, \tag{2}$$

where the effective mass attenuation coefficient

$$\mu = \mu_a + \left(\frac{\mu_w}{t_a} - \frac{\mu_a}{t_w}\right) \frac{m}{h}. \tag{3}$$

μ_w and μ_a are the mass attenuation coefficients of water and air, respectively.

t_a is the density of air.

$\bar{r}^\circ$ is the unite vector from point of the ground to the direction of the gamma detector. r is the distance between the point and detector.

The function $D(\bar{r}^\circ)$ is the detector area (perpendicular to the vector $\bar{r}^\circ$) times the probability to detect the photon.

$I(\bar{r}^\circ)$ is the intensity distribution of the counted photons at ground point.

The dependence of the intensity $I(\bar{r}^\circ)$ on $\bar{r}^\circ$ is determined by the radioatom distribution, soil density and, in a smaller degree, its elemental (H) composition. When the atoms are on the ground then $I(\bar{r}^\circ)$ does not depend on the direction of photon emission.

In Finland where the water equivalent in common is below 250 H_2Omm the measurement above the ^{137}Cs surface 30 kBq/m^2 is more accurate than that above the semi-infinite ^{40}K soil (Kasi 1988a, 1988b). Also the source of the ^{40}K gamma (1461 keV) radiation is often below the organic soil surface. For instance,

the bogs may attenuate the ^{40}K photons entirely. Though the cesium photons attenuate more, the cesium method (because the ^{137}Cs atoms are so near the soil surface) is now very useful.

For water catchment basin (the area A) the total snow mass

$$M = \int_A m \, dA$$

surely is an important quantity. For (e.g. the models of) any basin the mass distribution m is also useful.

I have performed the first experiments in the southern part of the fallout region in the central Finland. The curves in Fig. 3 are optimized to the experimental results. Kasi, 1988b, explains them in detail.

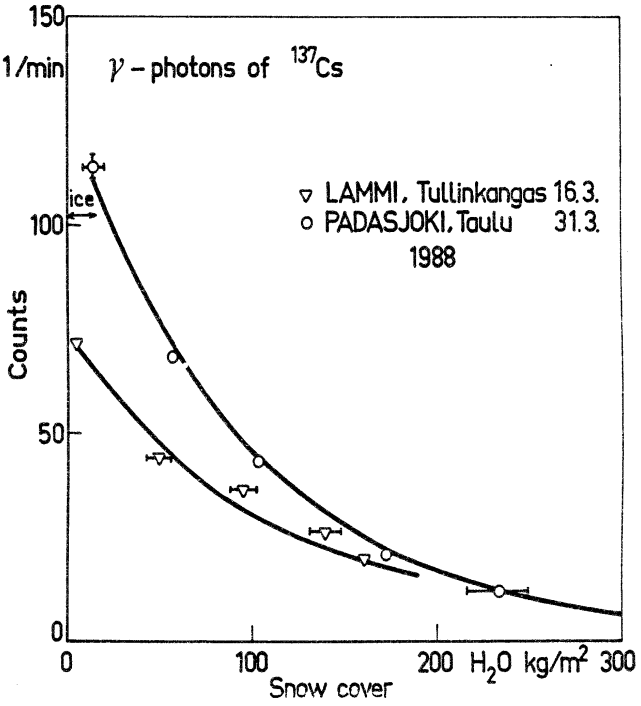

Fig. 3. Experimental evidence of the method

In these preliminary measurements with the probe A of Fig. 1 the scintillation crystal has a very minimal size, 13 cm^3. Therefore the counting rates in Fig. 3 are small. The sum volume of the crystals used in the aeroplane measurements in Finland is 25 dm^3. The sensitivity of the latter is almost 1000 times greater.

The gamma radiation above the ground can be measured in a vehicle in air or, e.g., on snow. The lead around the probe A of Fig 1 confines the directions of the incoming photons so that D(r°) is more optimal, and diminishes the radiation from the space. In the measurement the counts caused by the Compton scattered photons must be subtracted. They include scattered photons of the radon daughters. It is important that the window of the cesium-137 peak in scintillation measurements should be at so sufficiently high energies that the strong 609 keV photon of ^{214}Bi is not counted. Bristow, 1983, gives introduction in the spectrometry of the terrestial gamma radiation gauges.

REFERENCES

Arvela, H., Blomqvist, L., Lemmelä, H., Savolainen, A.L. and Sarkkula, S. (1987) Environmental gamma radiation measurements in Finland and the influence of the meteorological conditions after the Chernobyl accident in 1986. *STUK-A65*, Supplement 10 to Annual Report STUK-A55, Finnish Centre for Radiation and Nuclear Safety, Helsinki.

Bristow, Q. (1983) Airborne γ-ray spectrometry in uranium exploration. Principles and current practice. *Int. J. Appl. Radiat. Isot., 34, p. 199-229.*

Coughtrey, P.J. and Thorne, M.C. (1983) *Radionuclide distribution and transport in terrestial and aquatic ecosystems. A critical review of data. Vol. 1,* Chapter 7, Caesium. A. A. Balkema, Rotterdam, p. 321-424

Kasi, S.S.H. (1988a) Cesium-137 now for snow cover water equivalent measurement. To be published in a forthcoming issue of *IRPS-News, Newsletter of the International Radiation Physics Society.*

Kasi, S.S.H. (1988b) Cesium-137 for snow cover measurements. Submitted to *Nordic Hydrology.*

Schell, W.R. and Massey, C.D. (1987) Environmental radionuclide tracers of transport and diffusion in organic rich soil of the unsaturated zone. In: *Isotope texhniques in water resources development*, proceedings of the international symposium on the use of isotope texhniques in water resources development IAEA-SM-299, International Atomic Energy Agency, Vienna, Austria, p. 781-783.

Text VIII

PERGAMON

Radiation Physics and Chemistry 61 (2001) 673–675

Radiation Physics and Chemistry

www.elsevier.com/locate/radphyschem

Cesium deposition in soil and its effects

S.S.H. Kasi*

Helsinki University of Technology, P.O. Box 1000, FIN-02015 HUT, Finland

Abstract

Stabilization of the ^{137}Cs profile after 1986, has been observed in a mineral soil in southern Finland. An inversion calculation is presented to determine the ^{137}Cs profile from the photo-peak (662 keV) counting rate profile. Snow water equivalent (snow mass) can be accurately determined by using snow attenuation of the cesium radiation. When counting, at the same time, the 1461 keV photons of ^{40}K as well, it may then be possible to determine the surface soil moisture. The ^{137}Cs profile information is also important for the determination of its contribution to human dose.

Keywords: ^{137}Cs; Snow; Soil water; Dose

1. Cesium deposition and profiles in soils

In the 20th century, the natural environment has been contaminated by artificial radioactivity. In the northern hemisphere the atom bomb explosions increased the radioactivity, most significantly in the first half of the 1960s. In 1986 after the Chernobyl accident, the deposition of radioactive cesium increased (Fig. 1) considerably in large areas of Europe. In the southern half of Finland there was a 20 kBq/m^2 average deposition of ^{137}Cs.

The profile of ^{137}Cs was measured with a NaI(Tl) $\varnothing 1 \times 1''$ scintillator in steel tubes which were set vertically in soil (before 1986) or in holes in peat. Because cesium is an alkali metal, its ions easily find adsorption sites at soil grain surfaces. The time for its thorough fixation on surfaces of soil particles is more than one year (Konoplev et al., 1996). After that time the mobility of ^{137}Cs is similar to that of the stable isotope ^{133}Cs (Riise et al., 1990). The radiocesium profile seems to be stabilised in this way in forest soil in Lammi, southern Finland (Fig. 2). In 1986–1989 the first profile determinations in four other sites of mineral soil and in two peat sites in Finland were also made, and one in peat repeated in 1997.

2. Cesium profile determination

The profile concept assumes that the cesium distribution is one-dimensional and vertical. The coordinate of the vertical dimension is z. The geometry of the profile measurement is illustrated in Fig. 3. The response of the scintillator detector is the photo-peak counting rate of cesium 662 keV photons. The effects of small-angle inelastic and elastic scatterings are small. ^{137}Cs activity profile $q(z)$ is to be calculated from the measured counting rate profiles $c(z)$. For the calculation, it must also be assumed that the density $\rho(z)$ is one-dimensional as well.

The counting rate for a detector at z_0 is given by

$$c(z_0) = \int_{-\infty}^{\infty} q(z)K(z_0, z)\,\mathrm{d}z,$$

where the kernel

$$K(z_0, z) = \int_{x_0}^{\infty} D(r)\exp\left[-\int_{x_0/\sin\phi}^{r} \mu\rho(z')\mathrm{d}r\right] x\,\mathrm{d}x/2r^2$$

calculates the effects of geometry, attenuation μ in medium and detection efficiency η. $D(r) = \eta A(r)$ where

*HUT, Otakaari 1, Espoo, Finland. Tel.: +358-9-2428550.
E-mail address: servo.kasi@helsinki.fi (S.S.H. Kasi).

0969-806X/01/$ - see front matter
PII: S0969-806X(01)00368-1

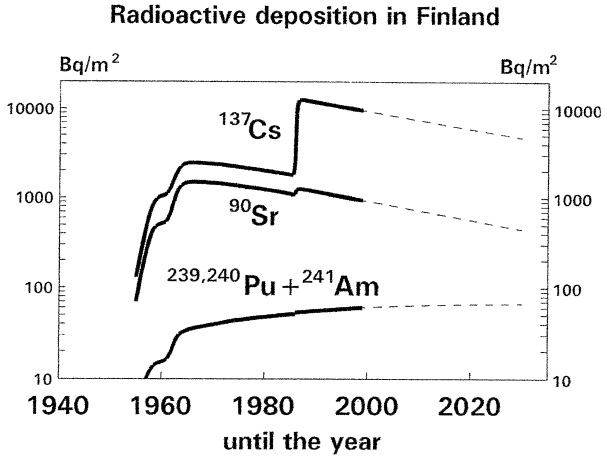

Fig. 1. Deposit of radioactive long-lived elements from atom bombs and accidents.

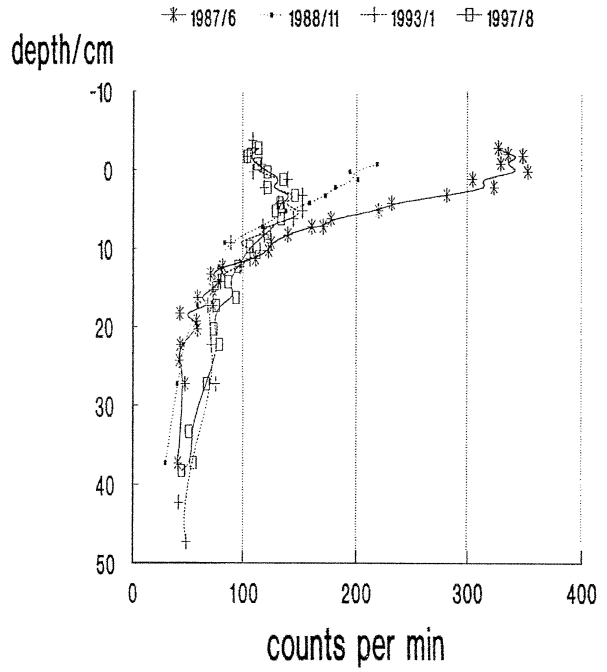

Fig. 2. Evidence of cesium profile stabilization in a mineral soil.

$A(r)$ is the cross section of detector against the direction of photon. Also $\eta = \eta(r)$, and can be determined experimentally. $dr = dz/\cos\phi$ and $2x_0$ is the diameter of hole or tube. In this application the iterative calculation of $q(z)$ from $c(z)$ has been rather fast. The $c(z)$ is the total photo-peak counting rate without the background. The density distribution $\rho(z)$ must be known accurately enough. It also may vary temporally.

Fig. 4 is a cesium profile result. The density profile used in the calculation was a rough three-step presentation. The effect of huge density profile variations was found in practice to be almost insignificant. The purpose is, however, to apply more adequate density profiles.

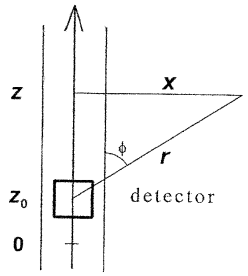

Fig. 3. Geometry for a relatively small photopeak detector in a vertical tube or hole.

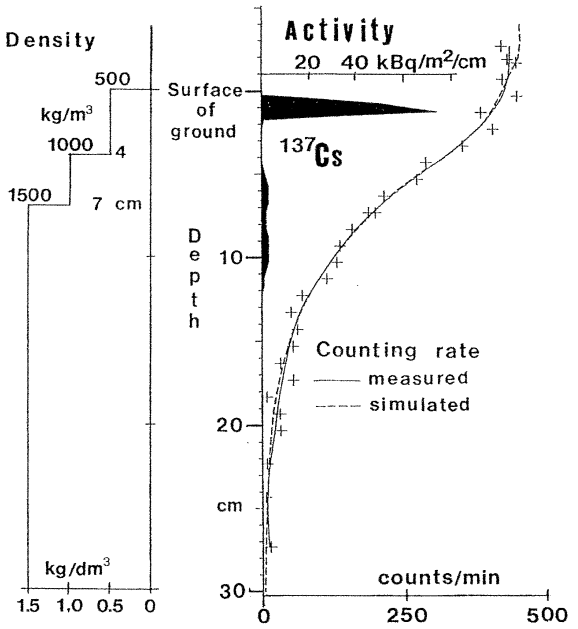

Fig. 4. The ^{137}Cs profile determined from the year 1987 counting rate profile of Fig. 2.

3. Snow water equivalent by using deposited cesium

Cesium photons are attenuated by soil and also by snow on the ground. This attenuation effect of snow can be used for measuring snow cover thicknesses, i.e. its weight burden (kg/m^2), or its water equivalent (H_2O mm). Soon after the accident some field experiments were performed with the $1 \times 1''$ NaI scintillator 1 m above the soil surface in Finland, in Lammi and Padasjoki. The scintillator (so big as a 161 package has been used) may be mounted in a vehicle, in an airplane or on a steep-sided hill. Kasi (1988, 1998) has pointed out that the cesium radiation can often determine the water equivalent more accurately than potassium radiation.

4. Use today of two photon sources in nature

In a single scintillator, in addition to the cesium 662 keV photons, potassium 1461 keV photons can be measured (Kasi, 1998). Because the cesium source is near the soil surface, but the ^{40}K source is almost uniform in soil, the water content near the soil surface can be determined, in summer and winter.

5. Personal dose caused by radiocesium

Gale et al. (1964) measured cesium activity in soil using ionisation chambers and then also found profile information. Knowledge of the profile is also needed for the determination of cesium contribution to the dose of a person on the soil surface. When the cesium profile is stabilized, the dose contribution of cesium activity follows the half-life 30.03 a of ^{137}Cs.

References

Gale, H.J., Humphreys, D.L.O., Fisher, E.M.R., 1964. Weathering of Cesium-137 in soil. Nature 201 (4916), 257–261.

Kasi, S., 1988. Cesium-137 for snow cover water equivalent measurement. IRPS-News (Newsletter of the International Radiation Physics Society) 2(2), 3–7; 2(3), 24.

Kasi, S.S.H., 1998. Determination of water content in soil below the ground surface using radioactive cesium and potassium in: XX Nordic Hydrological Conference. Rapport NHP-44 2, 413–422.

Konoplev, A.V., Bulgakov, A.A., Popov, V.E., Hilton, J., Comans, R.N.J., 1996. Long-term investigation of ^{137}Cs fixation by soils. Radiation Protection Dosimetry 64 (1/2), 15–18.

Riise, G., Bjornstad, H.E., Lien, H.N., Oughton, D.H., Salbu, B., 1990. A study on radionuclide association with soil components using a sequential extraction procedure. J. Radianal. Nucl. Chem. 142, 531–538.

Text IX

Nondestructive determination of gamma- active nuclide profiles in soil

Servo KASI
homepage: http://www.helsinki.fi/people/servo.kasi
Kajavankatu 6 B 45, FIN-04230 Kerava, Finland.
email: servo.kasi@helsinki.fi

Radiactivity profile changes, in the same profile, can be followed nondestructively

A scintillator is set in tube or hole in soil (Fig. 1,3) and it measures the counting rate profile $c(z)$ of gamma-active nuclide photopeak. An inversion calculation, from this profile, is presented to determine the activity profile $q(z)$ of radioactive nuclide in soil. The stratified or plane symmetry of the nuclide distribution is assumed, so that q and c depend only on z. In inversion calculation the $q(z)$ is determined by iteration with the integral

$$c(z) = \int_0^\infty K(z', z) q(z') dz'$$

so long that fitting is the best. The kernel $K(z', z)$ is in [1].

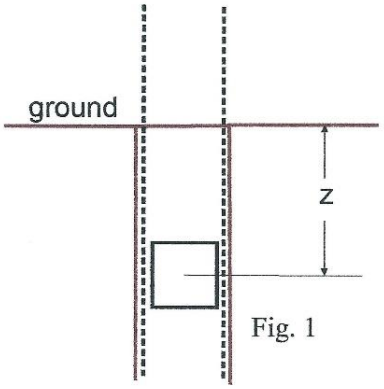

Fig. 1

^{137}Cs activity profiles, from the photo-peak (662 keV) profiles, are determined by using a 1" NaI(Tl) scintillator in tubes, which were in soils before Chernobyl, or in holes in peat. I started 1986 and the first result is in Fig. 3. In spring of 1987 STUK took my project concerning the cesium activities on swimming shores. I determined surface activities (the arrangement **a** of Fig. 2) in southern Finland , and also there in the tubes of the ground- and soil water sites of Hydrological office (today in Environmental Institute) I then used the arrangement **b** of the equipment in Fig. 2 for cesium profile determinations. ^{134}Cs was also in interests. Its disturbing effects in ^{137}Cs determinations were tried to eliminate. In profile calculations the density profile $\rho(z)$ ought to be considered. Its increase with water content can be determined by neutron moisture measurement or in other ways. In calculations I tried to consider the tube walls and snow on the ground. The Rayleigh scatterings (Fig. 4) have so small scattering angles that they cause no troubles. Polarization has effects in the both scatterings. The differential Klein-Nishina scattering cross section can be necessary to be multiplied by $S(x, Z)$ [2], where $x = \sin(\theta / 2) / \lambda$; λ is the initial photon wave length, θ scattering angle and Z atomic number. $S \in [0,1]$ and $S(0,Z) = 0$ for all elements. The compilation of $S(x,Z)$ in [3] I have used. The instrument in Fig. 2 is not so pulse height stabilized as should be. In future measurements the peat density instrument [4,5] I shall use, because it has the good stabilisation, from Nucletronics.

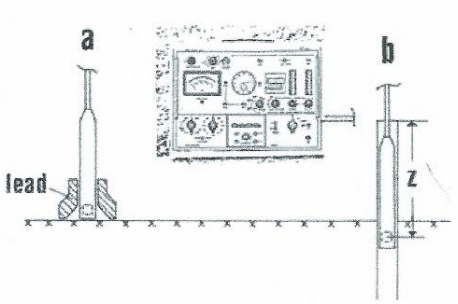

Figure 2. *Scintillator 1" NaI(Tl) and BASC scaler used in Cs surface activity (Bq/m^2) and soil profile measurement.*

In the first measurement and inversion calculation (Fig. 3) it was assumed ^{137}Cs layer with constant activity content. The forest soil profile in Tullinkangas in Lammi [1] I have measured most, but 1986-88 I started profile measurements also in Jämijärvi, Oripää, Orivesi and Elimäki in mineral soil, and in

Asikkala and Orimattila in peat. In the later calculations it was used the step wise constant approximation for $\rho(z)$ [1].

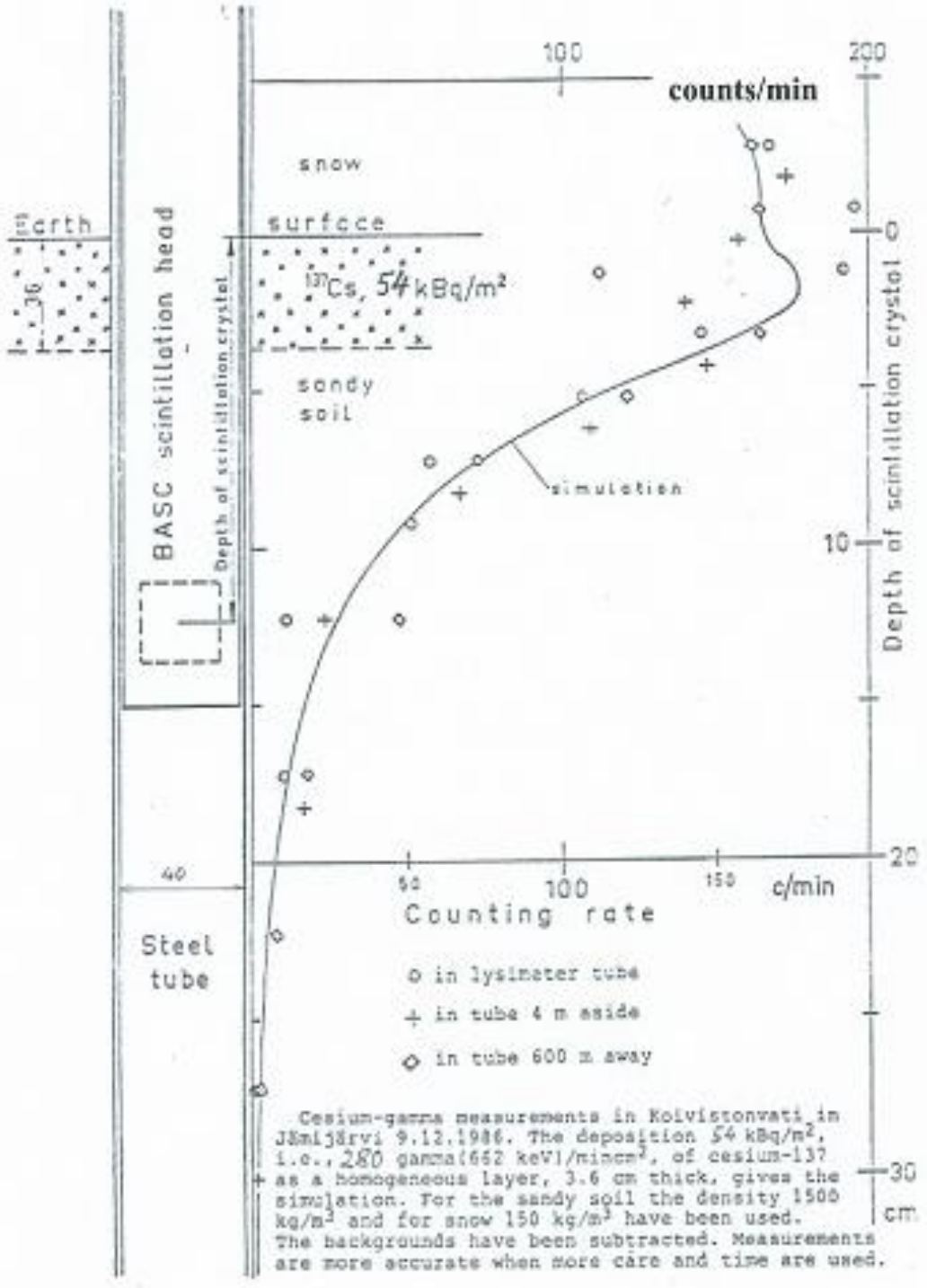

Figure 3. Cs-137 layer depth and activity determination with inversion calculation from the counting rates in 3 tubes in Koivistonvati, Finland, in 1986.

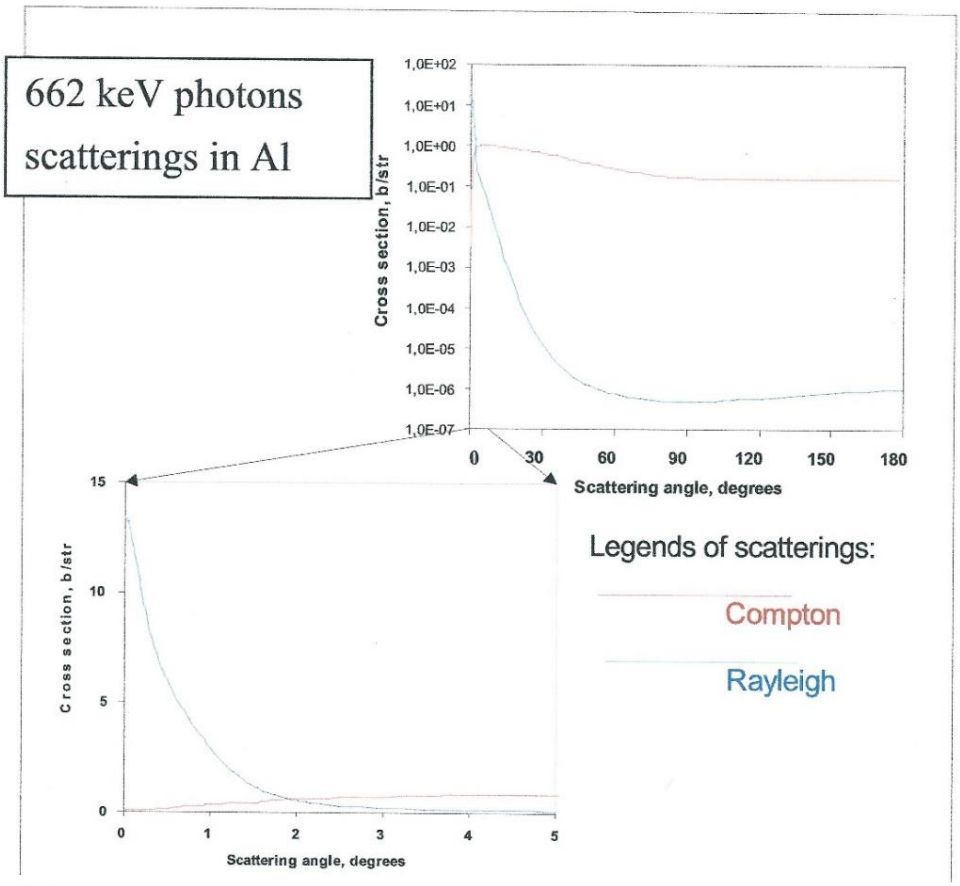

Figure 4. *Compton and Rayleigh cross sections on different scattering angles.*

After 1988 only one profile has been repeated in mineral soil site, and only 2 times [1], and once in peat. In the mineral soil, in Lammi in southern Finland, the stabilization of the ^{137}Cs profile has been observed [1], site B in Fig. 5. The site A is Koivistonvati of Fig. 3. Today I will verify the results in B and repeat all other profile determinations and make relevant new ones.

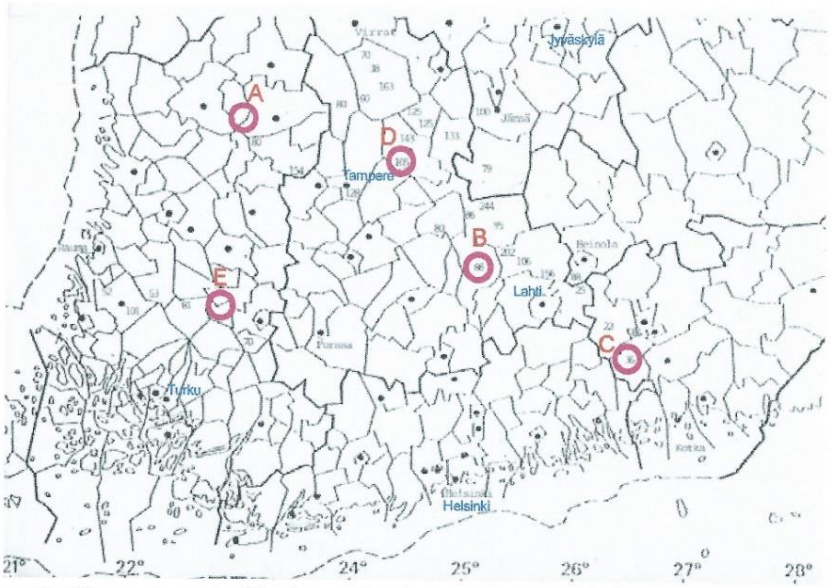

Figure 5. *The cesium profile determinations sites in red. The numerical values are cesium depositions in kBq/m^2 determined by the arrangement* ***a*** *in Fig. 2.*

The ^{137}Cs profile information is also important for determination of its contribution to human dose. In 1987 remarkable drifting of surface sand with its ^{137}Cs were found. In a sand pit to south-east from A the deposition was 80 kBq/m^2, but the drifting was found to cause this be increased even 5..6 times higher, mentioned also in [6].

In my poster in [7] there were presented the activities at the bottom of a pool in Padasjoki.

Potassium is used as a fertilizer. To follow its profile by using the 1461 keV photons of ^{40}K, I think, is interesting. I found plenty of findings of potassium fertilizers in web-search.

Snow water equivalent (snow mass) can be accurately determined by using snow attenuation of the cesium radiation. When counting, at the same time, the 1461 keV photons of ^{40}K as well, it may then be possible to determine the surface soil moisture. [6,7,8].

References

[1] S.S.H. Kasi Cesium deposition in soil and its effects, p. 673-675 in Radiation Physics and Chemistry 61(3-6), ed. by D A Bradley and L Musilek, Proceedings of 8th International Symposium on Radiation Physics - ISRP8, Prague, Czech Republic, 5 - 9 June 2000. In http://www.sciencedirect.com/science/journal/0969806X

[2] R. Ribberfors, K.-F. Berggren, Phys. Rev. A 26 (1982) 3325.

[3] J.H. Hubbell, W.J. Veigele, E.A. Briggs, R.T. Brown, D.T. Cromer, R.J. Howerton, J. Phys. Chem. Ref. Data 4 (1975) 471.

[4] S. Kasi, Soil water content more accurately by nuclear methods, XI Nordic Hydrological Conference, in Uppsala 26-30.6.2000, NHP Report 46, Vol. 2, 549-554.

[5] S.S.H. Kasi, Modelling, calibration and errors of γ- and n-gauges, a poster in International Symposium on Radiation Physics - ISRP10, http://www.mv.helsinki.fi/home/skasi/G10.pdf Coimbra, Portugal, 5 - 9 June 2006.

[6] S. Kasi, Aktuella hydrologiska cesium-137 mätningar (Actual hydrological Cs-137 measurements), Nordisk Hydrologisk Konferens, 1.-3.8.1988, Rovaniemi, Finland, NHP Report 22, Vol. 2, 263-270.

[7] S. Kasi, Hydrological use of radiocesium fallen down, Nordisk Hydrologisk Konferanse 4.-6.8.1992, Alta, Norge, NHP rapport 30, 574-583.

[8] S. Kasi, To modify and improve nuclear snow survey methods because of cesium deposit, Nordic Hydrological Conference, 4.-7. August 2002, Röros, Norge, NHP rapport 47, Vol. 1, 11-16.